Hydration and durability of fast hardening binders incorporating supplementary cementitious materials

Présentée le 22 juillet 2022

Faculté des sciences et techniques de l'ingénieur
Laboratoire des matériaux de construction
Programme doctoral en science et génie des matériaux

pour l'obtention du grade de Docteur ès Sciences

par

Sarra EL HOUSSEINI

Acceptée sur proposition du jury

Prof. A. Mortensen, président du jury
Prof. K. Scrivener, Prof. B. Lothenbach, directrices de thèse
Prof. S. Bishnoi, rapporteur
Prof. T. Matschei, rapporteur
Prof. A. Fontcuberta i Morral , rapporteuse

École
polytechnique
fédérale
de Lausanne

2022

Per Aspera ad Astra

Through hardships to the stars

For my parents, my husband and my lovely daughter

Acknowledgements

I would like to express my deepest appreciation to all persons who made these four years an unforgettable experience with a lot of fun.

To begin with, needless to say I had the opportunity to have two important persons without whome this thesis would not be possible. First, I am extremely grateful to the person who made this dream come true, Prof. Karen Scrivener. Thank you for believing in me, for being always a great support at all stages, and for your profound belief in my work. I would also like to extend my sincere gratitude to my cosupervisor Prof. Barbara Lothenbach for being always available and for solving all my GEMS problems. Without your guidance and continuous help, this accomplishment would not have been possible.

I would also like to express the deepest appreciation to all members of the jury committee: Prof. Andreas Mortensen, Prof. Anna Fontcuberta i Morral, Prof. Shashank Bishnoi and Prof. Thomas Matschei, who kindly agreed to invest their time in reviewing and discussing my work.

I am extremely grateful to Imerys Aluminates for financing this research work. Special thanks to Dr. Hervé Fryda, Dr. Barbara Benevenutti, Dr. Camille Nalet, Dr. Stéphane Berger for all their helpful advice and support.

Thanks to Dr. Mohsen Ben Haha from Heidelberg cement for always accepting my urgent MIP analysis and Luigi Brunetti from EMPA for the time spent on analysing all my pore solutions.

I would like to extend my sincere thanks to all my colleagues at EPFL and in particular LMC laboratory members. Thanks to my office mates Wiola, Mama Mink, Romain, Priscilla, Philipp and Andrea. It was great to work and to spend an important fraction of my time with you. I would also like to thank all members of LMC, Diana for being a good friend and for the helpful tips with the XRD quantification issues, Khalil for all the nice moments, Hisham for your generosity and your encouragements, Solène for the fructuous discussions during lunch together, Qiao for the tasty Chinese food, Maya for asking about my news every time I disappear and Meenakshi for spreading your good mood. Thanks also to Lenka for late evening lab discussions, Mai and Jinfeng for your great helping attitude. My appreciation and gratitude to Franco, Anna, Ziga, Julien, Alex, Alex.P, Monisha, Shishi, Yu Yan, William, Fabien and finally to Emmanuelle for your help with TEM.

I am also very grateful to people who have already left LMC but with whome relation went beyond the boundaries of the lab: Yosra (a great advisor), Mahsa (I will never ever forget your kindness), François (for scientific discussions and the nice days spent in the chalet). Anna (for organizing nice afterwork plans and for all the badminton games), Sreejith and Baghat (for introducing me to the great Indian culture), Julien, Alex. P and Monisha.

Several people have played an important role throughout this journey. I would like to thank Lionel (for solving all the challenging machine related issues and your sepcial French words), Jean (for never saying no and for being a good TP assistant partner), Antonio (for your smiling attitude), Maxime, Nathan and Noah.

I would like to thank my students: Fabiano and Andrea and extend these thanks to LMC administrative staff: Maude, Fabio, Adrien and Mira for your helpful advice, and for helping me out with my office queries.

I would also like to extend my thanks to all my friends: Marina (thank you for being my friend doctor and always being there whenever I need you), Chiheb for the ways back and the infinite discussions, Sonia for the unforgettable Swiss hikes and plans. My lovely Jennyfer and Nordin thank you for visiting me in Lausanne whenever possible. Dorsaf, Cyrine, Yosra, Asma, Fadwa, Fatnasa, Mariem and Lina thank you for keeping in touch although the distance.

Finally, I would like to express the special thanks to my beloved family. I would like to give my special thank to the Jemmali family for the nice dinners. Mom and Dad thank you for your unconditional love and endless support. Thanks to my sister who is always encouraging me to accomplish my goals. Big thanks to my wonderful parents and sisters in law for your support and for sending me Tunisian food whenever possible. Very special thanks to my husband Raouf who endured this long process, for always supporting me in tough times, for always saying "I do believe that one day, you will be awarded a Nobel prize!", for cooking and doing all the staff that you might hate but nevertheless does for the sake of love. And finally, thanks to my future daughter who survived all the writing process and the last months of my PhD. You are a strong girl !

Abstract

The use of supplementary cementitious materials (SCMs) is widely considered the most promising approach to reduce CO_2 emissions relative to cement production. SCMs are not commonly present in binders used for special applications. On the other hand, due to their low reactivity at early age, cements incorporating SCMs such as Limestone calcined clay cement (LC^3) exhibit low early age strength when compared to PC. This could restrict their field of applications and therefore solutions have to be found.

This thesis focused on two main axes. The first one is to lower the CO_2 footprint of ternary blends composed of Portland cement (PC), calcium aluminate cement (CAC) and calcium sulfate (Cs) using calcined clay as clinker substitute. The hydration of simple systems composed of PC with an increasing amount of CAC and Cs with and without calcined clay from 3 hours up to 90 days of hydration helped to understand and identify the contribution of each component. The results showed that increasing the CAC and Cs content in a PC system with and without calcined clay led to an increase of the ettringite content and a decrease of the portlandite content due to the portlandite consumption to form ettringite. The C_3S hydration was not delayed in presence of CAC and Cs. However, the presence of CAC, Cs and calcined clay led to slightly lower degree of hydration especially at later ages. The hydration and strength of a more realistic system "a fixing mortar formulation" with and without calcined clay was investigated. Overall, results showed that calcined clay can replace Portland cement by up to 20% with acceptable strength results.

The second aspect on which this thesis focused was the influence of incorporating CAC and Cs as limestone substitute in LC^3. The effect of the C/A molar ratio of the used CAC and its content were the main parameters investigated. The incorporation of 10%(CAC, Cs) improved the strength compared to LC^3 at all ages. The massive ettringite formation during the first hours of hydration explained the early age strength improvement. Results showed that the C_3S hydration was hindered when the C/A ratio of the CAC is equal to 1.7. The calculation of saturation indices indicated that a super saturation with respect to portlandite is likely needed to trigger the C_3S hydration. The high late age strength in LC^3-CAC blends was explained by a high volume occupied by hydrates in comparison with LC^3 blends. In terms of durability, the resistance to chloride ion penetration was investigated through the mini-migration method. LC^3-CAC blends showed a better chloride resistance than LC^3, which is mainly explained by the porosity refinement compared to PC, and the decrease of the total porosity in comparison with LC^3. On the other hand, the natural carbonation study showed that LC^3-CAC blends have a higher carbonation rate when compared to PC. Contrary to PC, forced carbonation of LC^3 and LC^3-CAC blends resulted in a decrease of the strength. However, the strength of carbonated LC^3-CAC specimens is still at least similar to the non-carbonated PC specimen.

Keywords SCMs, LC^3, fixing mortar formulation, hydration, C/A ratio, LC^3-CAC, durability.

Résumé

L'utilisation de matériaux cimentaires de substitution (MCS) est largement considérée comme l'approche la plus prometteuse pour réduire les émissions de CO_2 liées à la production de ciment. Les SCMs ne sont pas couramment présents dans les liants utilisés pour les applications spéciales. D'autre part, en raison de leur faible réactivité à jeune âge, les ciments incorporant des MCS, tels que le ciment calcaire argiles calcinées (LC^3), présentent une faible résistance au jeune âge par rapport au PC. Cela pourrait restreindre leur champ d'application et il faut donc trouver des solutions.

Cette thèse s'est focalisée sur deux axes principaux. Le premier consiste à réduire l'empreinte CO_2 des mélanges ternaires composés de ciment Portland (PC), de ciment d'aluminate de calcium (CAC) et de sulfate de calcium (Cs) en utilisant l'argile calcinée comme substitut de clinker. L'hydratation de systèmes simples composés de PC avec une quantité croissante de CAC et de Cs avec et sans argile calcinée de 3 heures jusqu'à 90 jours d'hydratation a permis de comprendre et d'identifier la contribution de chaque composant. Les résultats ont montré que l'augmentation de la teneur en CAC et Cs dans un système PC avec et sans argile calcinée a entraîné une augmentation de la quantité d'ettringite et une diminution de la quantité de portlandite. Ceci est dû à la consommation de portlandite pour former de l'ettringite. L'hydratation du C_3S n'a pas été retardée en présence de CAC et de Cs. Cependant, la présence de CAC, Cs et d'argile calcinée a conduit à un degré d'hydratation légèrement plus faible, surtout à long terme. L'hydratation et la résistance d'un système plus réaliste "une formulation de mortier de fixation" avec et sans argile calcinée a été étudiée. Dans l'ensemble, les résultats ont montré que l'argile calcinée peut remplacer le ciment Portland jusqu'à 20% avec des résultats de résistance acceptables.

Le deuxième aspect sur lequel cette thèse s'est focalisée était l'influence de l'incorporation de CAC et Cs comme substitut du calcaire dans le LC^3. L'effet du rapport molaire C/A du CAC utilisé et sa teneur ont été les principaux paramètres étudiés. L'incorporation de 10% (CAC, Cs) a amélioré la résistance par rapport au LC^3 à tous les âges. La formation massive d'ettringite pendant les premières heures d'hydratation explique l'amélioration de la résistance au jeune âge. Les résultats ont montré que l'hydratation du C_3S était réduite lorsque le rapport C/A du CAC est égal à 1.7. Les calculs des indices de saturation ont montré qu'une super saturation par rapport à la portlandite est probablement nécessaire pour déclencher l'hydratation du C_3S. La résistance élevée à long terme dans les mélanges LC^3-CAC s'explique par un volume d'hydrates élevé en comparaison avec le LC^3. La résistance aux ions chlorures a été testée par la méthode de la mini-migration. Les mélanges LC^3-CAC ont montré une meilleure résistance aux chlorures que le LC^3. Ce résultat s'explique principalement par l'affinement de la porosité par rapport au PC et la diminution de la porosité totale par rapport au LC^3. D'autre part, l'étude de la carbonatation naturelle a montré que les mélanges LC^3-CAC ont une vitesse de carbonatation plus élevée par rapport au PC. Contrairement au PC, la carbonatation forcée des mélanges LC^3 et LC^3-CAC a entraîné une diminution de la résistance. Cependant, la résistance des spécimens LC^3-CAC carbonatés est toujours au moins similaire à celle du spécimen PC non carbonaté.

Mots-clés SCMs, LC^3, formulation de mortier de fixation, hydratation, rapport C/A, LC^3-CAC, durabilité.

Contents

List of Figures

List of Tables

Glossary

Cement notation is used throughout the document:

A= Al_2O_3, C= CaO, S= SiO_2, F= Fe_2O_3, s= SO_3, c=CO_3, H= H_2O

For SO_3 and CO_3, s and c were used instead of $\overline{S}$ and $\overline{C}$ to simplify the typing.

Materials

PC	Portland cement
SCMs	Supplementary cementitious materials
CAC	Calcium aluminate cement
CsH_x	Anhydrite for x=0, Hemihydrate for x= 0.5, Gypsum for x=2)
CClay	Calcined clay
LC^3	Limestone calcined clay cements
Cc	Limestone

General abbreviations

C/A	Calcium oxide to aluminum oxide molar ratio
w/b	Water to binder ratio
wt .%	Weight percentage

Methods

XRF	X-Ray Fluorescence
PSD	Particle Size Distribution
XRD	X-Ray Diffraction analysis
MIP	Mercury intrusion porosimetry
GEMS	Gibbs energy minimization software
IC	Ion chromatography
SEM	Scanning electron microscopy

Definition

"Building chemistry" refers to the use of formulated cementitious mixes in applications such as tile adhesives and self levelling floor screeds. These are special blends that are usually made of calcium aluminate cement, Portland cement and calcium sulfate as well as chemical admixtures in powder form [1] .

Chapter 1   Introduction

1.1   Background of the thesis

Concrete is the second most consumed substance on earth after water, with more than 4 billon tons produced per year. This material is composed of basic ingredients water, cement, and aggregates (sand and gravels). Concrete is one of the most energy-efficient construction material [2]. However, the continuous rise in world population, means there is an increasing need for concrete as a key factor for human development. This does not come without an environmental cost. The extensive production of concrete and thus of cement is responsible for approximately 7% of the global carbon dioxide (CO_2) emissions [3]. Specifically, one ton of cement produced releases about 0.8 ton of CO_2 [4].

In the cement industry, the production of clinker is the most significant source of greenhouse-effect gases and CO_2 is the main greenhouse gas of concern. Clinker is a key ingredient of cement that is obtained by calcining limestone and clay at about 1450°C. At about 700-800°C, limestone decomposes ($CaCO_3 \rightarrow CaO+CO_2$) and this accounts for about 60% of the total CO_2 emissions. The rest arises from the combustion of fuel needed to reach 1450°C.

Several sustainable approaches have been proposed to reduce cement CO_2 emissions [3,5,6]. One of the proposed approaches suggests to reduce the use of conventional fossil fuels and to maximize the use of alternative fuels to produce cement. The most commonly used ones are waste materials and biomass. The most interesting approach focuses on reducing the clinker to cement ratio by using supplementary cementitious materials (SCMs) such as slag, fly ash and silica fume, limestone and calcined clay. The availability of blast furnace slag and fly ash is not in the range of massive cement production [7], whereas, Kaolinitic clays (suitable for calcination) and limestone are some of the most abundant materials worldwide [7].

1.2   Portland cement

In concrete, cement acts as the glue that holds the aggregates together. Portland cement (PC) consists of a mixture of clinker and a calcium sulfate source in a ratio of about 95:5 [8]. Clinker is a multi-phase compound that comprises four main phases:

- Alite, tricalcium silicate (C_3S: Ca_3SiO_5)
- Belite, dicalcium silicate (C_2S: Ca_2SiO_4)
- Tricalcium aluminate (C_3A: $Ca_3Al_2O_6$)
- Ferrite solid solution ($C_2(A,F)$, $(CaO)_2((Al_2O_3)_x, (Fe_2O_3)_{1-x}$)

Hydration is the used term to describe the reaction of water with cement. Hydration is a complex phenomenon that leads to the precipitation of hydrates from the dissolution of the above-mentioned anhydrous phases. Most of cement hydration reactions are exothermic and the overall heat released during the process can be followed with isothermal calorimetry [9]. A typical calorimetry curve up to 50 hours of hydration is shown in Fig. 1-1.
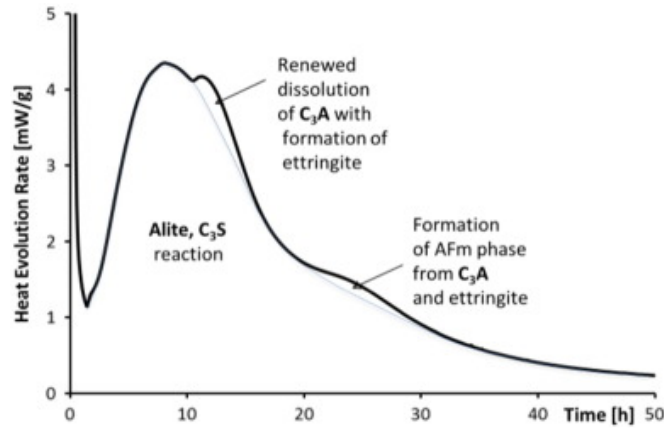
Fig. 1-1 Heat release during a typical PC hydration [8].

The hydration of alite is a dissolution-precipitation process leading to the formation of crystalline calcium hydroxide (Ca(OH)$_2$ or CH), known as portlandite, and calcium silicate hydrate (C-S-H) as described in Eq.1. It is well known that C-S-H is the major hydration product in cement paste and determines the mechanical properties of cementitious material. The hydration reaction of belite is slower and same hydration products are formed according to Eq.2.

$$yC_3S + H \rightarrow (3y - x)CH + C_x - S_y - H \tag{1}$$

$$yC_2S + H \rightarrow (2y - x)CH + C_x - S_y - H \tag{2}$$
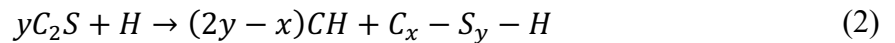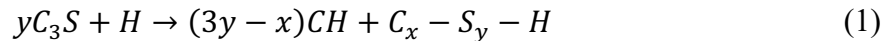
C$_3$A reaction with water leads to fast setting and calcium aluminate hydrates are formed as shown in Eq.3.

$$2C_3A + 21H \rightarrow C_4AH_{13} + C_2AH_8 \tag{3}$$

The addition of gypsum (CsH$_2$) or any other sulfate source delays its reaction and ettringite ($C_6As_3H_{32}$) also known as AFt (Aluminate Ferrite trisulfate) is formed according to Eq.4.

$$C_3A + 3CsH_2 + 26H \rightarrow C_6As_3H_{32} \tag{4}$$
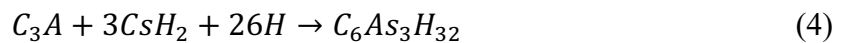
Once all the sulfate is depleted, ettringite reacts with the remained aluminate phase. Monosulfate phase AFm (Aluminate Ferrite monosulfate) is formed [10] according to Eq.5.

$$2C_3A + C_6As_3H_{32} + 4H \rightarrow 3C_4AsH_{12} \tag{5}$$
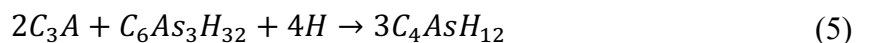
The hydration of Ferrite solid solution C$_2$(A,F) is slower than C$_3$A.

1.3   Clinker with Supplementary Cementitious Materials (SCMs)

Blending clinker with SCMs has a great potential to save clinker costs and use. Among all the commonly used SCMs, limestone and calcined clay are the most widely-available materials in sufficient quantities to reduce the clinker factor on a large scale of production [7]. Calcined kaolinitic clays are of particular interest due to their high reactivity.

There are different types of clays. These clays need to be thermally-activated to become reactive. Kaolinitic clays were shown to be the most reactive after calcination [11]. During the calcination process, the dehydroxylation of kaolinite (AS_2H_2) occurs between 400°C to 600°C and gives rise to an amorphous metastable phase that is called metakaolin (AS_2) [12]. Metakaolin is composed of alumina and silica and is formed according to Eq. 6.

$$AS_2H_2 \rightarrow AS_2 + 2H \tag{6}$$

Previous studies have shown that the high reactivity of metakaolin is linked to the change in the coordination number of aluminum and especially the presence of Al (V) in its structure [13,14]. Since aluminum groups are at the surface, they are directly exposed on metakaolin surface [14].

Substituting clinker with SCMs has two distinct effects: physical and chemical. During the first hours of hydration, the physical presence of SCMs enhances the hydration of cement. This is explained by a higher shearing during mixing since the interparticle distance is reduced by adding fine SCMs to the system [15]. Second, SCMs act as a nucleating agent. They provide nucleation sites for hydration products [15,16]. Moreover, replacing clinker with SCM results in an effective increase in the water to cement while the water to solid ratio is constant. More space is thus available for hydrates to form. The physical effect is usually known as the filler effect. Limestone and calcined clay are also known to chemically react. After sulfate depletion, limestone reacts with aluminates to form Hc and Mc (hemicarbo- and monocarbo- aluminate phases) [17]. In presence of limestone, ettringite dissolution is reduced after sulfate depletion [18]. Eq.7 and 8 summarizes the reactions. The limestone reaction is limited by the amount of alumina available to react. During the hydration of Portland cements, only 2-5% of limestone reacts [19,20].

$$C_3A + 0.5Cc + 0.5CH + 11.5H \rightarrow C_4Ac_{0.5}H_{12} \qquad \text{Hc} \tag{7}$$

$$C_3A + Cc + 11H \rightarrow C_4AcH_{11} \qquad \text{Mc} \tag{8}$$
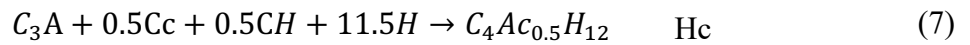
Metakaolin reacts as a pozzolanic material. This aluminosilicate amorphous phase reacts in presence of water and portlandite (CH) to form additional hydrates, mainly C-A-S-H and strätlingite (C_2ASH_8) [21,22] as presented in Eq.9. This reaction results in higher compressive strength.

$$AS_2 + CH + 6H \rightarrow C - A - S - H + C_2ASH_8 \tag{9}$$
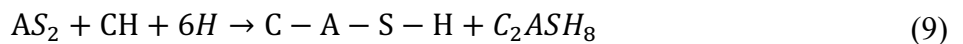
Limestone calcined clay cement is one of the most promising alternative cements. The combination of calcined kaolinitic clays and limestone allow the clinker content to be reduced by around 50% while maintaining similar strength to PC from 7 days onwards [23]. This is explained by the limestone reaction (Eq.7 and Eq.8), the pozzolanic reaction of metakaolin (Eq.9), and the synergetic reaction between alumina in calcined clay and limestone as presented in Eq.10. Thanks to the synergetic

reaction more carboaluminate phases are formed which results in an important porosity refinement and strength development [24].

$$A \text{ (from } AS_2) + Cc + 3CH + 11H \rightarrow C_4AcH_{11} \tag{10}$$
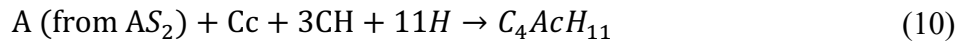
Nearly all concrete has an early age strength requirement. As shown in Fig. 1-2, the 1 day strength performance of LC^3 is relatively low compared to PC. This means that LC^3 formulations needs to be adapted to make it suitable. Few studies have focused on enhancing the early age strength performance of LC^3 and on identifying hydration mechanisms responsible for strength development. Adjusting the sulfate content showed a positive influence on the early age strength [23]. However, using a proper sulfation did not allow to reach equivalent strength to PC at 1 day. The other proposed way was to add alkanolamines. These alkanolamines are known to improve the grindability of cement as well as its hydration. Huang et al. studied the effect of triethanolamine (TEA) or triisopropanolamine (TIPA) on the hydration and strength performance [25]. The use of TEA was observed to enhance the strength at all curing ages which was not the case for TIPA [25]. TIPA has been found to positively impact the later age strength [26]. Zunino et al. confirmed that the use of TEA has a high potential to improve the early age strength [27]. These studies showed an enhancement compared to the LC^3 reference but no comparison with PC was made. Additionally, at 1 day, the observed improvement compared to the LC^3 reference, was about 3MPa and the strength tests were carried out on paste and with a water to binder ratio of 0.4. Furthermore, the use of alkali such as KOH was observed to improve the 1 day strength but negatively impacts the later ages strength [28]. A new solution that consists in incorporating CAC and Cs in LC^3 formulation is proposed in this study.
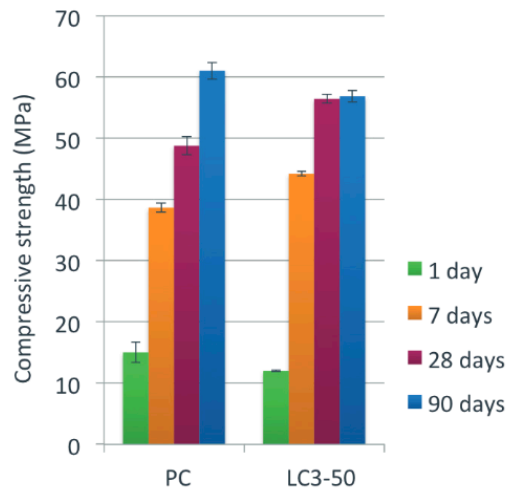
Fig. 1-2 Compressive strength of PC and LC3-50 from [23].

Corrosion of steel reinforcement is due to the chemical attack of chloride ions. LC^3 blends are known to have a better chloride resistance than PC. Important factors behind this improvement in resistance include the alkalinity of the pore solution, the binding capacity and the porosity refinement [29,30]. On the other hand, carbonation of blends incorporating SCMs (such as LC^3 blends) is known to be

higher than PC [31,32]. It was shown that the carbonation resistance of LC^3 blends can be improved by increasing the curing time [28].

1.4 Calcium aluminate cement

Calcium aluminate cement (CAC) is one of the most important non-Portland cements. This cement offers unique mechanical properties and chemical resistance [33–36] which makes it suitable for special applications such as refractory concrete, chemical resistant concrete and building chemistry products. The building chemistry market is one of the main markets of CAC, it offers a range of products such as specialist mortars for fixing, self-leveling compounds, tile adhesives and fast repairs. Depending on the alumina content, CAC is produced rather by sintering or fusing a mixture of low silica bauxite and limestone (T= 1450-1600°C). Reactive aluminate phases are formed. Monocalcium aluminate (CA) is the main anhydrous phase. Amorphous CACs are more reactive than crystalline CACs [37]. They consist in a chemically reactive phase composed of Al_2O_3 and CaO with some iron oxide (Fe_2O_3) and Magnesium oxide (MgO) present as impurities.

1.4.1 Hydration of calcium aluminate cement

As for PC, the hydration of calcium aluminate cement is driven by a dissolution and precipitation process. The hydration of CA at a temperature below 15°C leads to the formation of metastable calcium aluminum hydrates (CAH_{10}) according to Eq.11. At temperatures between 15 to 27°C, CAH_{10} coexists with C_2AH_8 and AH_3 as described in Eq.12. At T >50°C, stable hydrogarnet (C_3AH_6) is formed as shown in Eq.13.

$$CA + 10H \rightarrow CAH_{10} \qquad \text{T} < 15°C \qquad (11)$$

$$2CA + 11H \rightarrow C_2AH_8 + AH_3 \; ; \; CA + 10H \rightarrow CAH_{10} \quad 15°C < \text{T} < 27°C \quad (12)$$

$$3CA + 12H \rightarrow C_3AH_6 + 2AH_3 \qquad \text{T} > 50°C \qquad (13)$$
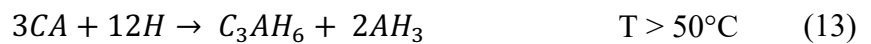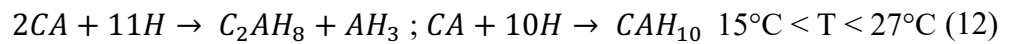
Metastable hydrates transform over time to the stable hydrogarnet (C_3AH_6) according to Eq.14 and Eq.15 [10,38]. The final hydration product has a higher density than metastable calcium aluminate hydrate. This reaction termed "conversion" is known to induce a volume modification and more precisely an increase of porosity [33]. As a result, the strength decreases which leads to a considerable susceptibility to failure [39].

$$2CAH_{10} \rightarrow C_2AH_8 + AH_3 + 9H \qquad (14)$$

$$3C_2AH_8 \rightarrow 2C_3AH_6 + AH_3 + 9H \qquad (15)$$
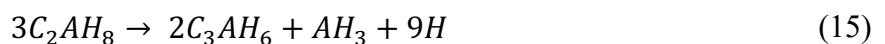
1.4.2 Hydration of calcium aluminate cement with calcium sulfate

Metastable aluminate hydrates formation can be avoided by adding a sulfate source [40]. New hydrates are formed and the setting is delayed. The hydration of binary blends composed of CAC and

sulfate source (CsH$_x$) leads to ettringite (AFt, C$_3$A·3Cs·32H$_2$O) and amorphous aluminum hydroxide (AH$_3$) as described in Eq.16.

$$3CA + 3CsH_x + (38 - 3x)H \rightarrow C_3A \cdot 3Cs \cdot H_{32} + 2AH_3 \tag{16}$$
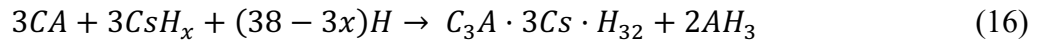
with x=0 for anhydrite, x=0.5 for hemihydrate and x=2 for gypsum.

If the amount of calcium sulfate is below the stochiometric ratio, the non-reacted CA will react with ettringite and as a result calcium monosulfoaluminate phases (AFm, 3C$_3$A.Cs.H$_{12}$) and aluminum hydroxide (AH$_3$) will form according to Eq.17.

$$6CA + C_3A \cdot 3Cs \cdot H_{32} + 16H \rightarrow 3C_3A \cdot Cs \cdot H_{12} + 4AH_3 \tag{17}$$
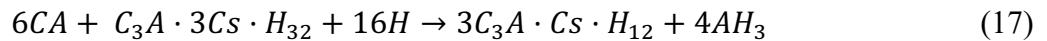
1.4.3   Hydration of systems composed of CAC/PC/CsH$_x$

CAC is a versatile material that can be blended with PC and CsH$_x$ when specific properties are required. These ternary binders are used to achieve strength much faster than Portland cement. Additional properties such as shrinkage compensation and fast setting are provided. Depending on application requirements, the mix proportions of CAC, Cs and PC can be varied. Fig. 1-3 shows three interesting areas for applications [41]:

▪ Area 1: Mixes of PC and CAC. These binary mixes can be only used in small repairs work since such mixes give quick or flash setting and have low strength.

▪ Area 2: This range contains mainly PC and a limited amount of CAC and Cs. Systems in this area are known as PC-rich formulations. Mixes with such a composition are generally used to produce fixing mortars, tile adhesives and fast repairs. The early ettringite formation offers high early strength (e.g. 20MPa at 3h), a better shrinkage compensation and accelerated hardening compared to PC.

▪ Area 3: CAC and Cs are the main binders. Systems in this area are known as CAC-rich mixes. A small amount of PC is added to provide extra lime to enhance ettringite formation. Higher CAC content means higher costs. This area provides higher early age strength, better shrinkage compensation and faster moisture reduction ("drying") compared to area 2. Such a mix is used for floor leveling. The need for specific properties justifies the higher cost of cement.
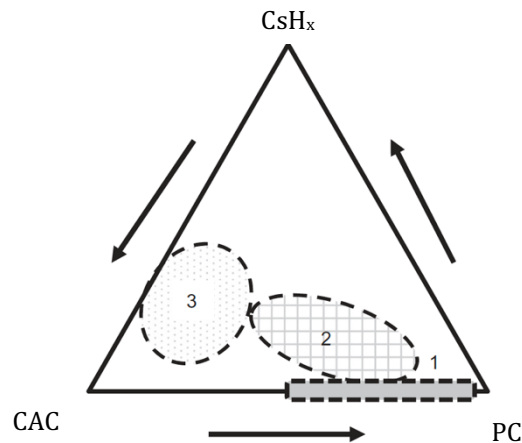
Fig. 1-3 Areas of interest in PC, CAC, CsH$_x$ ternary diagram [42].

In presence of calcium hydroxide, more ettringite can form relative to aluminum hydroxide, according to Eq.18.

$$(3 - y)\, CA + 3\, CsH_x + y\, CH + (38 - 3x - 4y)\, H \rightarrow C_3A \cdot 3Cs \cdot H_{32} + (2 - y)\, AH_3 \quad (18)$$
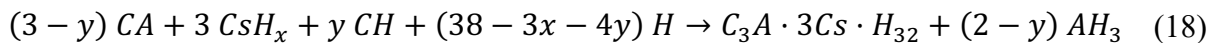
with x=0 for anhydrite, x=0.5 for hemihydrate and x=2 for gypsum.

The hydration of ternary binders is different from that of the individual cements. The sequence of hydration reactions varies with the initial mix composition of the ternary blends. Many researchers reported the hydration mechanisms taking place in ternary binders [42–46]. Amathieu et al. [47] and Kighelman et al. [45] showed that in these ternary binders ettringite is a key hydrate. The reactivity and the amount of calcium sulfate has been observed to control the amount and the kinetics of ettringite formation [46]. Nehring et al. highlighted the importance of the PC/CAC on the kinetics of hydration [42]. The principal hydration mechanisms taking place were described in [42,43,48]. These studies showed that the hydration is always first dominated by the ettringite formation then followed by PC hydration.

There is little literature on the effect of incorporating SCMs in CAC rich or PC rich formulations (area 2 or 3). Previous studies were focused on mixes made of CAC/SCM [49] or CAC/Cs/SCM (slag, limestone, fly ash) [44,50,51]. In ternary binders, the effect of incorporating SCMs was only investigated in CAC rich systems (area 3) and in most of cases slag was used as SCM [52,53]. However, no systematic study investigated the effect of incorporating calcined clay as a potential SCM in ternary binders specifically PC rich systems. More generally, the influence of calcined clay on the hydration mechanisms, the phase assemblage and strength performance of PC rich binders is unknown.

1.4.4 Objectives and content of the thesis

The aim of this thesis is to identify and understand hydration mechanisms taking place in PC, CAC, Cs based formulations incorporating SCMs particularly limestone and calcined clay. The long-term properties such as late age strength, chloride ingress and carbonation were also studied.

As a first step, the influence of incorporating calcined clay in a PC rich system more precisely a fixing mortar formulation was investigated. This study provides insights that could allow the replacement of calcined clay in ternary binders based on PC, CAC and Cs.

Second, to improve the early age strength performance of LC^3 blends, the effect of adding a CAC and Cs (1:1) to LC^3 was investigated. The effect of the CAC content and its C/A ratio on the strength and hydration mechanisms was studied. Then, particular attention was given to understanding the reasons for the delay of alite hydration in LC^3 incorporating low C/A ratio CAC.

Finally, understanding the long-term properties is of great importance to ensure the serviceability of LC^3-CAC blends over their lifespan. For this reason, a part of this project was dedicated to the investigation of the long-term properties. The main focus was on understanding the later age strength. Additionally, the resistance of LC^3-CAC blends to chloride and carbonation was assessed. Most of the chapters detailed below are written in the form of papers prepared for submission in peer-reviewed journals. They will be further edited before submission. A patent on LC^3-CAC blends was aleady submitted.

The outline of the thesis is organized as follows:

Chapter 2: focuses on understanding interactions between calcined clay, Portland cement, calcium aluminate cement and calcium sulfate in fixing mortar formulation. The first step in this chapter is to study the hydration of simple systems (PC with an increasing amount of CAC + Cs with and without calcined clay). The goal is to better see the effect of each component on the hydration and phase assemblage. This study gives better insights on reaction mechanisms taking place in a complex fixing mortar formulation with and without calcined clay.

Chapter 3: provides a first insights on the effect of calcium aluminate cement addition on the hydration and strength of LC^3. The effect of the C/A molar ratio of CAC and its content were the investigated parameters.

Chapter 4: investigates the reason of delaying alite hydration in LC^3-CAC formulation using low C/A ratio CAC. The effect of adding calcium hydroxide was also studied.

Chapter 5: focuses on understanding the late age strength of LC^3-CAC blends. The phase assemblage, the microstructure and the pore saturated limit were investigated.

Chapter 6: reports the results related to durability properties of LC^3-CAC blends. The resistance of LC^3-CAC blends to chloride was assessed using the mini-migration test method and compared with well-known systems: PC and LC^3. Regarding the carbonation study, both natural and forced carbonation were studied.

Chapter 7: summarizes the conclusions and gives suggestions for the future work.

1.4.5 Methodology

1.4.5.1 Characterization of the raw materials

The particle size distribution (PSD) and specific surface area (SSA) are important parameters that provide information about the fineness of a powder which is known to have an impact on the fluidity of cementitious materials and their reactivity. The particle size distribution was measured by laser diffraction. Mie theory was used to estimate the size of the particles. The specific surface area was determined using the gas adsorption technique. The SSA of the investigated materials was determined based on the BET theory.

1.4.5.2 Methods to investigate cement hydration and strength

Compressive strength

To assess the mechanical performance of the investigated systems, compressive strength tests were carried out on mortar cubes.

Isothermal calorimetry

Hydration of cementitious materials is an exothermic process. Isothermal calorimetry measures the heat release from hydration reactions. This technique provides reliable information about the kinetics of hydration.

X-Ray diffraction (XRD)

This technique was used to identify the crystalline phases present during hydration. Rietveld analysis allowed to quantify formed and consumed crystalline phases during hydration. In-situ XRD was also carried out to identify hydration reactions taking place at early age.

Scanning electron microscopy (SEM)

This technique provides useful information about the topography, morphology and phase composition. To observe the microstructure, backscattered electron images (SEM-BSE) was carried out. The C-A-S-H composition was obtained by energy dispersive X-Ray spectroscopy (EDX) point analysis on inner C-S-H. SEM-EDS mapping together with image analysis was carried out to identify and confirm the presence of phases of interest.

Mercury intrusion porosimetry (MIP)

Mercury intrusion porosimetry is a powerful technique to characterize the pore structure of cementitious materials down to 2 nm. In this project, MIP was used for different puroposes: study the effect of changing the mix compostion on the pore structure (Chapter 2), assess the evolution of the pork network at late age (Chapter 5) and investigate the effect of carbonation on the pore structure (Chapter 6).

Thermodynamic modelling

The geochemical gibbs free energy minimization software (GEMS) [54,55] together with the PSI-nagra thermodynamic database [56] and Cemdata 18 [55] were used to estimate the degree of reaction of metakaolin (DoR_{MK}) in blends containing calcined clay (Chapter 2 and 3), calculate saturation indices at early age (Chapter 4) and preditct the phase assemblage at 28 days (Chapter 5).

Internal relative humidity (RH)

To understand the late age strength, measurements of the internal relative humidity (RH) of cement paste samples and their pore solution were carried out. Based on the Kelvin Laplace equation, the water filled pore limit was estimated. Above the estimated pore limit, vapor rather than water is present and precipitation of hydrates should not be possible.

Transimission electron microscopy (TEM)

This technique provides details that can not be obtained with SEM. It allows a very local observation of the sample. In this study, this technique was used to compare the C-S-H morphology between systems of interest.

1.4.5.3 Methods to assess the durability

One of the most durability problems in reinforced concrete structures is corrosion of steel rebars. To ensure the serviceability of the investigated blends throughout their working life, the resistance of blends to chloride ingress and carbonation was assessed.

Mini-migration test method

This method allows to estimate the effective diffusion coefficient (D_{eff}) at cement paste scale. It measures D_{eff} without having the contribution of macro-scale effects and chloride binding. Additional techniques such as XRD and SEM-EDS were used to estimate the chemically and physically bound chloride.

Carbonation

The estimation of the carbonation coefficient based on the carbonation depth under natural conditions gives a good idea about the resistance of the investigated systems to natural carbonation. The effect of natural carbonation on the phase assemblage, the microstructure development and the C-S-H chemical composition were investigated using XRD, MIP and SEM.

Carbonation of mortar cubes under a high CO_2 concentration was studied. After 6 months of exposure, strength test was carried out. The aim was to study the impact of carbonation on the strength.

Chapter 2   Understanding interactions between calcined clay, Portland cement, calcium aluminate cement and calcium sulfate in a fixing mortar formulation

Note: This chapter is based on an article in preparation for submission to a peer reviewed journal

Contribution of the doctoral candidate: conceptualization, methodology, experiments, analysis and writing of the first manuscript draft.

Abstract

Blends composed of Portland cement, calcium aluminate cement and calcium sulfate are often used when rapid strength development, rapid drying and shrinkage compensation are required such as in fixing mortar formulations. The aim of this study was to provide a fundamental understanding of the hydration mechanisms taking place in a fixing mortar formulation. First, the hydration and the microstructure development of simple systems composed of PC+CAC+Cs with and without calcined clay was investigated. The results showed that substituting PC by CAC and Cs leads to a lower portlandite amount. This was explained by the portlandite consumption to form ettringite. The AFm content (the sum of hemicarboaluminate and monosulfoaluminate (Hc+Ms)), decreases after 3 days of hydration when CAC, Cs and calcined clay were present, due to the clay reaction leading to a conversion of Ms to strätlingite. However, strätlingite was only detected by X-Ray diffraction (XRD) at 28 days. While CAC+ Cs or calcined clay alone with PC did not have an impact on the C_3S hydration at later age, combining them together reduced slightly the degree of C_3S hydration.

Subsequently, the influence of calcined clay on the hydration and strength performance of a fixing mortar formulation was investigated. Incorporating calcined clay in a fixing mortar formulation led to lower early age strength. At later age, although the degree of hydration of C_3S in presence of calcined clay was lower, similar strengths as for the reference were obtained, due to the pozzolanic reaction of metakaolin.

2.1   Introduction

Calcium aluminate cement (CAC) is an alternative cement to Portland cement (PC). It was first used in the United Kingdom after the World War I for constructions where rapid strength development and a good sulfate resistance were needed [1]. The volume used per year is very small compared to PC [1]. The small production level (less than one thousandth of the volume of PC) together with the high expense of bauxite needed for production makes it four to five times more expensive than PC [57]. This limits its use to specific applications.

The hydration of CAC leads initially to metastable phases formation, C_2AH_8 and CAH_{10}. These phases convert over time to a denser phase C_3AH_6 [10,38]. As a consequence, the pore volume increases and causes a decrease in the strength performance [39]. Calcium sulfate (Cs) changes the reactions and leads to the formation of ettringite ($C_3A \cdot 3Cs \cdot 32H_2O$), hydrous alumina hydroxide (AH_3) and eventually monosulfate (C_4AsH_{12}) formation [40].

Ternary blends composed of PC, CAC and Cs have been developed to benefit from the special properties that CAC offers while maintaining an acceptable product cost. These blends are widely used in building chemistry application where fast setting, rapid drying and shrinkage compensation are required [41].

Overall, the cement industry accounts for about 7% of man-made CO_2 emissions [3] while cement and concrete account for more than half of all materials produced. Nevertheless, due to its large scale of production, coupled with an increasing market demand, therefore, the need for a more sustainable cementitious materials becomes a major challenge. In order to limit the global warming, several potential solutions, have been proposed by the IEA/WBCSD Roadmap to reduce the CO_2 impact of cement [58]. Among the proposed solutions, partial replacement of clinker by supplementary cementitious materials (SCMs) is the most promising approach [7,59]. Limestone and clays (suitable for calcinaton) are the some of the most widely available materials and the potential of using them as SCMs has not been fully exploited. Kaolinitic clays are the most suitable type of clays. After calcination, metakaolin forms as a highly reactive aluminosilicate amorphous phase. Metakaolin is an excellent pozzolanic material that reacts with portlandite to form C-A-S-H and strätlingite [23,60].

Blending PC with calcined clay has been extensively investigated in PC based systems [61–63]. A few studies were done on the effect of incorporating SCMs, such as limestone or slag, in ternary binders based on PC, CAC and Cs [44,64–66]. However, there is no study on the influence of calcined clay as partial PC substitute in blends made of PC, CAC and Cs. More generally, information about the hydration mechanisms that could take place with and without calcined clay is missing. The aim of this chapter is to understand the hydration reactions taking place in a fixing mortar formulation with and without calcined clay.

First, simple systems were investigated:

- PC with various CAC and Cs amounts, to provide a baseline understanding of the effect of CAC and Cs addition on PC hydration.

- PC + calcined clay with an increasing amount of CAC and Cs, to see how the hydration reactions are influenced in the presence of calcined clay. The PC: calcined clay is always 4:1.

Several analytical techniques, such as X-Ray diffraction (XRD), scanning electron microscopy (SEM), mercury intrusion porosimetry (MIP) were used. The Gibbs energy minimization software (GEMS) was also used to estimate the degree of reaction of metakaolin.

Secondly, the effect of replacing a part of PC by calcined clay in a fixing mortar formulation in terms of kinetics of hydration, phase assemblage and mechanical performance was investigated. Isothermal calorimetry measurement together with XRD in-situ were used to identify the main hydration mechanisms taking place.

The evolution of the anhydrous and the hydrated phases over time was followed by XRD ex-situ combined with the Rietveld method. The evolution of compressive strength tests was measured to assess the feasibility of substituting PC by calcined clay in the fixing mortar formulation.

2.2 Materials and methods

2.2.1 Raw materials

PC from HeidelbergCement conforming to EN197-1 and classified as CEM I 52,5R was used. The CAC used in this study was provided from Imerys Technology Center Lyon (ITC Lyon). It is amorphous and it has a C/A molar ratio of 1.7. The Cs is a natural anhydrite. Calcined clay (CClay) was an Argical M-1200S from Imerys Refractory Minerals (IRM). The kaolinite content was estimated as ~ 80% from thermogravimetric analysis (TGA) of the raw clay, from the weight loss between 400°C-600°C [13], as detailed in [63]. The oxide composition of the materials was measured by X-ray fluorescence (XRF) analysis. The particle size distribution (PSD) of the main materials, determined by laser diffraction with a Malvern Mastersizer is plotted in Fig. 2-1. The optical model parameters were selected according to [67]. The specific surface area was obtained by nitrogen adsorption using the BET model. The physicochemical properties of the PC, CAC, Cs and CClay are shown in Table 2-1. The phase composition of the main materials is shown in Table 2-2. XRD-Rietveld analysis is not shown for calcined clay as it is mainly amorphous. Citric acid (setting retarder, from Citrique Belge, Fine granular 51N,) and Na_2CO_3 (setting accelerator, Solvay) were used as admixtures to control the setting time of cement. For mortar preparation, AFNOR sand was used.
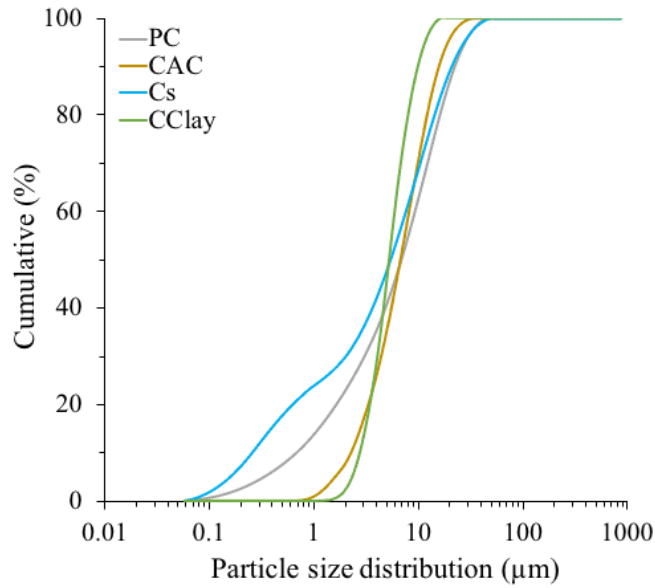
Fig. 2-1 PSD for the main materials.

Table 2-1 Physicochemical properties of PC, CAC, Cs and CClay.

(wt.%)	PC	CAC	Cs	CClay
Al_2O_3	3.88	45.71	0.00	38.88
SiO_2	22.47	4.75	0.00	54.06
CaO	65.88	43.68	42.0	0.12
Fe_2O_3	1.42	1.74	0.00	1.99
MgO	0.88	0.90	0.00	0.32
K_2O	0.71	0.26	0.00	1.22
Na_2O	0.27	0.07	0.00	0.07
P_2O_5	0.15	0.13	0.00	0.06
SO_3	3.37	0.10	57.0	0.00
TiO_2	0.17	2.21	0.00	1.99
Cr_2O_3	<0.01	0.13	0.00	0.02
MnO	0.05	0.07	0.00	0.01
SrO	0.18	0.00	0.00	0.00
ZnO	0.02	0.00	0.00	0.00
CO_2	0.30	n.d	n.d	n.d
Specific surface area (m^2/g)	0.85	0.88	0.97	18.70
$D_{v\,50}$ (µm)	7.20	6.00	5.20	5.50

Table 2-2 Phase composition of PC, CAC and Cs.

Phase (wt.%)	PC	CAC	Cs
C_3S	65.8	-	-
C_2S	15	-	-
C_4AF	1.5	-	-
C_3A	11.5	-	-
Dolomite	0.6	-	-
CsH_2	0	-	-
Cs	4.3	-	99.4
Cc*	1.3	-	0.6
CA	-	7	-
C_2AS	-	0.15	-
CFT*	-	1	-
$C_{12}A_7$	-	0.45	-
Magnetite	-	-	-
Amorphous	-	91.40	-

*Cc: $CaCO_3$, CFT: Perovskite

2.2.2 Mixture design and sample preparation

In this study, simple systems (SSs) were first investigated. They consist in samples composed of PC with an increasing amount of CAC+Cs and samples composed of PC-CClay with an increasing amount of CAC+ Cs. The CAC: Cs was always 1:1. More details about all the mixes compositions are shown in Table 2-3. As a second step, a fixing mortar formulation with about 84.34% PC was used as a reference to investigate the influence of incorporating calcined clay on the hydration and strength performance. Then, 5, 15 and 20% of PC was substituted by CClay. For all the mixes, cement pastes were prepared by mixing distilled water with dry powder using a high-speed mixer at 1600 rotations per minute for 2 min. A water-to-binder ratio (w/b) of 0.46 was used for the study of pastes. To assess the compressive strength performance of fixing mortar formulations, mortars were prepared with a w/b ratio of 0.5.

Table 2-3 Mix compositions of the investigated systems (wt. %).

	Notation	PC	CAC	CClay	Cs	Citric acid	Na_2CO_3
SS	PC-0(CAC,Cs)	99.06	-	-	-	0.33	0.61
	PC-5(CAC,Cs)	94.10	2.47	-	2.47	0.33	0.61
	PC-10(CAC,Cs)	89.15	4.95	-	4.95	0.33	0.61
	PC-15(CAC,Cs)	84.21	7.42	-	7.42	0.33	0.61
SS- with 20CClay	PC-0(CAC,Cs)-20CClay	79.25	-	19.81	-	0.33	0.61
	PC-20CClay-5(CAC,Cs)	75.28	2.47	18.82	2.47	0.33	0.61
	PC-20CClay-10(CAC,Cs)	71.32	4.95	17.83	4.95	0.33	0.61
	PC-20CClay -15(CAC,Cs)	67.37	7.42	16.84	7.42	0.33	0.61
Fixing mortar formulation	0CClay	84.34	7.43	0	7.43	0.28	0.52
	5CClay	80.12	7.43	4.22	7.43	0.28	0.52
	15CClay	71.68	7.43	12.65	7.43	0.28	0.52
	20CClay	67.47	7.43	16.87	7.43	0.28	0.52

The admixture content is slightly higher in simple system compared to the ordinary fixing mortar formulation. To check the effect of such a difference on the hydration kinetics, the evolution of the heat of hydration was followed by isothermal calorimetry for 20CClay and the simple system: PC-20CClay-15(CAC,Cs). The latter has the same mix composition as 20CClay but with higher citric acid and Na_2CO_3 contents. The calorimetry results presented in Fig. 2-1, show a small difference in terms of kinetics of hydration, but three main peaks are observed in both cases. The hydration peaks (#1, #2 and #3) are slightly delayed in the fixing mortar formulation where lower admixtures contents are used.
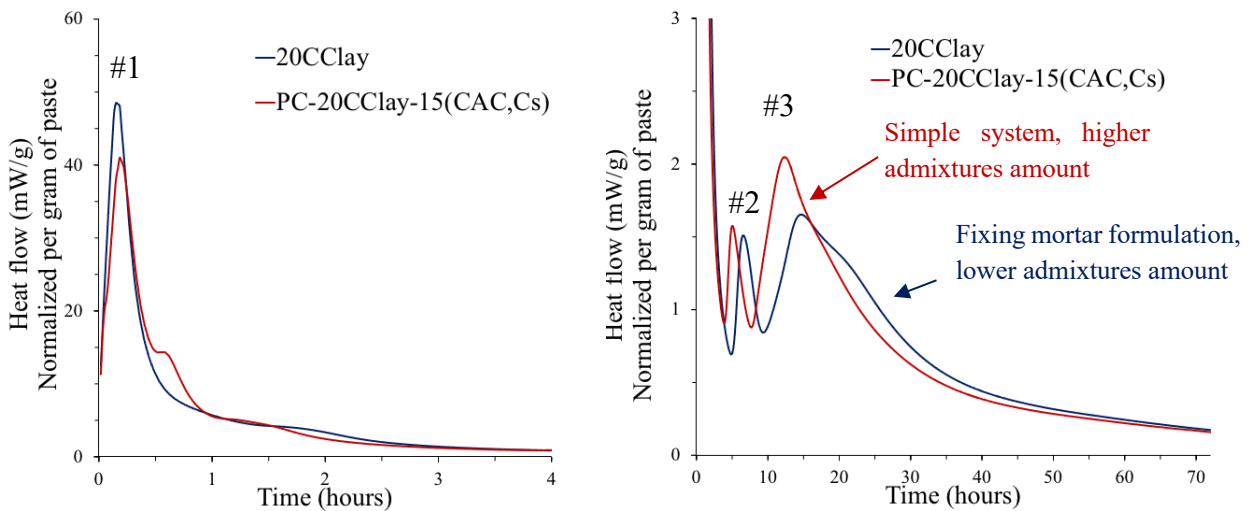
Fig. 2-2 Heat release per gram of paste for 20CClay and PC-20CClay-15(CAC,Cs).

2.2.3 Methods

For the simple system study, the following methods were used:

After mixing, the cement pastes were placed in plastic cylinders bottles and sealed with parafilm. At the required age, a fresh slice of cement paste of few mm thickness was cut with a saw and then analyzed by XRD. Experiments were carried out on fresh cement paste slices at 3 hours, 1, 3, 7, 28 and 90 days. For the first sample (nominally 3 hours), the measurement was made when paste is hard enough to cut a slice. Measurements were made with a PANalytical X'pert Pro with a copper source working at 45kV and 40mA. Scans were collected between 5 and 70° 2θ with a 1/2° divergence slit in 15 minutes, which represents a step size of 0.017° 2θ. Anhydrous and hydrated phases were quantified with the Rietveld method using HighScore Plus program. The external standard method was used to get the K factor of the device and the amorphous phases in the paste. A scan of Rutile powder was used to calculate the K factor.

XRD-Rietveld data on fresh paste at time, t, are per 100g of paste. For cement powder carried-out at t_0, results are measured per 100g of solid. To calculate the degree of hydration and compare between t_0 and t, results on paste need to be rescaled according to Eq.1. The quantification is normalized per 100g of solid according to the water to binder ratio (w/b) used:

$$Wt_{i,rescaled} = \left(Wt_{i,Rietveld} \cdot \left(1 + \frac{w}{b}\right)\right) \tag{1}$$

Wt is the weight percent of a phase at a t time.

From the Rietveld quantification data, the hydration degree of C_3S (DoH_{C3S}) was determined according to Eq. 2.

$$Hydration\ degree\ of\ C_3S\ (t) = \frac{C_3S_{(t)} - C_3S_{(t0)}}{C_3S_{(t0)}} \tag{2}$$

Where C_3S (t) is the amount of the unreacted C_3S (g/100g of solid) from XRD-Rietveld analysis at a t time. C_3S (t_0) is the amount of the initial C_3S obtained from the Rietveld quantification of the initial dry mix.

The microstructural development was studied with scanning electron microscopy (SEM) (FEI Quanta 200 equipped with BrukerXFlash 4030 energy dispersive spectroscopy (EDS) detector). The cement hydration was stopped by solvent exchange with isopropanol [67]. At a specific age, 2 slices of 2 mm thickness were immersed in 200 mL isopropanol for 7 days. The solvent was replaced after 1 hour, 1, 3 and 5 days. After stopping the hydration, samples were dried and stored in a dessicator under vacuum for at least 48 hours to ensure a complete evaporation of the remaining isopropanol. Afterwards, a small piece of dried cement paste was impregnated in low viscosity resin then polished using a diamond abrasive sprays from 9μm to 1μm and finally carbon coated. An accelerating voltage of 15 kV and a working distance of 12.5 mm were used. The C-A-S-H composition at 90 days was determined by SEM- EDS according to the method of Rossen [68].

The Gibbs energy minimization software GEMS [54] was used to estimate the degree of reaction of metakaolin at 90 days. The PSI-Nagra database [56] and the Cemdata18 database [55] were used. The CSHQ model for C-S-H was selected. The C-A-S-H composition was corrected for Al uptake based on the estimated composition from SEM-EDS. The degree of hydration of anhydrous phases (C_3S, C_2S, C_3A, C_4AF, Cs) calculated from the Rietveld refinement at 90 days was used as input. GEMS gives the evolution of the portlandite content as a function of the degree of reaction of metakaolin. Knowing the amount of the portlandite content at 90 days from XRD-Rietveld method, it is possible to determine the DoR_{MK}. The amount of reacted metakaolin was calculated according to Eq.3.

$$Amount\ of\ reacted\ metakaolin\ = DoR_{MK}\ .wt\ calcined\ clay.calcined\ kaolinite\ content \quad (3)$$

Where DoR_{MK} is the degree of reaction of metakaolin from GEMS (g/100g of solid), wt calcined clay is the amount of calcined clay in the formulation (g/100g of solid) and the calcined kaolinite content is given by TGA.

For the fixing mortar formulation study, the following methods were used:

To follow the kinetics of hydration, the heat released during the hydration of cement was monitored by a TAM air isothermal calorimeter at 20°C for up to 7 days. After mixing, 10g of paste was placed into a glass ampoule. The ampoule was then sealed and introduced inside the calorimeter.

To relate the phase development of the cement paste to the hydration kinetics, in-situ XRD was carried out. The sample preparation is the same as for the isothermal calorimetry experiment. After mixing, the cement paste was placed in a sample holder. To minimize the carbonation of the cement paste and water loss from evaporation, cement paste was covered with a Kapton film of 12.5μm thickness. Similar scan parameters were used as for the ex-situ XRD measurements except for the divergence slit which is 1°. A water-cooling system was used to ensure a constant temperature at 20°C. A diffractogram was recorded every 15 minutes during the first 2 hours of hydration and every 30 minutes between 5-12 hours of hydration, then every 2 hours up to ~ 72 hours of hydration. The Rietveld refinement was conducted using the HighScore Plus software. A scan of Rutile powder under the same measurements conditions was carried out to calculate the K factor. XRD on fresh slices as already described above was also carried out.

To assess the compressive strength, 4x4x4cm mortar cubes were used. Samples were prepared and stored in a humidity chamber until the testing date. Strength measurements were carried out at 1, 3, 7, 28 and 90 days of hydration. The loading rate was 2.4kN/s.

2.3 Results and discussion

2.3.1 Hydration of simple systems with and without calcined clay

2.3.1.1 Impact of the CAC and Cs amount without calcined clay

The influence of increasing the CAC and Cs amount on the ettringite content is shown in Fig. 2-3(a). The control system (PC) has the lowest ettringite amount at all ages. An important increase of ettringite is observed between 1 and 3 days. The citric acid can retard both the CAC and PC hydration. Contrary to systems that contain CAC and Cs, citric acid in the PC system is fully available to delay the aluminate phases (C_3A, C_4AF) from clinker to react and to form ettringite. From 3 days onwards, the ettringite content remains unchanged. The ettringite content significantly increases when the CAC and Cs are added. As both hemicarboaluminate (Hc, $C_4Ac_{0.5}H_{12}$) and monosulfate (Ms, C_4AsH_{12}) were detected in XRD, results are shown as the sum of these two AFm phases in Fig. 2-3(b). The quantification of the AFm phases by XRD-Rietveld is challenging due to the poor crystallinity of these phases and their variable compositions leading to a change in their peak positions and intensities [69]. However, it can is clear that an increase of the CAC and Cs amount leads to an increase of the AFm amount. For PC-10 (CAC, Cs), a slight decrease of the AFm content is observed but the difference is within the error.

a)   b)
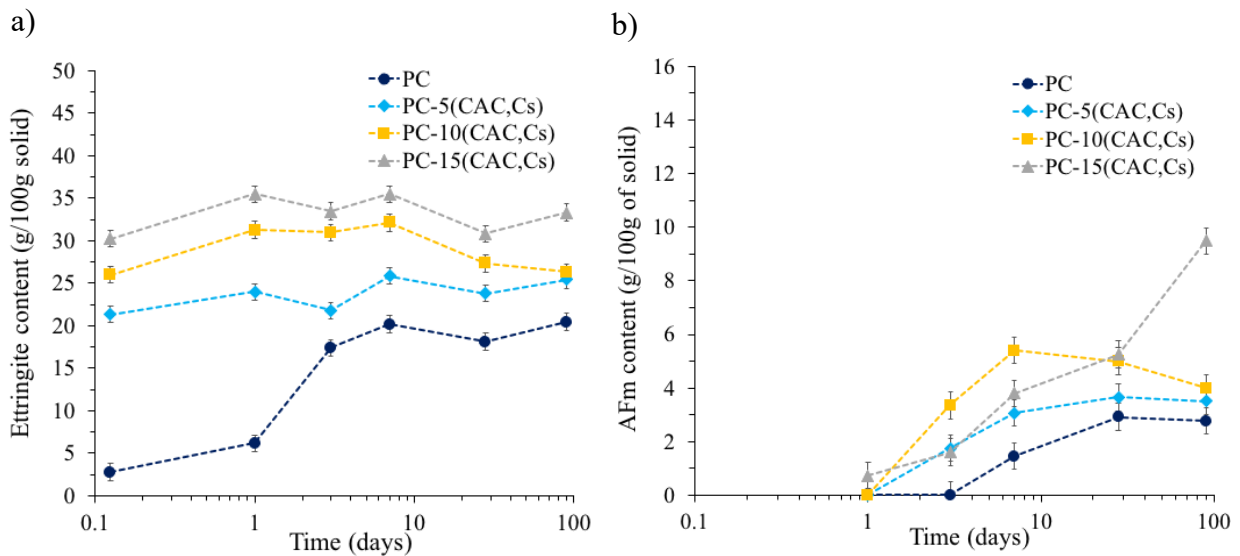
Fig. 2-3 Ettringite (a) and AFm (Hc+Ms) Rietveld quantification for the reference PC and PC systems containing 5, 10 and 15(CAC,Cs).

Fig. 2-4 shows the degree of hydration of alite (DoH_{C3S}) for the PC reference system and systems containing 5, 10 and 15% of CAC and Cs. In the PC system, the degree of hydration of C_3S is low, at 1 day. This is attributed to a delaying effect caused by citric acid. It can be seen that at 1 day a higher DoH_{C3S} is observed when CAC and Cs are present. In the reference, citric acid is more available to delay the C_3S hydration. However, when CAC and Cs are added, citric acid will act first on the early ettringite formation. Thus, it might be less available to delay alite hydration that occurs later. In the PC system, there is an important increase of C_3S hydration between 1 and 3 days. From

3 days onwards, the hydration of alite seems to be similar between all the systems. The small differences are within the error. This indicates that the use of CAC and Cs does not have an impact on the C_3S hydration.
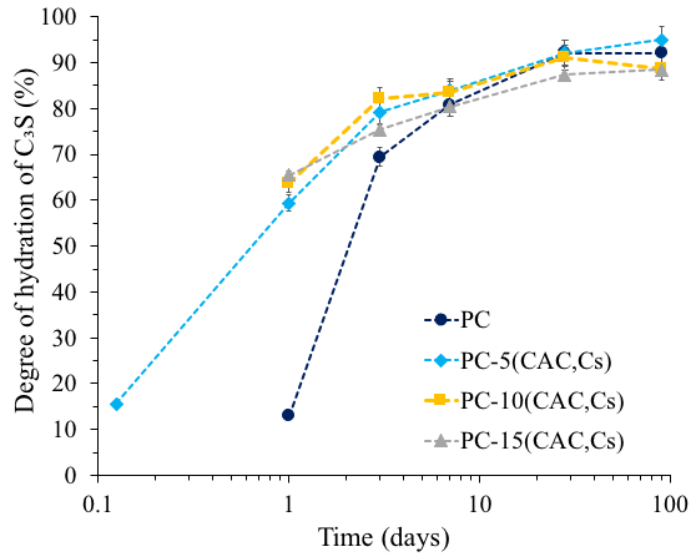
Fig. 2-4 Degree of hydration of alite (DoH$_{C3S}$) for the reference PC and systems with 5,10 and 15(CAC,Cs).

The quantitative analysis of portlandite by XRD-Rietveld is shown in Fig. 2-5(a). To remove the effect of differences in terms of cement content and degree of hydration of C_3S, the portlandite content was also normalized per the amount of reacted C_3S. Results are shown in Fig. 2-5(b). It is evident that the portlandite content, as a proportion of C_3S reacting, decreases with the CAC and Cs content. The higher the CAC and Cs content, the higher the ettringite content, but the lower the portlandite content is. This can be explained by the fact that a part of the calcium hydroxide is used to form ettringite (Chapter 1, Eq.18).
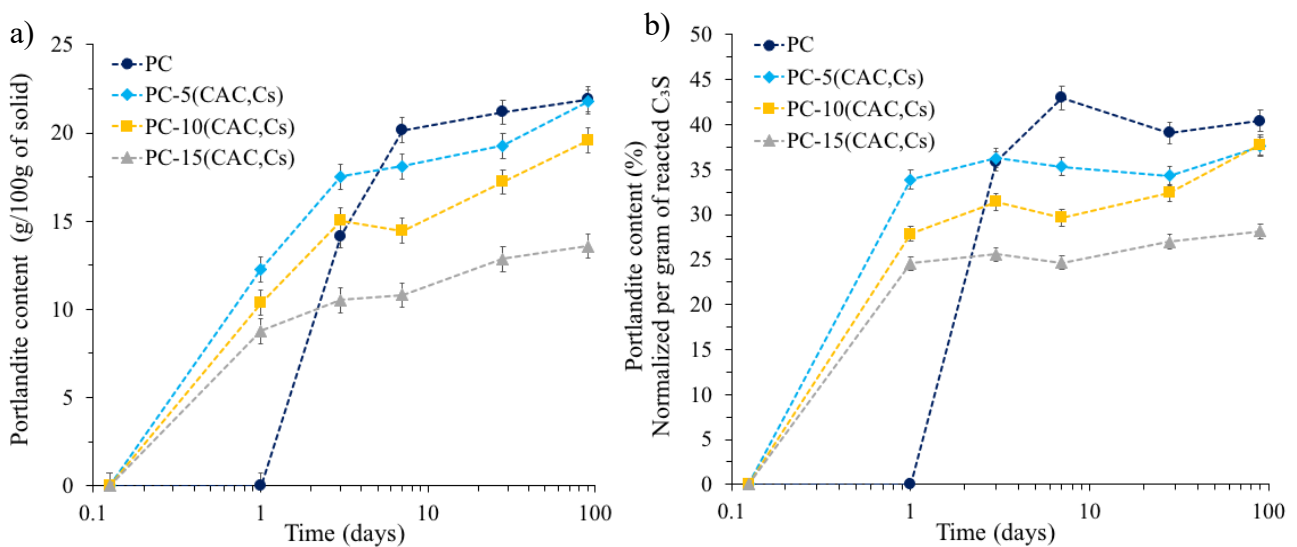
Fig. 2-5 Portlandite content per 100g of solid (a) and per amount of reacted C_3S (b) for PC reference and systems with 5, 10 and 15(CAC,Cs).

2.3.1.2 Impact of the CAC and Cs amount with calcined clay

The evolution of the ettringite content over time is plotted in Fig. 2-6(a). As for systems without calcined clay, the ettringite content increases with the CAC and Cs amount. The quantification of AFm phases is shown in Fig. 2-6(b) as the sum of Ms and Hc. It can be seen that AFm phases start to form from 1 day in presence of CAC and Cs. AFm phases are detected later (at 3 days) for the reference system (PC). This could be explained by the different Al/S ratio and also a delay caused by the citric acid. The AFm amount in systems containing CAC and Cs, in presence of calcined clay, starts to decrease after 3 days. This could be due to the strätlingite formation. By XRD, the two characteristic peaks of strätlingite (7° and 21°) were only detected from 28 days in systems that contain CAC, Cs and calcined clay.

a)   b)
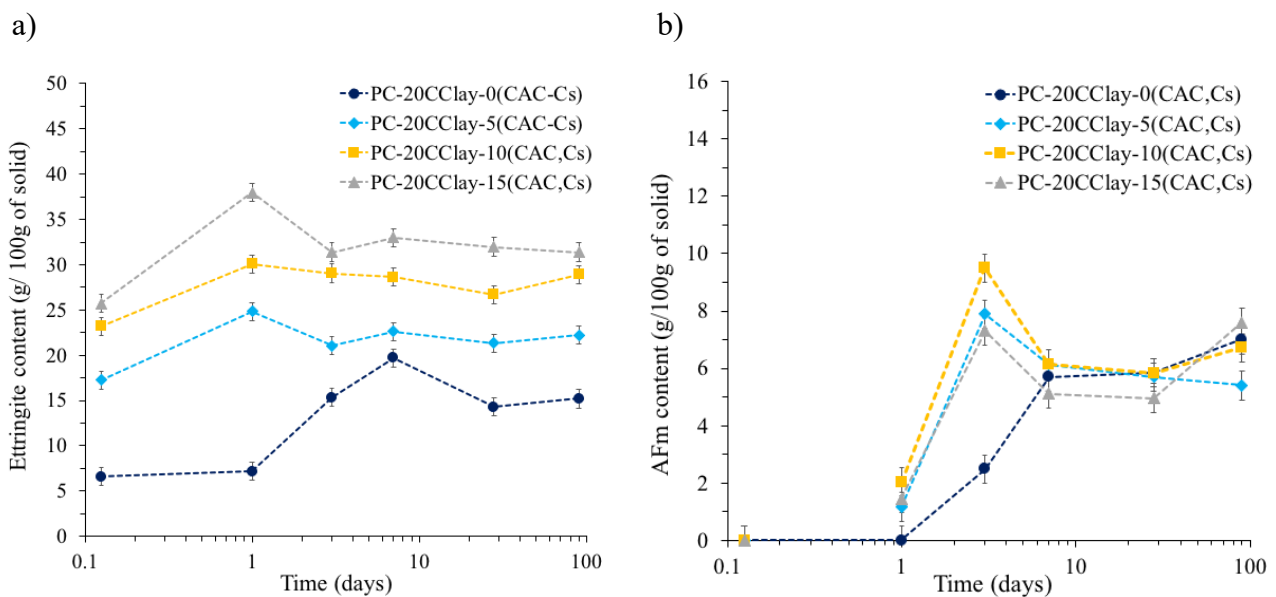
Fig. 2-6 Ettringite (a) and AFm (Ms+Hc) Rietved quantification for PC-20CClay reference system and PC-20CClay with 5, 10, 15(CAC,Cs).

The degree of hydration of alite for PC-20CClay and PC-20CClay- with 5 ,10 and 15 (CAC, Cs) is plotted in Fig. 2-7. The C_3S hydration is delayed in PC-20CClay and mainly occurs between 1 and 3 days. As it was previously explained, this is a citric acid delaying effect. For the system with both 20CClay and 15 (CAC, Cs), it can be seen that a lower degree of hydration is obtained at all ages. This shows that the combination of CAC, Cs and calcined clay slows down the hydration of alite.
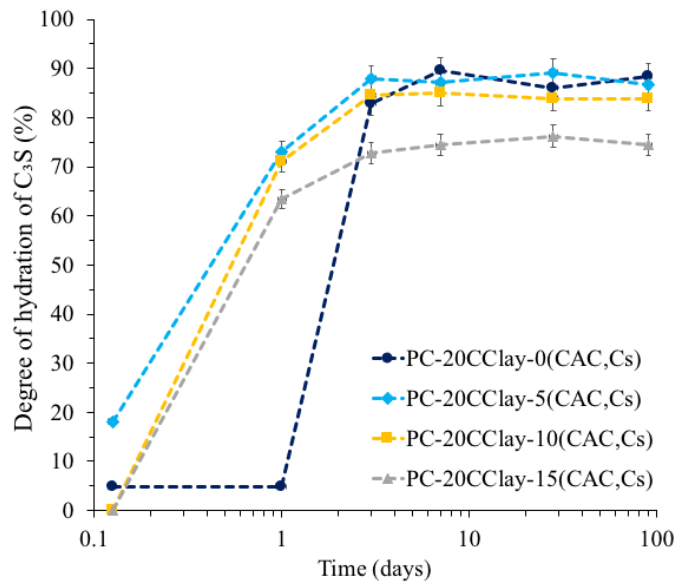
Fig. 2-7 Degree of hydration of alite (DoH$_{C3S}$) for the reference PC-20CClay and PC-20CClay with 5,10 and 15 (CAC,Cs).

Fig. 2-8(a) shows the evolution of the portlandite content normalized per 100g of solid. To remove the effect of differences in terms of cement content and degree of hydration of C_3S, the portlandite content was also normalized per the amount of reacted C_3S, as shown in Fig. 2-8(b). It is clear that higher CAC and Cs leads to a lower portlandite content. It can be also observed that the portlandite content decreases mainly between 1 and 28 days. This can be explained by the pozzolanic reaction of metakaolin.
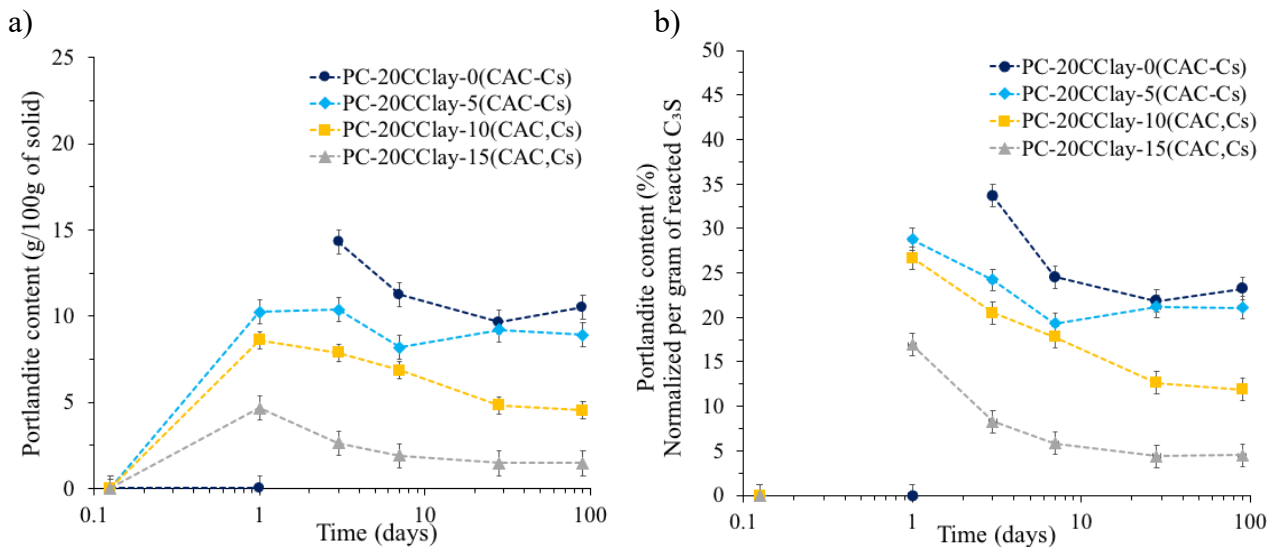
Fig. 2-8 Portlandite content per 100g of solid (a) and per amount of reacted C_3S (b) for the reference PC-20CClay and PC-20CClay with 5,10 and 15(CAC,Cs).

2.3.1.3 Assessment of metakaolin reactivity

To check whether the calcined clay contributes to form additional ettringite or not, the ettringite content of various systems was plotted in Fig. 2-9(a). It can be seen that similar ettringite amounts are obtained when Portland cement is substituted by calcined clay. Fig. 2-9(b) shows the portlandite content normalized per amount of reacted C_3S as a function of the amount of CAC and Cs at 7 and 28 days. It is clear that with and without calcined clay the amount of portlandite decreases by increasing the amount of CAC and Cs. In addition, a slight decrease in the portlandite content is observed in some systems between 7 and 28 days. This can be explained by the pozzolanic reaction of metakaolin. Independently of the CAC and Cs amount, the portlandite content is lower in presence of calcined clay, which shows the portlandite consumption by the reaction of the calcined clay.
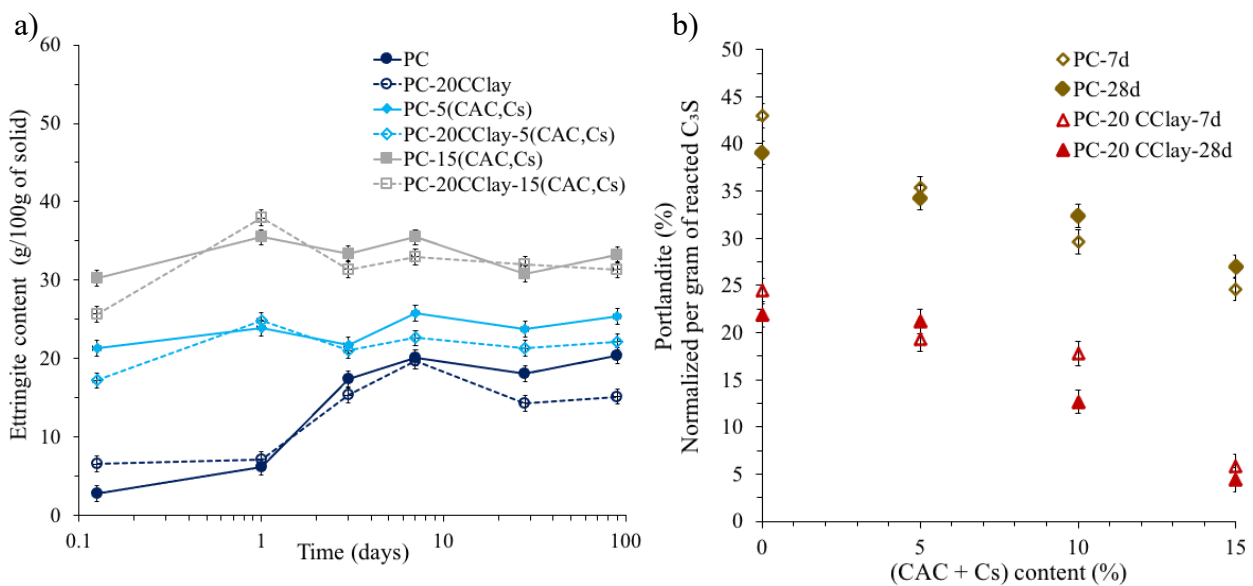
Fig. 2-9 Effect of calcined clay on the ettringite content (a) and on the portlandite content (b) as a function of the amount of CAC and Cs.

Fig. 2-10(a) shows the degree of reaction of metakaolin at 90 days estimated from the comparison of the amount of portlandite measured with the amount predicted by thermodynamic simulation by GEMS. Results show that a higher degree of reaction of metakaolin is obtained at 90 days of hydration with PC-20CClay-15(CAC,Cs) compared to PC-20CClay. However, the amount of reacted metakaolin is more or less the same, as shown in Fig. 2-10(b). This indicates that the combination of CAC and Cs together with calcined clay does not negatively affect the pozzolanic reaction of metakaolin. Since the overall amount of calcined clay reacted is quite small, it should be possible to use lower grade calcined clay.
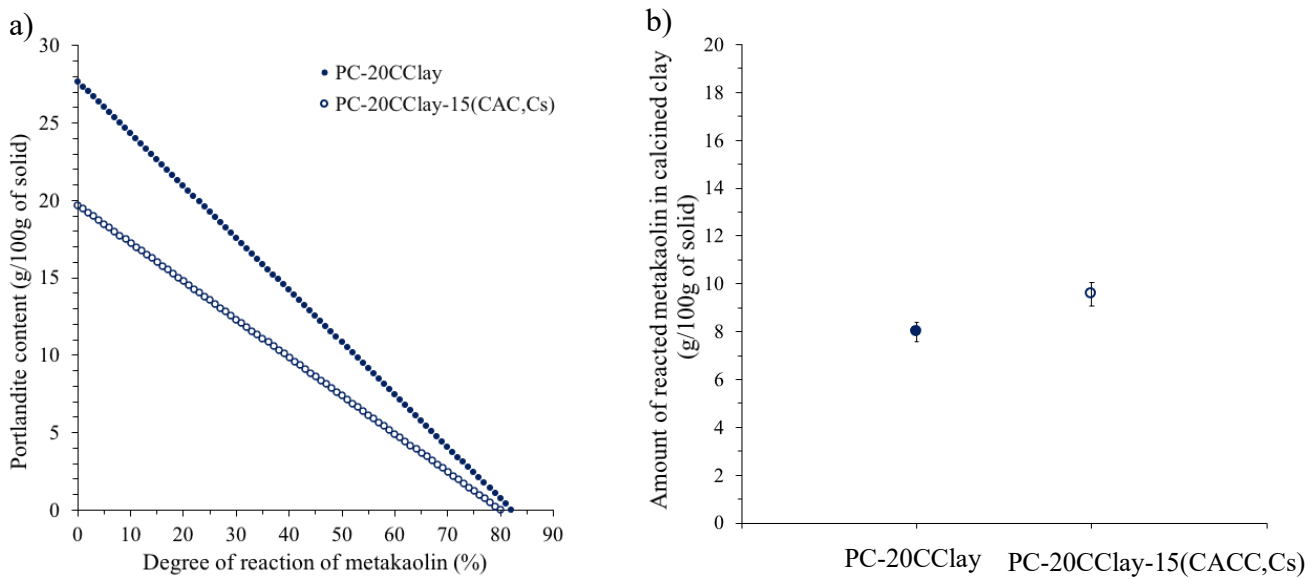
Fig. 2-10 Determination of the degree of reaction of metakaolin by thermodynamic modelling (a) and the amount of reacted metakaolin in calcined clay (b) for PC-20CClay and PC-20CClay-10(CAC,Cs) at 90 days.

2.3.1.4 Microstructure observation at 7 and 28 days

SEM pictures of the microstructure of PC, PC-20CClay, PC-15(CAC,Cs) and PC-20CClay-15(CAC,Cs) at 7 and 28 days are shown in Fig. 2-11. At 7 days, PC system with both 20 CClay and 15(CAC,Cs) has a less porous structure compared to the other systems. It is also more difficult to observe portlandite (light grey) compared to PC-20CClay. This is in agreement with the portlandite Rietveld quantification results, presented in Fig. 2-9 (b), where it was shown that PC blended with CAC, Cs and CClay has a much lower portlandite amount compared to the system with only 20% CClay. At 28 days, it can be seen that for all systems the porosity is reduced. A dense structure is observed for PC-20CClay-15(CAC,Cs) compared to PC with only 15(CAC,Cs).
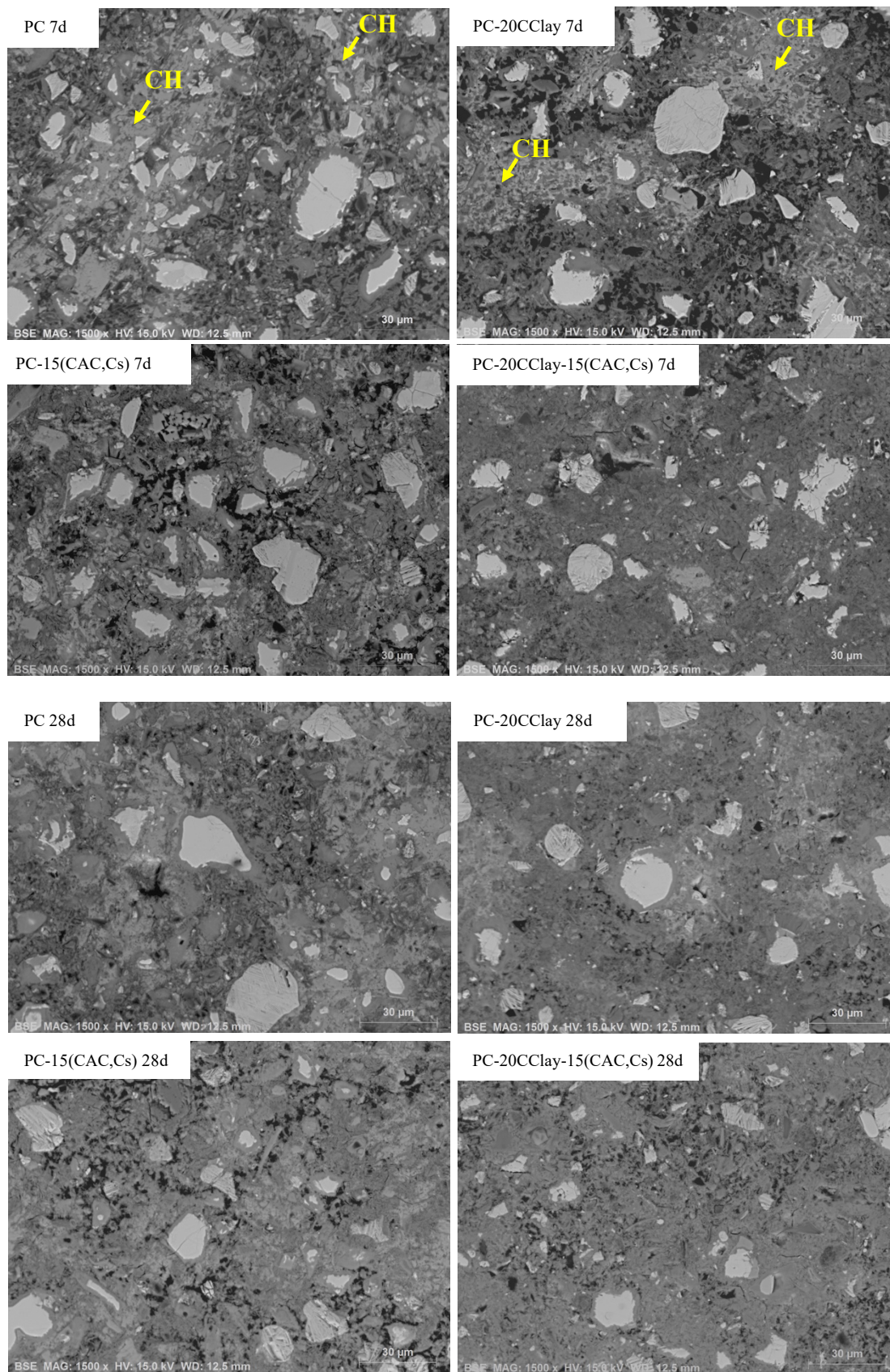
Fig. 2-11 SEM pictures of PC, PC-20 CClay, PC-15(CAC, Cs) and PC-20 CClay-15(CAC,Cs) at 7 and 28 days for 1500x magnification.

2.3.1.5 Porosity characterization at 28 days

The pore size distribution plots for PC, PC-20CClay, PC-15(CAC, Cs) and PC-20CClay-15(CAC, Cs) at 28 days are shown in Fig. 2-12. The PC reference has the smallest breakthrough pore entry radius (~40 nm), which corresponds to the point at which the mercury starts to intrude throughout the cement matrix. PC with calcined clay or PC with CAC, Cs gives bigger breakthrough radius and higher porosity compared to PC reference. The breakthrough radius of CAC, Cs together with calcined clay is smaller than either of the two alone and only slightly bigger than PC reference. PC-20CClay-15(CAC,Cs) has a similar relative low total porosity as PC. Although the C_3S hydration was limited when CAC, Cs and CClay are incorporated, smaller total porosity and lower breakthrough pore entry radius are reached compared to PC-20CClay.
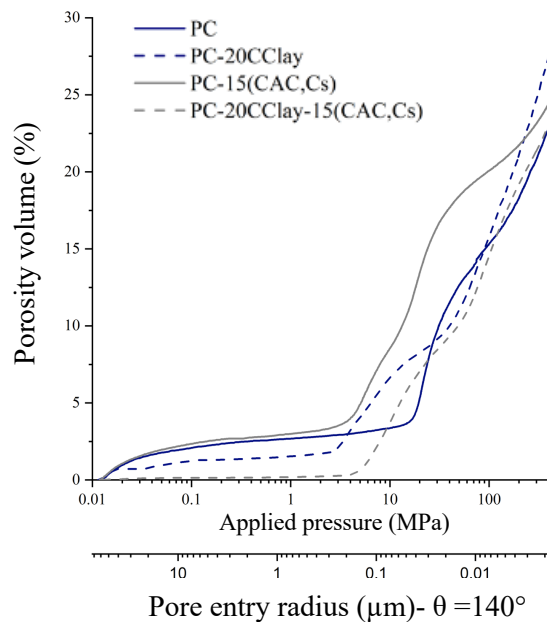
Fig. 2-12 Cumulative pore volume curves for PC, PC-20CClay, PC-15(CAC,Cs) and PC-20CClay-15(CAC,Cs) at 28 days.

2.3.2 Hydration and strength development of fixing mortar formulation with CClay

In order to identify reaction mechanisms taking place, isothermal calorimetry was carried out together with XRD in-situ. The heat of hydration and the phase assemblage quantification are shown in Fig. 2-13(a) and (b) for the reference system "0CClay". Results up to ~72 hours of hydration are shown. The calorimetry curves show five main peaks. During the first hour of hydration a high intensity peak is observed (#1). A part of this peak can be attributed to introducing the ampoule into the calorimeter. As the C_3S amount is lower after 0.33 hour compared to t= 0h, this peak is partially also due to the dissolution of C_3S. Afterwards, a second peak (#2) is observed, at this stage the amount of ettringite increases rapidly and anhydrite is dissolving. This confirms that the second reaction peak is the ettringite formation resulting from the hydration of amorphous CAC with sulfate from anhydrite. The C_3S and C_2S contents are not changing. After 3 hours of hydration, a third peak (#3) is observed. This peak is better seen in Fig. 2-13(b). It corresponds to an ettringite formation and also

a small amount of C_3S dissolution. After 6 hours of hydration, a fourth peak (#4) is observed, which is mainly attributed to the dissolution of C_3S. Portlandite starts to precipitate after 12 hours. The anhydrite amount becomes very low (<1%) after ~13 hours. The C_3S hydration is delayed in this ternary binder formulation compared to a typical heat flow curve of PC system. A hump (#5) is observed in calorimetry results. This might correspond to AFm formation after sulfate depletion, although no AFm phases were detected. This might be due to their poor crystallinity at this stage and also due to the presence of a hump (from the Kapton film) in the diffractogram close to their peak position.

The heat release during the first 72 hours of hydration together with XRD in-situ results are shown in Fig. 2-13(c) and (d) for the fixing mortar formulation incorporating 20% CClay "20CClay". Similar events to the reference system can be identified (peak #1, #2, #3, #4). The difference to the reference system is that when 20%CClay is added, the clinker from PC hydration looks more like an ordinary PC hydration. The fifth peak (#5) represents the sulfate depletion peak also known as the second ettringite formation peak. At the same time, portlandite starts to form. Its formation occurs 10 hours later compared to the reference system. It can be noticed, that its formation is occurring when the sulfate is depleted in presence of CClay while it starts before the sulfate depletion in the reference system. In addition to that, 50% less CH is formed when CClay is added to the system.
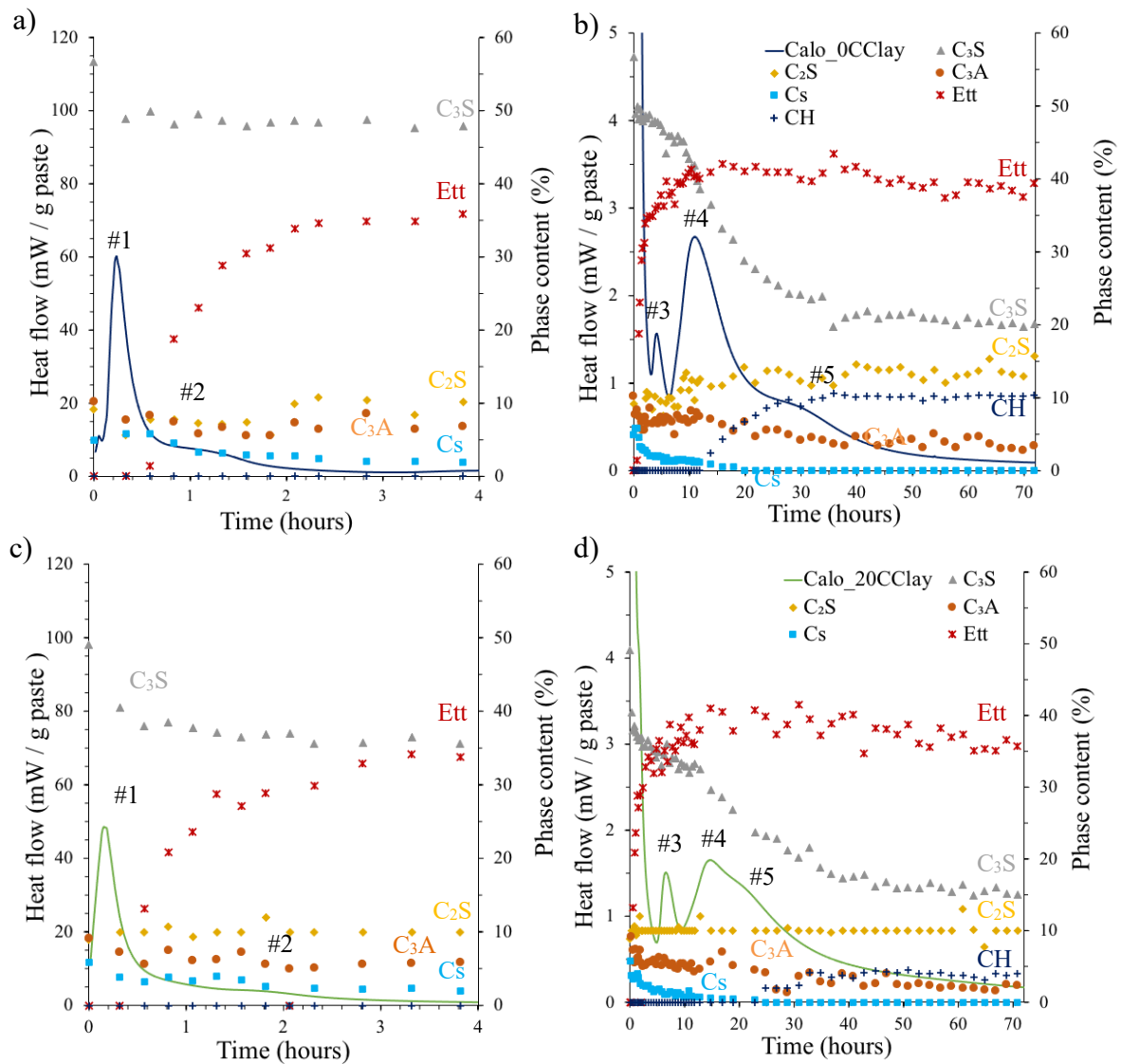
Fig. 2-13 Phase assemblage by in-situ XRD up to 4 hours (a,c) and up to 72 hours (b,d) for 0CClay and 20CClay.

Results of the heat released per gram of paste during the first days of hydration for systems containing 0, 5, 15 and 20CClay are plotted in Fig. 2-14(a) and (b). Only peak #1, #3, #4 and #5 will be discussed. The height of the first peak (#1) decreases as the CClay content increases. As a part of this peak represents the C_3S dissolution peak, decreasing the PC content and thus the C_3S content by substituting PC by calcined clay have an impact on this peak. Calorimetry results of Fig. 2-14(c) show similar peak height when the results are normalized per gram of PC. A third peak (#3) is observed for all the systems. This peak is delayed by increasing the calcined clay content. The onset of this peak is respectively reached after 3.1, 3.1, 3.2, 4.1 and 5 hours for 0, 5, 10, 15 and 20% of calcined clay. As this peak represents the ettringite formation and a small C_3S dissolution, calcined clay incorporation seems to have an impact on the C_3S hydration. This peak is followed by the main C_3S hydration peak (#4). It is also delayed as the calcined clay content increases. The height of this peak also decreases by increasing the substitution rate. Fig. 2-14(d) shows that the clinker hydration that is mainly the C_3S hydration (#4) is diminished at higher calcined clay content.
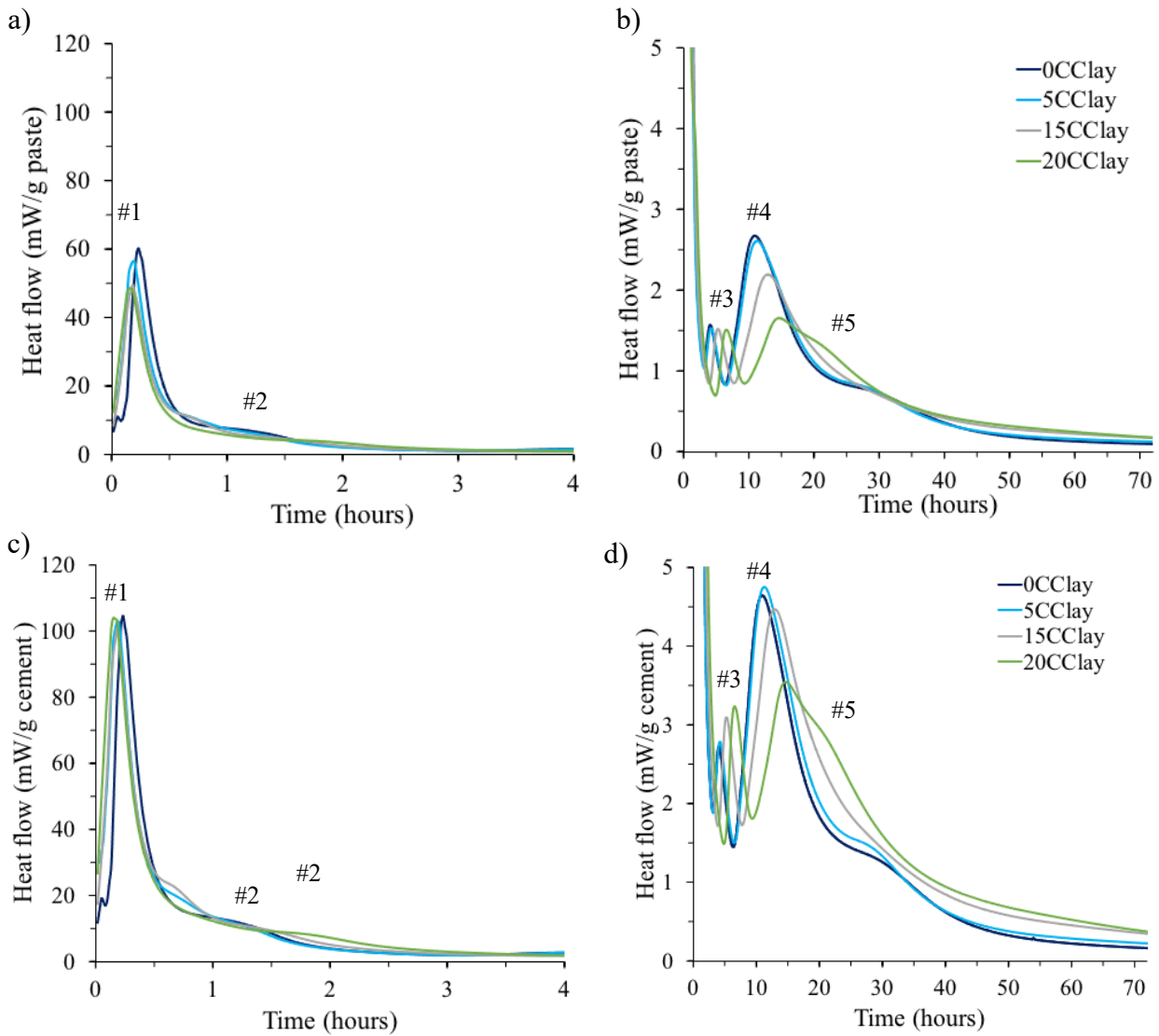
Fig. 2-14 Heat release per gram of paste (a,b) and per gram of cement (c,d) of fixing mortar formulations with 0, 5, 15 and 20CClay.

The evolution of the ettringite content over time is shown in Fig. 2-15(a). Increasing the calcined clay content did not increase the ettringite content. This indicates that the amount of ettringite formed is determined by the Cs addition. Furthermore, lower ettringite is observed at higher calcined clay content. The lower PC content (and thus C_3A content and Cs in PC) at higher calcined clay content could explain the lower ettringite obtained. The AFm phases quantification results are plotted in Fig. 2-15(b). Similar to the simple systems study, both Hc and Ms were detected in the investigated systems. Thus, the results will be presented as the sum of these two phases. The reference system (0 CClay) has lower Hc+Ms amounts compared to the other systems up to 28 days. The addition of CClay leads to an increase of the Hc+Ms content. As the addition of calcined kaolinitic clay provides additional Al_2O_3, the Hc+Ms amount is higher in CClay blends compared to 0CClay. However, results show at higher calcined clay content no further increase in the Hc+Ms content. It can be seen that for higher CClay content (20CClay), the Hc+Ms content is reduced from 3 days onwards, while silicate

containing AFm, C_2ASH_8, was detected in the 20 CClay at 28 days. This result can explain the decrease of the Hc+Ms content, more particularly of the Ms content.
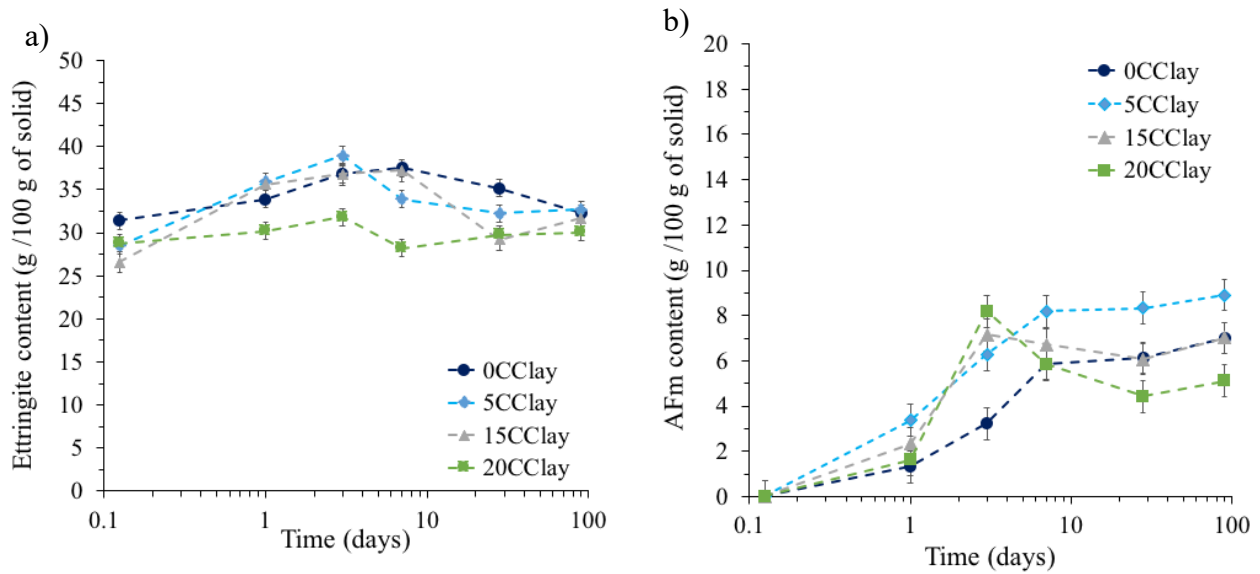
Fig. 2-15 Ettringite (a) and AFm (Hc+Ms) (b) Rietveld quantification for systems containing 0, 5, 15 and 20CClay.

Fig. 2-16(a) shows the evolution of the degree of hydration of alite (DoH$_{C3S}$) of systems with 0, 5, 15 and 20CClay. Lower DoH$_{C3S}$ are observed in the system containing 20 CClay up to 90 days, in comparison with the control system. This is in agreement with calorimetry results where a lower intensity C_3S hydration peak was observed with 20CClay. At 90 days, the hydration of C_3S is enhanced with 15CClay compared to 28 days but it is still lower than the control system. For 20CClay, the hydration of C_3S did not further improve. When the absolute amount of reacted C_3S is plotted in Fig. 2-16(b), it is clear that it decreases with decreasing the cement content.
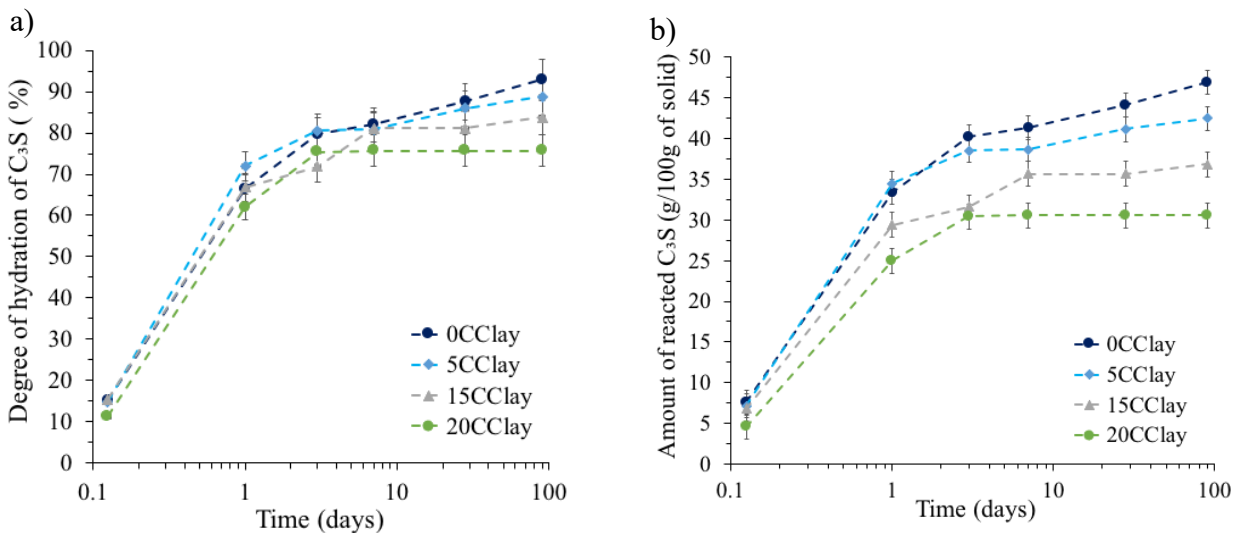
Fig. 2-16 Degree of hydration of alite (DoH$_{C3S}$) (a) and the amount of reacted C_3S (b) for systems with 0, 5, 15 and 20CClay.

Fig. 2-17(a) shows the evolution of the portlandite content normalized per gram of cement. Results demonstrate that a higher calcined clay content leads to a lower portlandite amount. This indicates the portlandite consumption by metakaolin. To consider both the different cement contents and the different degree of hydration of C_3S, the portlandite content was normalized per the relative amount of reacted C_3S as shown in Fig. 2-17(b). Systems with 15 and 20CClay, the portlandite content is lower compared to the reference.

a)

b)
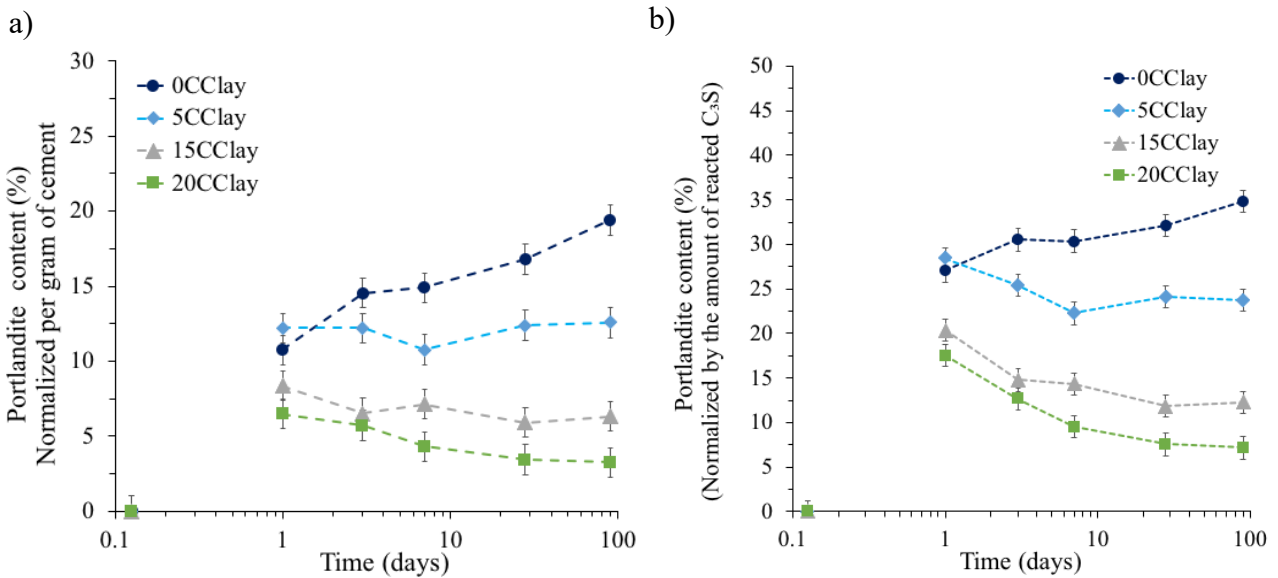
Fig. 2-17 Portlandite content per gram of PC (a) and per amount of reacted C_3S in a fixing mortar formulation containing 0, 5, 15 and 20CClay.

Fig. 2-18 shows the effect of the calcined clay content on the mortar compressive strengths. Increasing the calcined clay amount (except 5CClay) decreases the strength at 1 and 3 days. At early age (1 and 3 days), calcined clay incorporation did not show a positive impact yet and thus the loss in strength due to the lower PC content and the lower amount of reacted C_3S is not compensated neither by the filler effect nor by the pozzolanic reaction of calcined clay. From 7 days onwards, although a lower amount of C_3S has reacted, similar or even higher strengths compared to the control system are observed. This highlights the positive impact of incorporating CClay in fixing mortar formulation. At 90 days, although a lower amount of C_3S had reacted at high CClay contents, similar strengths are obtained for different CClay content. In fact, the portlandite consumption over time in systems containing CClay, as presented in Fig. 2-17(b), shows the pozzolanic reaction of calcined clay and explains the improvement of strength compared to the reference system. Results also show that higher substitution of PC by CClay is possible.
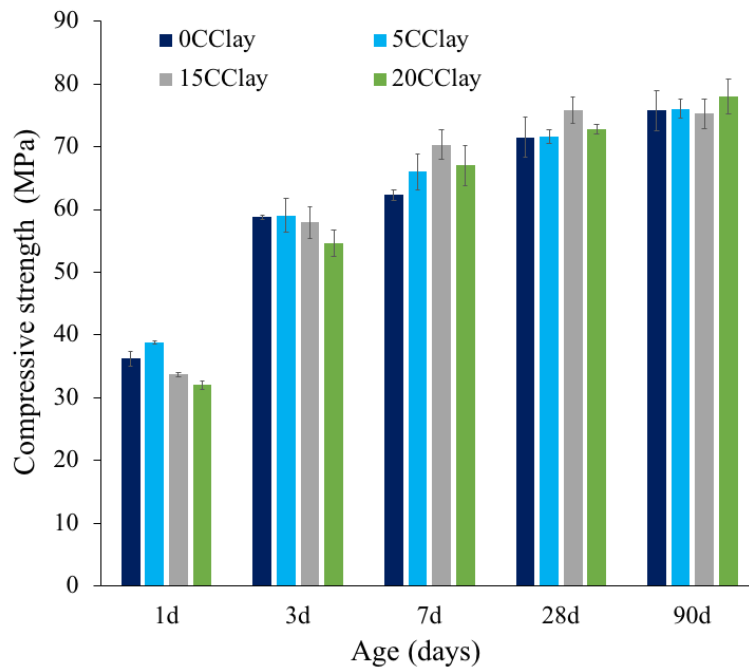
Fig. 2-18 Compressive strength development for fixing mortar formulation with 0, 5, 15 and 20CClay.

2.4   Conclusions

In this study, the effect of incorporating calcined in ternary binders composed of PC, CAC and Cs blends was investigated. In the first part, blends called "simple systems", were studied:

- PC with an increasing amount of (CAC+ Cs)

- PC-20CClay with and increasing amount of (CAC + Cs)

The main findings of the simple systems study are summarized below:

- The higher the CAC and Cs dosage the higher the ettringite but the lower the portlandite content. However, the decrease in the portlandite content seems to not have a negative impact on the pozzolanic reaction of metakaolin.

- The content of Hc+Ms decreases after 3 days of hydration when CAC, Cs and calcined clay are used which was not the case when only CAC and Cs are added to the PC system. The reason is the conversion of Ms to strätlingite.
- The CAC and Cs addition alone to PC does not delay the C_3S hydration. However, combining CAC, Cs and CClay leads to lower degree of hydration of C_3S, even at later age.

In the second part, the effect of substituting a part of Portland cement by calcined clay in a realistic mix design: a fixing mortar formulation was assessed. The effect on the hydration kinetics, phase assemblage and compressive strength was particularly investigated. Lower strengths were obtained

at early age due to the lower amount of reacted C_3S at higher calcined clay substitution. From 7 days onwards, similar or even higher strengths are obtained with higher CClay substitutions. This was explained by the pozzolanic reaction of metakaolin.

Chapter 3   Effect of calcium aluminate cement addition on the hydration and strength of Limestone calcined clay cement

Note: This chapter is based on an article in preparation for submission to a peer reviewed journal

Contribution of the doctoral candidate: conceptualization, methodology, experiments, analysis and writing of the first manuscript draft.

Abstract

The effect of incorporating calcium aluminate cement and calcium sulfate on the hydration and strength of LC^3 system was investigated. The influence of the C/A molar ratio and the amount of CAC were studied. Two types of amorphous CAC were studied: ACAC1.7 with a C/A = 1.7 and ACAC2.2 with a C/A = 2.2. An improvement of strength development compared to LC^3 was observed, which is explained by ettringite formation during the first hours of hydration.

ACAC1.7 showed slower strength development and reached PC performance only from 7 days onwards due to a delay of the C_3S hydration. At higher ACAC1.7 contents, the C_3S hydration was more delayed and led to lower strengths. When ACAC2.2 is used, particularly 10%(ACAC2.2,Cs), at least similar strengths to PC were obtained from 1 day onwards due to the combined massive ettringite formation and the C_3S hydration.

3.1   Introduction

The global rise in concern about the environment pushes industries to find solutions and approaches to cut their CO_2 emissions. The cement industry is involved as the clinker production accounts for about 7% of man-made CO_2 emissions [3] and those emissions are expected to rise with the growth of the world population and urbanisation. To obtain large scale CO_2 reductions, the incorporation of supplementary cementitious materials (SCMs) as a partial replacement for clinker seems to be the most successful strategy.

Limestone calcined clay cement (LC^3) is an alternative cement that allows reduction by up to 40% of the CO_2 emissions per ton of cement produced. With this green, binder it is possible to replace up to 50% or more of Portland cement (PC) by combining two widely available SCMs: limestone and

calcined clay. Kaolinitic clays are the most suitable clays to produce reactive calcined clays. These two materials are available in sufficient quantities for the scale of cement production and well distributed in the earth crust [7]. From durability point of view, this eco-efficient binder shows a better chloride resistance than PC and alkali-silica-reaction (ASR)[28,70,71].

At 40% calcined kaolinite content, LC^3 can reach equivalent mechanical strength performance to PC from only 7 days onwards [63]. LC^3 blends have lower strength before 7 days due to the low reactivity of calcined clay at early age [72].

Calcium aluminate cement (CAC) is also an alternative cement. This type of cement is preferred to conventional cement, for special requirements which cannot be attained with PC. Calcium aluminate cement is usually used in blends with calcium sulfate (CsH$_x$) and Portland cement. Ettringite (C$_3$A·3Cs·32H$_2$O) is the first hydration product that forms from the hydration of CAC with CsH$_x$. It is responsible for rapid strength development, fast setting and shrinkage compensation [73].

Early age strength enables fast demolding on the field. It is also a key parameter for specific applications such as precast concrete. Few studies have proposed solutions to boost the early age strength performance of LC^3. Antoni et al. investigated the impact of the sulfate content addition in blends containing Portland cement, limestone and calcined clay on the strength [23]. The sulfate level controls the degree of aluminate reaction. It was found that using a proper sulfate addition, significantly improves the early age strength of the blend. However, the strength at 1 day did not achieve Portland cement strength performance. Huang et al. investigated the influence of alkanolamines addition on the strength performance of LC^3 [25] and found that triethanolamine (TEA) promotes the strength of LC^3 at all ages. It particularly accelerates the aluminate reaction and reduces the porosity at early age. Huang et al. showed that triisopropanolamine (TIPA) has a positive impact on the strength only from 28 days as TIPA causes the formation of large capillary pores at early age. Another study showed that going to high TEA content can alter the strength by delaying the C$_3$S hydration [74]. Early age strength of blended cements can be improved by separate grinding of clinker grains and SCMs.

In this paper, calcium aluminate cement and anhydrite (Cs) were used as a partial replacement of the limestone in LC^3. Two calcium aluminate cements with different C/A molar ratios were studied. To understand the reaction mechanisms underlying the strength results, the hydration kinetics and phase assemblages were investigated. To reduce costs, the effect of replacing a fraction of the overall LC^3 by CAC and Cs on the strength was investigated. This will also allow to use CAC + Cs as mineral accelerator on site.

3.2   Materials and methods

3.2.1 Raw materials

The Portland cement (PC) was a commercial clinker, ground with gypsum and classified as CEM I 42.5R. Two amorphous calcium aluminate cements provided by Imerys Technology Center (ITC) Lyon were used. The CAC "ACAC1.7" is amorphous and has a C/A molar ratio of 1.7. The CAC

"ACAC2.2" is also amorphous and has a C/A molar ratio of 2.2. These calcium aluminate cements are trial products. The limestone used was Imercarb3 from Imerys. Commercial gypsum (Emprove ESSENTIAL) from Sigma Aldrich (CsH_2) was added to ensure a proper sulfation of the LC^3 blends. Natural anhydrite (Cs) was also added with the CAC at a CAC/Cs mass ratio equal to 1. Calcined clay (CClay1) was an Argical M-1000S from Imerys Refractory Minerals (IRM). The kaolinite content of the raw clay, as determined by Thermogravimetric Analysis (TGA) using the tangential method [67], is about ~ 71%. Citric acid (setting retarder, Citrique Belge, Fine granular 51N) and Na_2CO_3 (setting accelerator, Solvay) were used as admixtures to control the reactivity of the CAC. The particle size distribution (PSD) was estimated by laser diffraction with a Malvern MasterSizer S and are presented for all the materials in Fig. 3-1. The specific surface area was measured by nitrogen adsorption technique using the BET model with a Micromeritics Tristar II plus apparatus. The physicochemical properties of PC, ACAC1.7, ACAC2.2, Cs and CClay1 are presented in Table 3-1. The phase composition of the different cements, shown in Table 3-2, was computed by the X-ray diffraction-Rietveld quantification method [67]. For mortar samples, AFNOR sand was used.
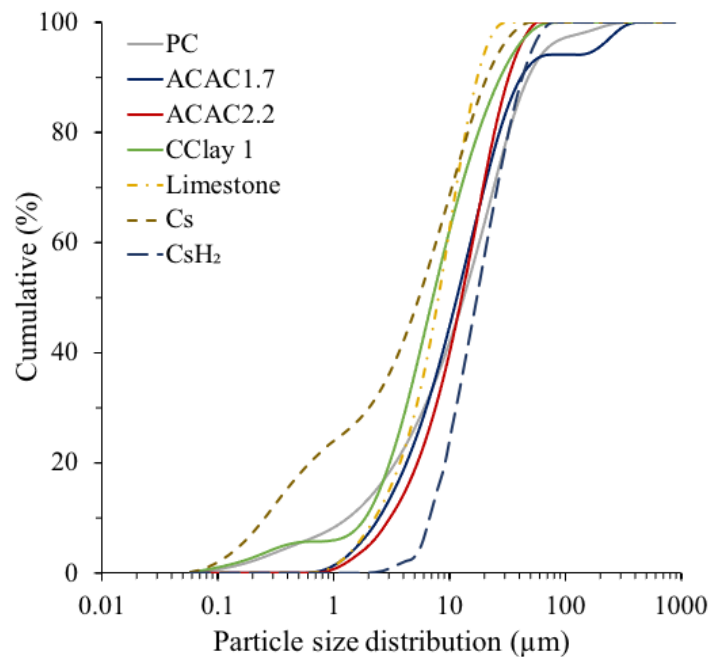
Fig. 3-1 PSD for all powders except admixtures.

Table 3-1 Physicochemical properties of PC, ACAC1.7, ACAC2.2, Anhydrite (Cs) and CClay1.

(wt.%)	PC	ACAC1.7	ACAC2.2	Cs	CClay1
Al_2O_3	4.56	45.71	40.12	-	31.74
SiO_2	20.08	4.75	4.55	0.18	62.91
CaO	63.59	43.68	49.36	42.00	0.07
Fe_2O_3	3.18	1.74	1.90	0.01	1.15
MgO	1.85	0.90	0.48	1.14	0.19
K_2O	0.95	0.26	0.23	-	0.42
Na_2O	0.16	0.07	0.06	-	0.00
P_2O_5	0.18	0.13	0.11	0.01	0.05
SO_3	3.27	0.10	0.04	56.62	-
TiO_2	0.35	2.21	1.78	-	1.50
Cr_2O_3	0.01	0.13	0.04	-	0.02
MnO	0.04	0.07	0.03	0.00	0.01
SrO	0.06	0.00	0.04	0.13	-
ZnO	0.00	0.00	0.00	0.02	0.00
CO_2	1.15	n.d	n.d	n.d	n.d
LOI*	1.65	0.10	0.12	-	2.3
SSA* (m^2/g)	1.41	0.50	0.70	0.97	17.24
$D_{v\,50}$ (µm)	13.67	11.75	12.7	5.20	7.31

*LOI Loss of ignition, SSA Specific surface area

Table 3-2 Cements phase composition from XRD-Rietveld analysis (wt. %).

Phase (wt.%)	PC	ACAC1.7	ACAC2.2
C_3S	70.4	-	-
C_2S	7.8	-	-
C_4AF	8.5	-	-
C_3A	6.3	-	-
Dolomite	0.9	-	-
CsH_2	2.4	-	-
Cs	0.3	-	-
Cc*	2.6	-	-
CA	-	7	-
C_2AS	-	0.15	-
CFT*	-	1	-
$C_{12}A_7$	-	0.45	7.3
Magnetite	-	-	-
Periclase	0.5	-	-
Amorphous	-	91.40	92.7

*Cc: $CaCO_3$, CFT: Perovskite

3.2.2 Mixture design and sample preparation

In this study, the systems investigated were PC, LC^3 and LC^3 with different CAC and Cs amounts. For LC^3-CAC mixes, the limestone was substituted with 5, 10 and 15% either by ACAC1.7 and Cs or by ACAC2.2 and Cs. The admixtures content was adjusted in LC^3 blends with 5%(CAC,Cs). The effect of substituting 10% of LC^3 with ACAC2.2 and Cs "90%LC^3-10%(ACAC2.2,Cs)" on the strength was also studied. The full mix compositions are detailed in Table 3-3.

Table 3-3 Mix compositions of the investigated systems (wt.%)

	PC	CAC	Cs	CClay	CsH_2	Cc	Citric acid	Na_2CO_3
PC	100	-	-	-	-	-	-	-
LC^3	52.66	-	-	25	2.34	20	-	-
LC^3-5%(ACAC1.7,Cs)	52.27	2.57	2.57	24.83	2.41	14.88	0.16	0.30
LC^3-10%(ACAC1.7,Cs)	52.15	5	5	24.76	2.34	9.81	0.33	0.61
LC^3-15%(ACAC1.7,Cs)	52.15	7.5	7.5	24.76	2.34	4.81	0.33	0.61
LC^3-5%(ACAC2.2,Cs)	52.27	2.57	2.57	24.83	2.41	14.88	0.16	0.30
LC^3-10%(ACAC2.2,Cs)	52.15	5	5	24.76	2.34	9.81	0.33	0.61
LC^3-15%(ACAC2.2,Cs)	52.15	7.5	7.5	24.76	2.34	4.81	0.33	0.61
90%LC^3-10%(ACAC2.2,Cs)	46.90	5	5	22.27	2.08	17.81	0.33	0.61

Cement paste samples were used to study hydration by isothermal calorimetry, X-Ray diffraction (XRD) and scanning election microscopy (SEM). Pastes were prepared with a water to binder ratio (w/b) of 0.4. A high-speed mixer was used to mix the cement paste for 2 minutes at 1600rpm. Samples were cast in a 50mL cylindrical polyethylene container (diameter: 35mm), which was sealed with parafilm and a lid. Samples were stored up to 90 days of hydration in a controlled temperature room (20°C). At a specific testing ages, two slices of 2-3mm thickness were cut from the hardened cement paste using a diamond saw and water as lubricant.

Mortar samples were prepared according to the European EN196-1 standard. The water /binder (w/b) ratio was 0.5 (which is roughly the same as 0.4 in paste due to extra water in the interfacial transition zone around aggregates). Mixing was conducted at room temperature. Mortars were cast in a steel moulds, then, demolded after 1 day. Prisms were cut to 4x4x4cm cubes and were kept in plastic bags in a humidity chamber ($\sim$ 95%) until the required testing age.

3.2.3 Methods

Compressive strength tests were performed according to EN196-1. Strengths were measured at 1, 3, 7, 28 and 90 days with a loading rate of 2.4kN/s. Three cubes were tested for each age.

Exothermic reactions taking place during cement hydration were followed by an isothermal calorimeter (TAM air) for $\sim$ 6-7 days of hydration. Directly after mixing, around 10g of fresh paste was introduced into a glass ampoule. After sealing the ampoule, it was placed in the calorimeter.

To identify observed peaks and quantify crystalline phases present during the first 70-72 hours of hydration, X-Ray diffraction (XRD) in-situ was done. After mixing, paste samples were put in a sample holder. To avoid water evaporation, a Kapton film of 12.7μm thickness was used to cover the sample holder and was secured with a ring. The temperature was fixed at 20°C and was controlled with a cooling system. The Bragg-Brentano mode with a X'Pert PANalytical diffractometer using a $CuK_{\alpha1\alpha2}$ source was used to analyze samples. The X-ray source was at 45kV and 40mA. Scans were recorded from 5 to 70° 2θ with a 1° divergence slit in 15 minutes with a step size of 0.017°2θ. A diffractogram was recorded every 1.25 hours during the first 10 hours of hydration, then every 2.5 hours up to ~ 70-72 hours of hydration. The quantification of consumed and formed crystalline phases during the hydration was conducted by XRD-Rietveld refinement method using the High Score Plus Software. To determine the total amount of amorphous phase, rutile was used as an external standard.

To identify and quantify more accurately the phase assemblage up to 90 days of hydration, X-Ray diffraction (XRD) was carried-out on the dry mix powder and fresh slices at 1,3, 7, 28 and 90 days. Similar parameters to XRD in-situ were used, except the divergence slit that was 1/2° in this case. According to Eq.1, the degree of hydration of C_3S was calculated at a time, t, from the mass fraction of remained C_3S relative to the initial C_3S amount.

$$Hydration\ degree\ of\ C_3S\ (t) = \frac{C_3S\ (t) - C_3S\ (t_0)}{C_3S(t_0)} \qquad (1)$$

XRD-Rietveld data on fresh paste at time, t, are per 100g of paste. For cement powder carried-out at t_0, results are measured per 100g of solid. To calculate the degree of hydration and compare between t_0 and t, results on paste need to be rescaled according to Eq.2. The quantification is normalized per 100g of solid according to the water to binder ratio (w/b) used:

$$Wt_{i,rescaled} = (Wt_{i,Rietveld} \cdot \left(1 + \frac{w}{b}\right)) \qquad (2)$$

Wt is the weight percent of a phase at a t time

Scanning electron microscope-energy dispersive X-Ray (SEM-EDX) was used to determine the C-A-S-H chemical composition at 28 days according to Rossen et al. [68] . Analysis were carried-out using a FEI Quanta 200 equipped with Bruker XFlash 4030 EDS detector. An accelerating voltage of 15kV on polished sections was used. The working distance was 12.5mm. Due to intermixing of C-A-S-H with other phases and for better accuracy, analysis was done on 150 points per sample. Before doing the analysis, samples were prepared as follows: the hydration was stopped at 28 days by the isopropanol solvent exchange method [67]. After 28 days of hydration, fresh slices were immersed in 200mL isopropanol for 7 days. Isopropanol was changed after 1 hour, 1 day, 3 and 5 days. After that slices were stored in a dessicator to dry for at least 2 days. A small piece of sample was impregnated under vacuum with a low viscosity resin. Samples were first manually pre-polished with a sand paper (SiC Paper #1200) to uncover the surface using isopropanol as lubricant. After that, samples were polished using an automatic polishing machine (Struers RotoForce-1 connected to Struers RotoPol-25). Samples were polished using polishing disc (MD Largo Struers) and diamond suspensions (DP-Spray M) of 9, 3, 1μm. Deodorized petroleum was used as lubricant. Samples were

stored under vacuum in a desiccator for 2 days to remove isopropanol and finally coated with carbon to achieve a conductive surface.

The degree of reaction of metakaolin was estimated by calculating the expected amount of portlandite by geochemical modelling with the Gibbs energy minimization software (GEMS) [54] and the Cemdata18 database [55] using the CSHQ model to represent C-S-H. The degree of hydration of anhydrous cement phases, limestone and gypsum from XRD-Rietveld at 28 days and the C-A-S-H composition were used as inputs. As it is amorphous, the amount of unreacted CAC could not be not quantified directly and was assumed to completely react in the simulations. Based on these inputs GEMS predicts the phase assemblage as a function of the degree of reaction of metakaolin. By comparing for each computed DoR_{MK} the predicted portlandite content with the experimental one given by XRD-Rietveld quantification method, it is possible to estimate the degree of reaction of metakaolin.

3.3   Results and discussion

3.3.1 Effect of the ACAC1.7 and Cs contents on the hydration and strength of LC^3

3.3.1.1 Strength development

The strength development of the reference PC, LC^3 and LC^3 blended with different ACAC1.7 and Cs contents are shown in Fig. 3-2. LC^3 starts to have strength close to PC from 7 days onwards, while lower strengths are obtained with LC^3 compared to PC at 1 and 3 days. The incorporation of ACAC1.7 together with Cs significantly improves the strength of LC^3 at 1 day. LC^3 with 5%(ACAC1.7,Cs) has a lower early age strength than PC at 1 and 3 days. LC^3 blended with 10%(ACAC1.7,Cs) gives almost similar strength to PC at 1 day and higher strength from 7 days onwards. The increase of the ACAC1.7 and Cs amount to 15% did not further improve the strength and lower strengths compared to the system with 10% were obtained at 3 and 7 days. At 28 and 90 days, systems with 10 and 15% show much higher strength compared to the reference PC; the maximum strength values are observed for 10%(ACAC1.7,Cs). The system with 5% was not further studied as it did not show a sufficient improvement of the strength at 1 day.
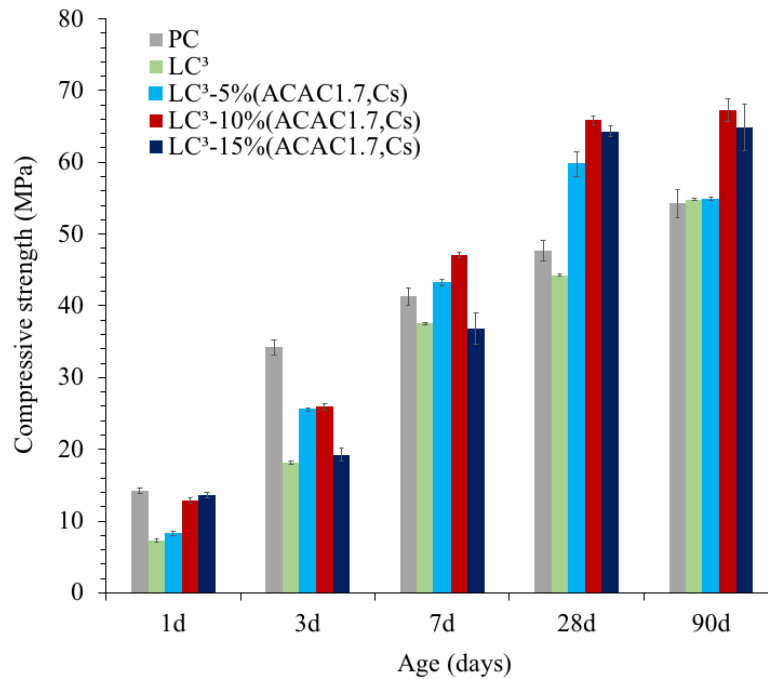
Fig. 3-2 Compressive strength development for PC, LC³, LC³ with different ACAC1.7 and Cs contents.

3.3.1.2 Kinetics of hydration

The heat release during the first 4 hours of hydration is shown in Fig. 3-3(a) and up to 150 hours of hydration in Fig. 3-3(b) for PC, LC³ and LC³-10%(ACAC1.7,Cs) and -15%(ACAC1.7,Cs). Fig. 3-3(a) shows a first peak (#) that is mainly due to the introduction of the ampoule into the calorimeter. This peak is followed by two peaks during the first hour in the case of the LC³-CAC blends. These two peaks correspond most probably to the early ettringite formation resulting from the fast reaction of ACAC1.7 and Cs. They are absent for the reference PC and LC³. Fig. 3-3(b) clearly shows the C_3S hydration main peak and the sulfate depletion peak for PC and LC³. The maximum of the C_3S hydration peak is reached after 11 hours of hydration for PC and after 8 hours for LC³. SCMs are known to accelerate the cement hydration due to their filler effect [75]. It can be seen that in the case of LC³ lower intensity peaks are observed, due to the lower clinker content in the LC³ system. The incorporation of -10%(ACAC1.7,Cs) leads to a two well separated peaks, which are more delayed and less intense at a ACAC1.7 and Cs content of 15%. These two events correspond most likely to PC hydration peaks, which are known to take place after the reaction of CAC and Cs, indicating a strong effect of CAC and Cs on the kinetics of PC reaction.
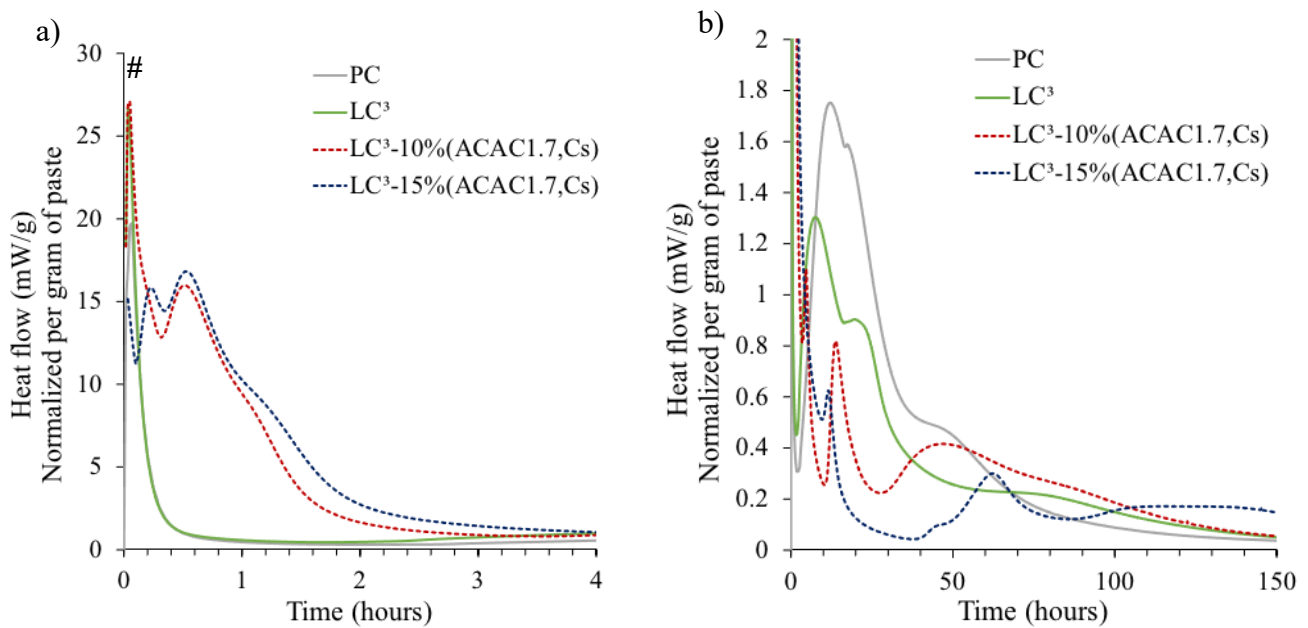
Fig. 3-3 Heat release per gram of paste during the first 4 hours (a) and up to 150 hours (b) for PC, LC^3, LC^3-10%(ACAC1.7,Cs) and -15%(ACAC1.7,Cs).

3.3.1.3 In-situ XRD

Fig. 3-4 shows the phase assemblage for LC^3-10%(ACAC1.7,Cs) up to 10 hours (a) and up to 70 hours of hydration (b). Fig. 3-4(a) shows that the 2nd peak (#2) following the introduction peak (#1) mainly represent the ettringite formation. The C_3S might be slightly dissolving. The amount of gypsum decreases and becomes very low after 2.5 hours of hydration. It can be seen that anhydrite is dissolving slower than the gypsum. Its content is below 1% after 5 hours of hydration. Fig. 3-4(b) shows that during the peaks (#3) and (#4), C_3S dissolves slowly. It can be also noted that portlandite did not start forming yet. The C_3A and the C_2S content as well as the limestone content are not changing.
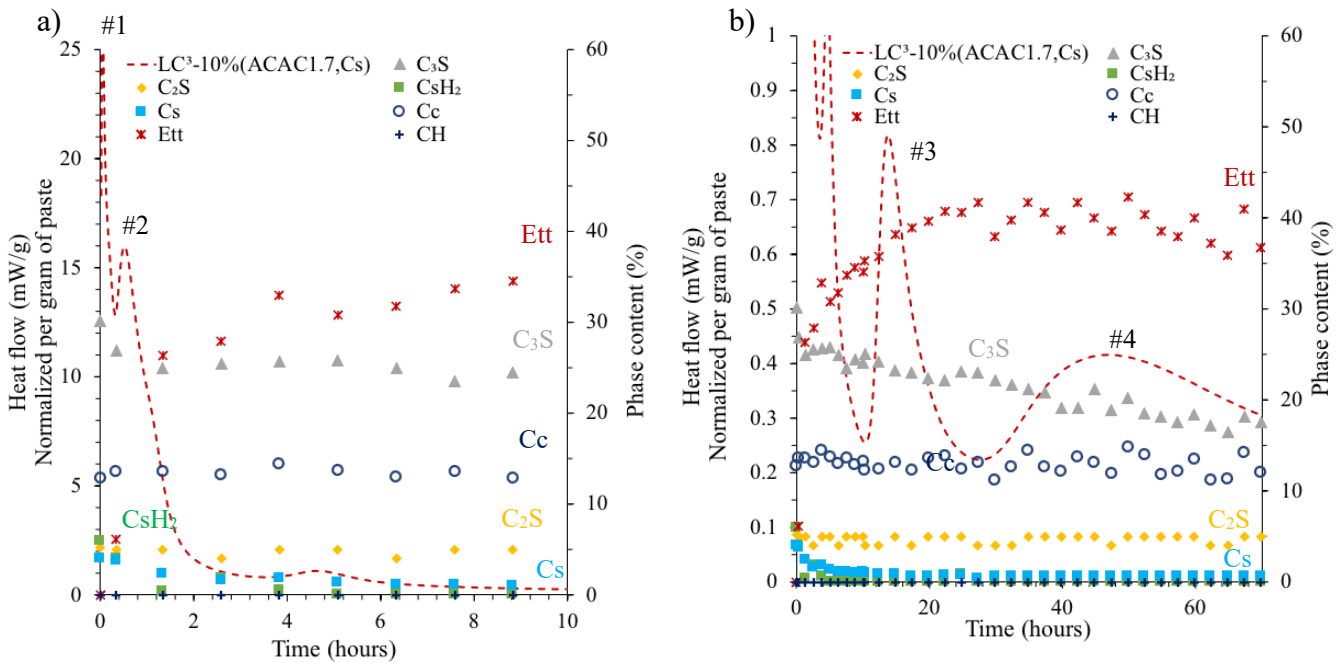
Fig. 3-4 Phase assemblage by in-situ XRD up to 10 hours (a) and up to 70 hours (b) for LC^3-10%(ACAC1.7,Cs).

3.3.1.4 Ettringite content

The evolution of the ettringite content for PC, LC^3, LC^3-10%(ACAC1.7,Cs) and -15%(ACAC1.7,Cs) over time is shown in Fig. 3-5. The ettringite content is higher for LC^3 blended with ACAC1.7 and Cs compared to PC and LC^3, because of the high aluminate reactive phase content in LC^3-ACAC1.7. For all ages, a higher amount of ACAC1.7 and Cs results in a higher ettringite content. The ettringite content of the reference PC decreases with time as monosulfate is formed at later reaction times as the PC has a relative low limestone content of 2.6 wt% (Table 3-2).
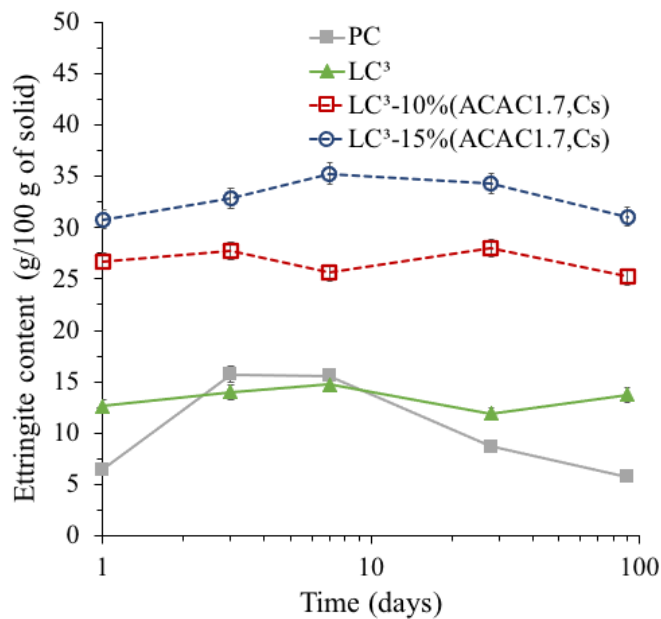
Fig. 3-5 Ettringite Rietveld quantification for PC, LC^3 and LC^3 with 10%(ACAC1.7,Cs) and 15%(ACAC1.7,Cs).

3.3.1.5 Degree of hydration of alite and the portlandite content

The degree of hydration of alite (C_3S) for PC, LC^3 and LC^3 with 10% and 15% ACAC1.7 and Cs is shown in Fig. 3-6(a). A higher degree of C_3S hydration is reached with LC^3 compared to PC, which can be explained by the filler effect. In the presence of ACAC1.7 and Cs, the hydration of C_3S becomes slower and with increasing amounts of ACAC1.7 and Cs also the reaction degrees are much lower at later ages. This explains the lower strength performance obtained when the ACAC1.7 and Cs content was increased. Fig. 3-6(b) shows the portlandite quantification by XRD-Rietveld over time. For PC, the portlandite content increases over time. For LC^3, the portlandite content is lower due to the lower clinker content and starts to decrease from 3 days onwards, showing that the pozzolanic reaction of metakaolin has started. For LC^3 systems blended with 10%(ACAC1.7,Cs), it can be seen that less portlandite is formed. For the blend with 15%(ACA1.7,Cs), no portlandite is detected. At early age, this can be explained by the low degree of hydration of C_3S. At later age although the C_3S hydration increases, no portlandite is detected indicating its consumption most likely by metakaolin.
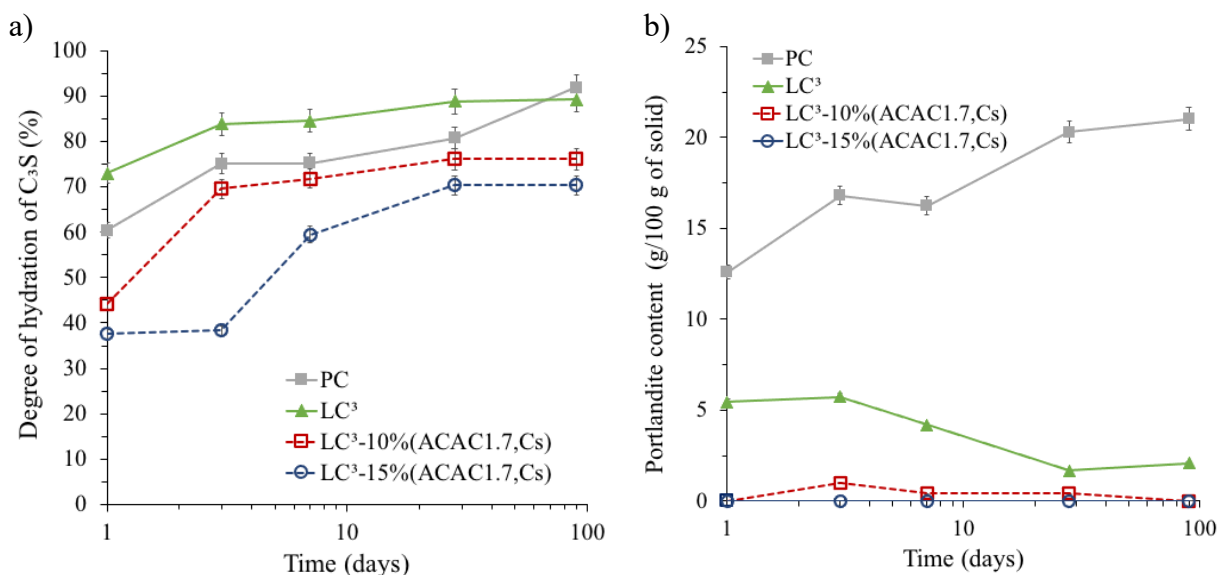
Fig. 3-6 Degree of hydration of alite (DoH$_{C3S}$) (a) and the portlandite content (b) for PC, LC^3 and LC^3 with 10%(ACAC1.7,Cs) and 15%(ACAC1.7,Cs).

3.3.1.6 AFm-type phases content

The AFm quantification results (the sum of hemicarbonate: Hc, monocarbonate: Mc and monosulfate: Ms) by XRD-Rietveld are plotted in Fig. 3-7. PC has the lowest AFm amount due to the lower amount of aluminate phases present in the system to react and also the small quantity of limestone present in the clinker resulting in less monocarbonate. AFm formation is delayed for LC^3 blended with 15%(ACAC1.7,Cs). This can be due to the delay of the C_3S hydration, which in turn causes a delay in the AFm formation.
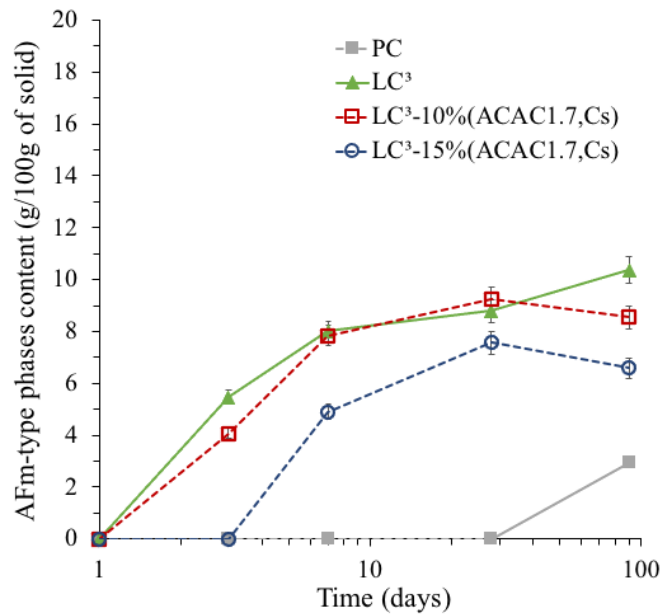
Fig. 3-7 AFm-type phases (Hc+Mc+Ms) Rietveld quantification for PC, LC^3 and LC^3 with 10%(ACAC1.7,Cs) and 15%(ACAC1.7,Cs).

3.3.2 Effect of the ACAC2.2 and Cs contents on the hydration and strength of LC^3

3.3.2.1 Strength development

Fig. 3-8 shows the strength development for PC, LC^3 and LC^3 blended with different amounts of ACAC2.2 and Cs. Using 5%(ACAC2.2,Cs) did not improve the strength at 1 day. At all ages, LC^3 blend with 10%(ACAC2.2,Cs) shows at least equivalent strength as PC; a higher ACAC2.2 and Cs amount results in higher strength. Contrary to ACAC1.7 blends, no decrease is observed at 15% of ACAC2.2 and Cs but a higher strength at all ages. The system with 5% was not further studied as it did not show equivalent strength to PC at 1 day.
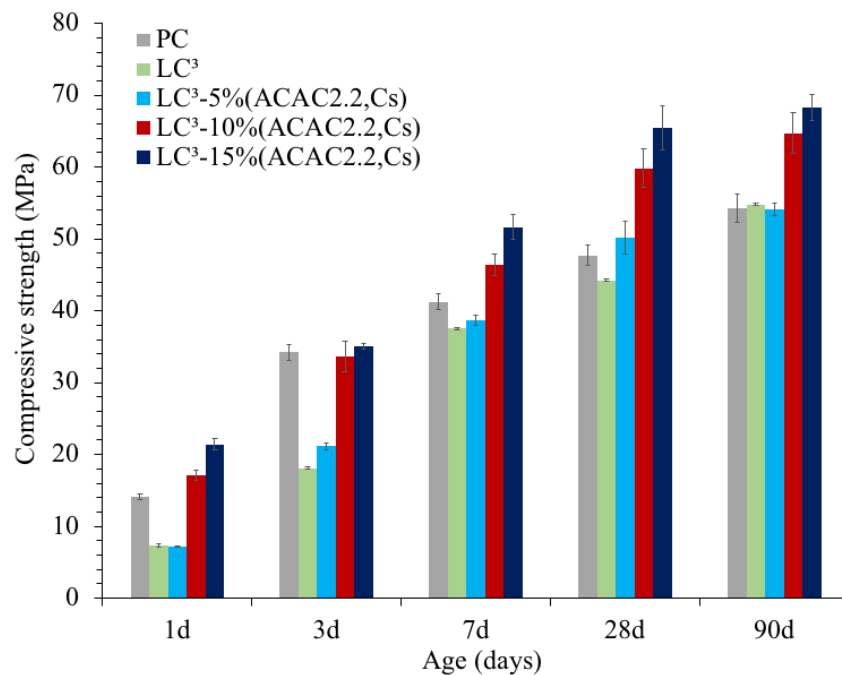
Fig. 3-8 Compressive strength development for PC, LC^3, LC^3 with different ACAC2.2 and Cs contents.

3.3.2.2 Kinetics of hydration

The heat released during the hydration of PC, LC^3 and LC^3 with 10% and 15% ACAC2.2 and Cs contents is shown up to 4 hours in Fig. 3-9(a) and up to 150 hours of hydration in Fig. 3-9(b). The peak following the introduction peak has a very high intensity, even higher than those observed for the ACAC1.7 blends. Fig. 3-9(b) shows that the main peaks observed for 10% and 15%(ACAC2.2,Cs) occur at a similar time and look similar to typical Portland cement hydration peaks.
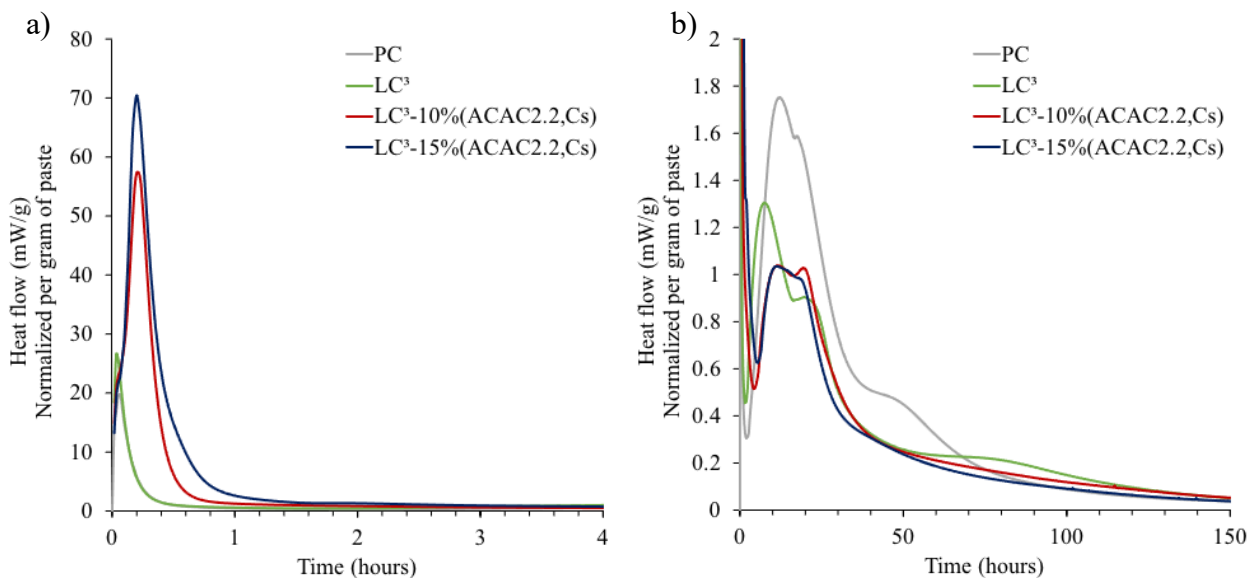
Fig. 3-9 Heat release per gram of paste during the first 4 hours (a) and up to 150 hours (b) for PC, LC^3 and LC^3 with -10%(ACAC2.2,Cs) and -15%(ACAC2.2,Cs).

3.3.2.3 In-situ XRD

The evolution of the phase assemblage during the first 72 hours of hydration for LC^3-10%(ACAC2.2,Cs) was quantified by in-situ XRD. Results up to 10 hours are presented in Fig. 3-10(a) and up to 72 hours in Fig. 3-10(b). Fig. 3-10(a) shows clear that the peak following the introduction peak (#1) mainly represents the ettringite formation (#2). Similarly to the LC^3 blended with 10%(ACAC1.7,Cs), CsH_2 is consumed faster than Cs. Fig. 3-10(b) shows a clear C_3S dissolution (#3) followed by anhydrite depletion after around 30 hours of hydration (#4). Contrary to ACAC1.7, portlandite starts forming after about 22 hours of hydration.
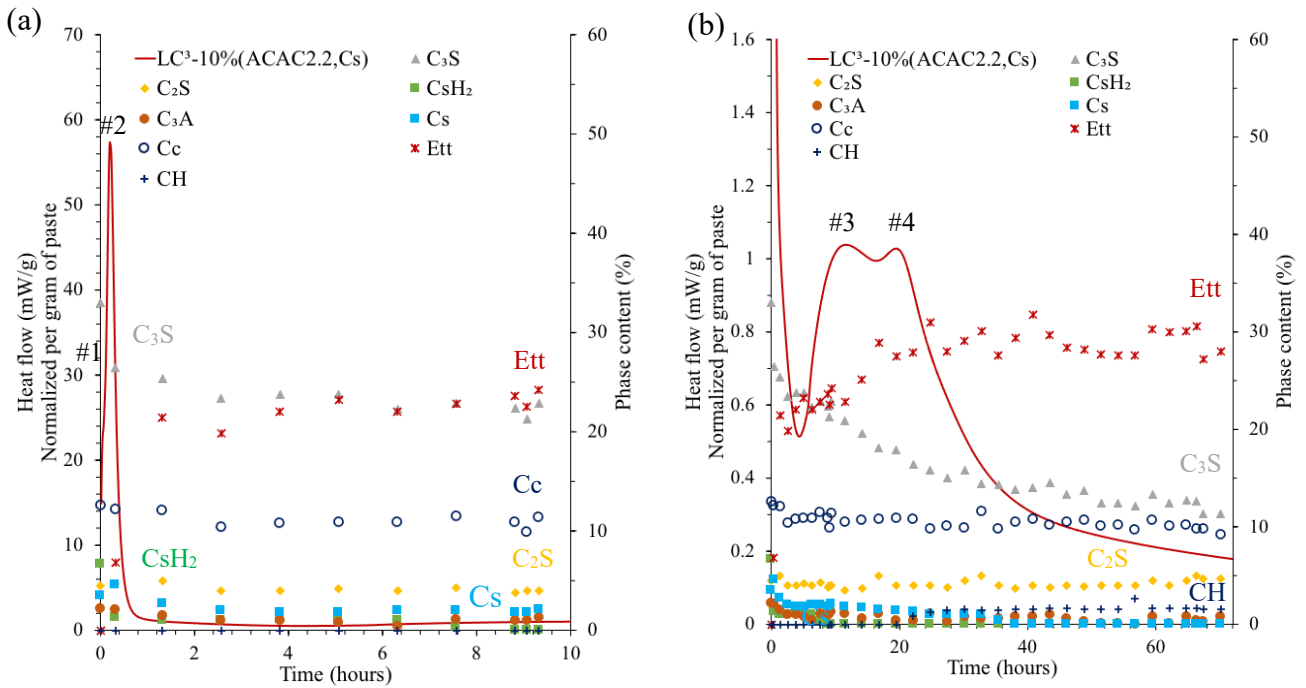
Fig. 3-10 Phase assemblage by in-situ XRD up to 10 hours (a) and up to 72 hours (b) for LC^3-10%(ACAC2.2,Cs).

3.3.2.4 Ettringite content

Fig. 3-11 shows the ettringite content determined by XRD-Rietveld analysis. At all ages, at higher ACAC2.2 and Cs content more ettringite is formed. The ettringite content is stable at later ages for LC^3 and LC^3 with different ACAC2.2 and Cs amounts. By comparing with 10%(ACAC1.7,Cs), it can be noted that the C/A ratio of the CAC does not have an impact on the ettringite content.
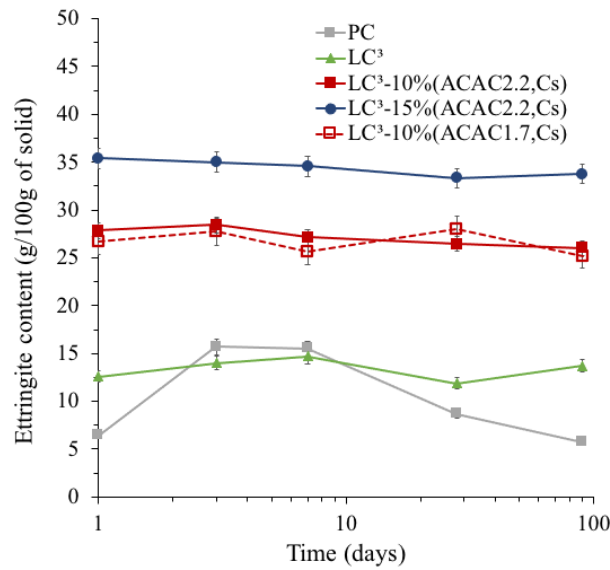
Fig. 3-11 Ettringite quantification by XRD-Rietveld for PC, LC³, LC³ blended with -10, -15%(ACAC2.2,Cs) and LC³-10%(ACAC1.7,Cs).

3.3.2.5 Degree of hydration of alite and the portlandite content

The degree of hydration of alite (C_3S) for PC, LC³ and LC³ with -10% and -15% (ACAC2.2, Cs) are plotted in Fig. 3-12(a). Interestingly, the delaying effect of ACAC1.7 on the C_3S hydration was not observed in the case of ACAC2.2. Increasing the amount of ACAC2.2 and Cs content up to 15%, did not significantly delay the C_3S hydration. However, the final alite reaction degree was lower at higher ACAC2.2 and Cs contents. The impact of increasing the ACAC2.2 content on the portlandite content was also investigated and plotted in Fig. 3-12(b). Contrary to the case of ACAC1.7, it is clear that the ACAC2.2 and Cs amount has no effect on the portlandite amount. The portlandite amount starts to slowly decrease from 3 days onwards. This can be explained by the pozzolanic reaction of metakaolin that consumes portlandite.
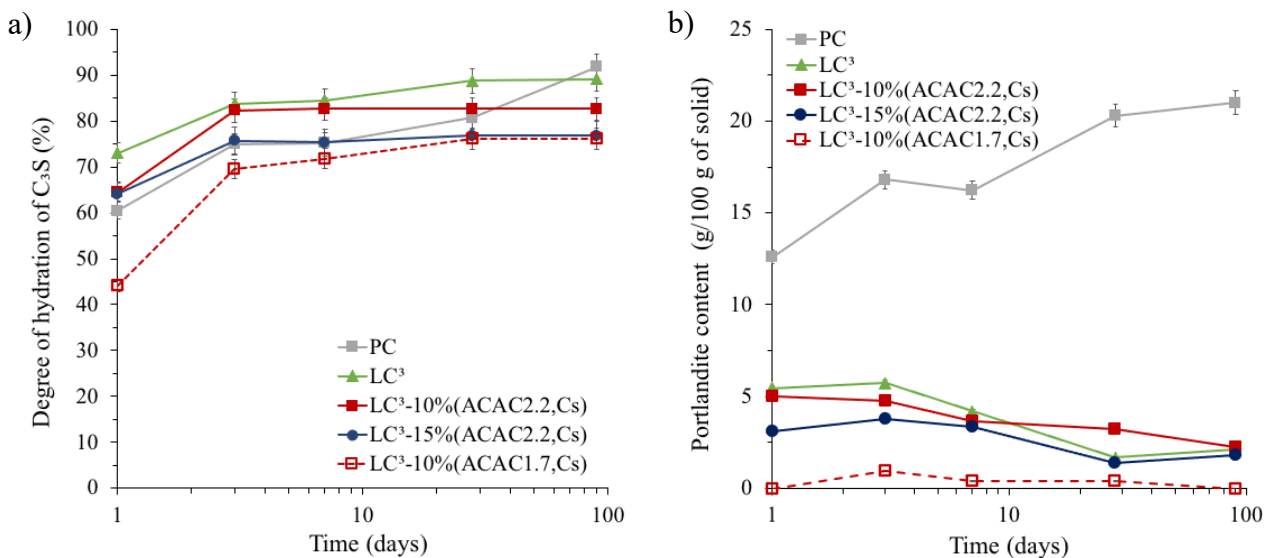
Fig. 3-12 Degree of hydration of alite (DoH$_{C3S}$) (a) and the portlandite content (b) for PC, LC³, LC³ blended with -10, -15%(ACAC2.2,Cs) and LC³-10%(ACAC1.7,Cs).

3.3.2.6 AFm-type phases

The evolution of the AFm-type phases (the sum of Hc, Mc and Ms) content is shown in Fig. 3-13. The difference is not significant between systems blended with ACAC2.2 and Cs. With 10%(ACAC1.7,Cs), from 7 days onwards, a high AFm- type phases amount is formed compared to 10%(ACAC2.2,Cs).
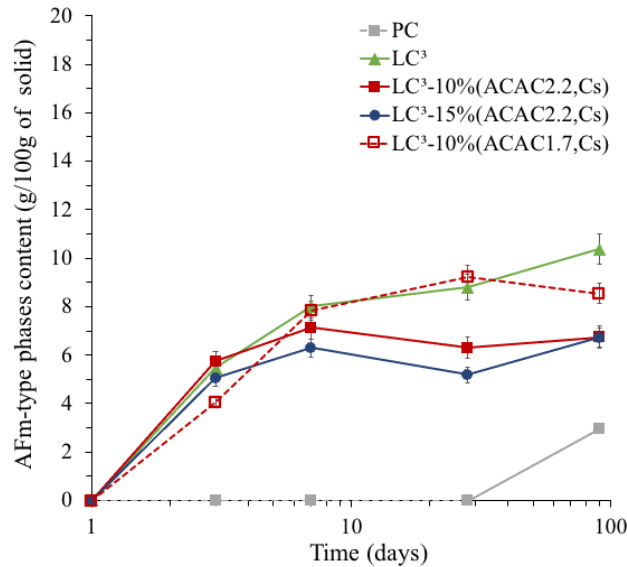
Fig. 3-13 AFm-type phases (Hc+Mc+Ms) quantification by XRD-Rietveld for PC, LC^3, LC^3 with -10%, -15%(ACAC2.2,Cs) and LC^3-10%(ACAC1.7,Cs).

3.3.3 Effect of CAC on C-A-S-H composition and the degree of metakaolin reaction

3.3.3.1 C-A-S-H composition

Fig. 3-14 shows the SEM-EDX results for LC^3, LC^3-10%(ACAC2.2,Cs) and LC^3-10%(ACAC1.7,Cs) at 28 days. The average C-A-S-H composition is determined from the plot of Al/Ca vs Si/Ca atomic ratios. The close intermixing of C-A-S-H with other phases such as AFm and ettringite is responsible for the spread of data points. More intermixing of C-A-S-H is observed in the case of LC^3-10%(ACAC1.7,Cs) as shown in Fig. 3-14(c). The determination of C-A-S-H in the case of ACAC1.7 was not easy task and more points were required. The likely error in the estimation is probably large in this case. Table 3-4 gives the Al/Ca and Si/Ca atomic ratios obtained by SEM-EDX. Similar Al incorporation is observed for all the systems. The Si/Ca ratio remains also unchanged by adding rather ACAC2.2 or ACAC1.7.
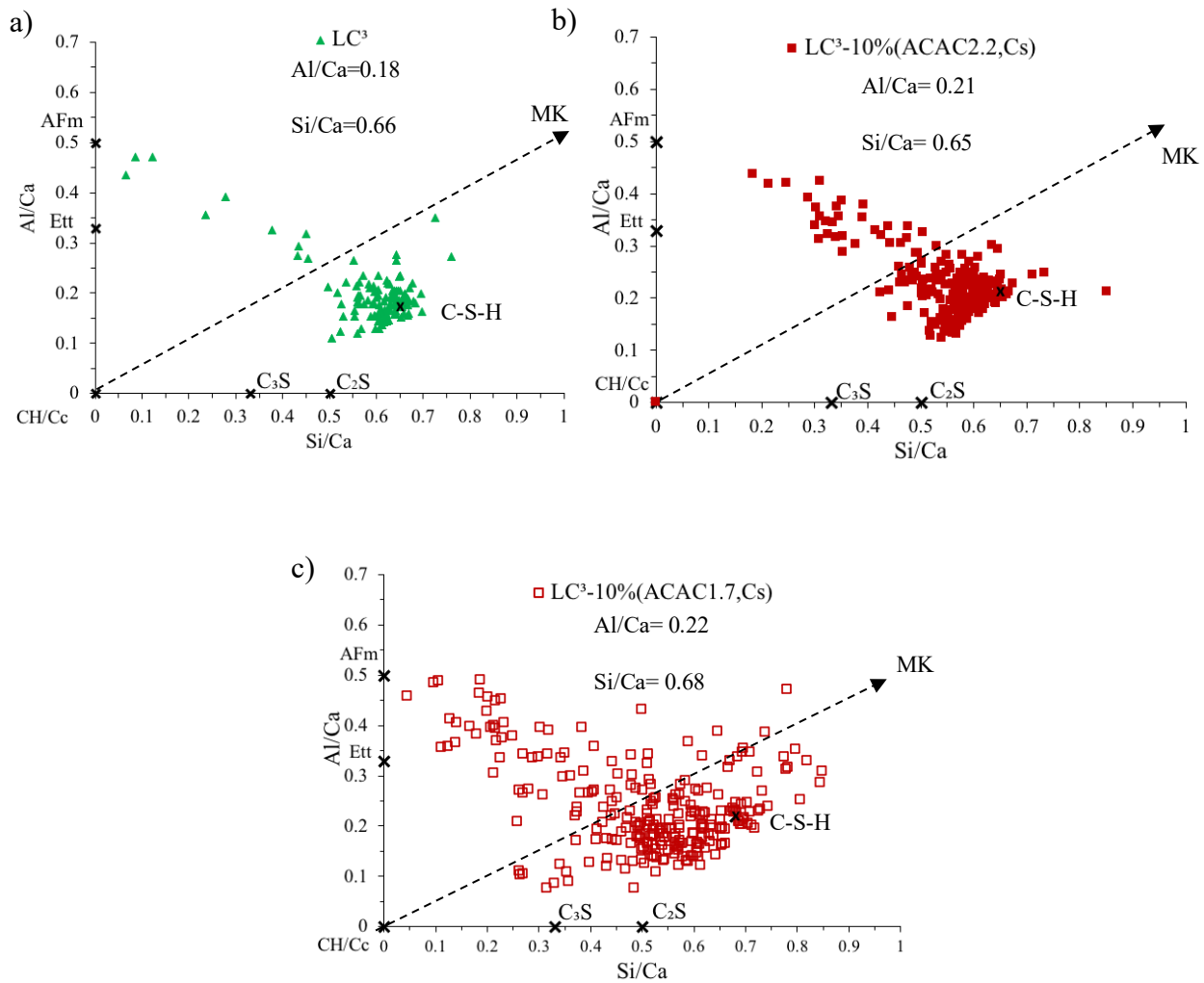
Fig. 3-14 Al/Ca atomic ratio as a function of Si/Ca atomic ratio determined by SEM-EDX for LC^3 (a), LC^3-10%(ACAC2.2,Cs) (b) and LC^3-10%(ACAC1.7,Cs) (c) at 28 days.

Table 3-4 Al/Ca, Si/Ca and Ca/Si atomic ratios of C-A-S-H by SEM-EDX at 28 days.

28 days	Al/Ca	Si/Ca	Ca/Si
LC^3	0.22±0.01	0.66±0.02	1.51±0.02
LC^3-10%(ACAC2.2,Cs)	0.21±0.02	0.65±0.02	1.53±0.02
LC^3-10%(ACAC1.7,Cs)	0.22±0.02	0.68±0.04	1.47±0.04

3.3.3.2 Determination of the degree of reaction of metakaolin

Fig. 3-15(a) shows the expected evolution of the portlandite content as a function of the degree of metakaolin reaction (in %), computed by thermodynamic modelling. The comparison with the experimental portlandite content determined by XRD-Rietveld method allows estimation of the degree of metakaolin reaction. Fig. 3-15(b) shows the degree of metakaolin reaction and the amount of reacted metakaolin for LC^3, LC^3-10%(ACAC1.7,Cs) and LC^3-10%(ACAC2.2,Cs). Higher DoR of

metakaolin of $\approx 40\%$ is obtained with LC^3 compared to LC^3-CAC blends ($\approx 30\%$). When ACAC1.7 is used, a higher DoR_{MK} is obtained compared to the ACAC2.2 blend.
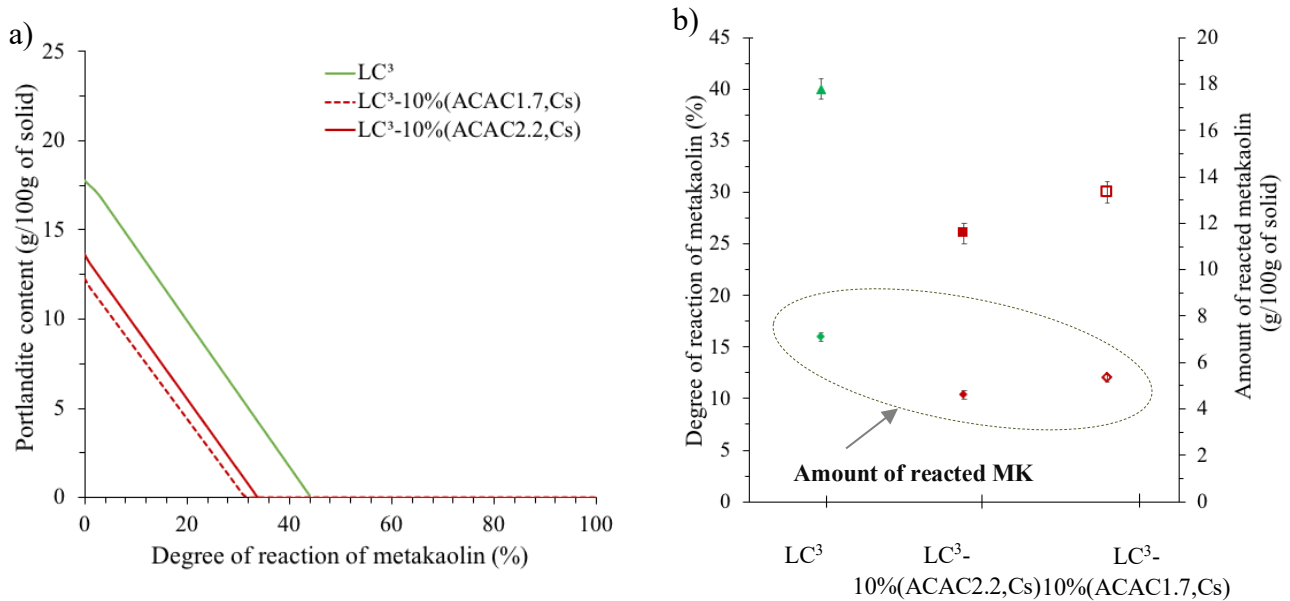
Fig. 3-15 Determination of the degree of reaction of metakaolin (%) by thermodynamic modelling (a) degree of reaction of metakaolin (%) and amount of reacted metakaolin (b) for LC^3, LC^3-10%(ACAC2.2,Cs) and - 10%(ACAC1.7,Cs) at 28 days .

3.3.4 LC^3 substitution by ACAC2.2 and Cs

In the previous sections, the effect of substituting the limestone part by CAC and Cs was investigated. In this section, the influence of substituting the overall LC^3 by ACAC2.2 and Cs on the strength was studied. Compressive strength results for PC, LC^3, LC^3 -10%(ACAC2.2,Cs) and 10% of LC^3 substituted by ACAC2.2 and Cs "90%LC^3-10%(ACAC2.2,Cs)" are shown in Fig. 3-16. It can be seen that substituting the overall of LC^3 by ACAC2.2 and Cs gives better strength than LC^3. Additionally, an equivalent strength to PC is obtained at 1 day and a higher strength from 7 days onwards.
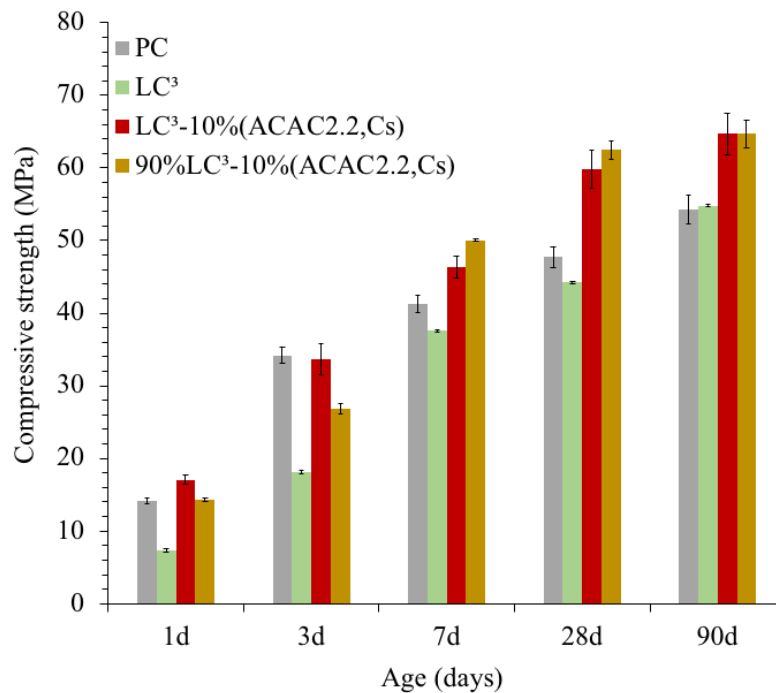
Fig. 3-16 Compressive strength development for PC, LC^3, LC^3-10%(ACAC2.2,Cs): limestone substitution by ACAC2.2 +Cs and 90%LC^3-10%(ACAC2.2,Cs): LC^3 substitution by ACAC2.2 +Cs.

3.4   Conclusions

The present study investigated the feasibility of incorporating calcium aluminate cement (CAC) in a LC^3 blend. The effect of C/A molar ratio and the CAC content were studied.

The substitution of a part of the limestone by ACAC1.7 and Cs improved the strength of LC^3 at 1 and 3 days, which is related to the massive ettringite formation during the first hours from the hydration of ACAC1.7 and Cs. However, higher strength than for PC is observed only from 7 days onwards as the addition of ACAC1.7 delayed the C$_3$S hydration. It is interesting to note that the addition of 15% ACAC1.7 and Cs dosage led to a lower early age strength and later C$_3$S reaction, which will be further investigated in the next chapter (Chapter 4). The early ettringite formation did not compensate the loss in strength. The portlandite content was reduced by increasing the ACAC1.7 dosage. The formation of AFm-type phases was delayed at 15%(ACAC1.7,Cs).

The substitution of a part of the limestone by ACAC2.2 and Cs considerably improved the strength at all ages. With 10%(ACAC2.2,Cs), at least the same strength was obtained as for PC from 1 day onwards. Higher ACAC2.2 contents increased the compressive strength. The improvement of strength at early age can be explained by the combination of early ettringite formation and the non-delayed C$_3$S hydration. Contrary to the case of ACAC1.7, higher ACAC2.2 and Cs dosage did not hinder C$_3$S hydration nor lowered the portlandite content.

The comparison of the two CACs showed that the ettringite formation does not depend on the C/A ratio of the CAC as a similar amount is obtained for LC^3 with ACAC2.2 and ACAC1.7. The ettringite however clearly increased with the amount of CAC plus Cs showing its dependence on the sulfate

content. The amount of portlandite depends mainly on the degree of C_3S hydration. As ACAC1.7 delayed the C_3S hydration, less portlandite was quantified at higher ACAC1.7 dosage. This however, did not affect the degree reaction of metakaolin and a slightly higher degree than in the ACAC2.2 system was obtained, indicating the amount of portlandite is not the main driver for the metakaolin reaction. For the 10%(ACAC1.7,Cs) blend, a higher amount of AFm-type phases was obtained after 28 days of hydration compared to 10%(ACAC2.2,Cs), due to the higher metakaolin reaction.

The incorporation of CAC and Cs in LC^3 lowered the metakaolin reaction degree slightly.

Finally, the substitution of the overall LC^3 with ACAC2.2 and Cs showed equivalent strength to PC at 1 day.

Chapter 4　Understanding reasons of delaying alite hydration in LC³ incorporating ACAC1.7

Note: This chapter is based on an article in preparation for submission to a peer reviewed journal

Contribution of the doctoral candidate: conceptualization, methodology, experiments, analysis and writing of the first manuscript draft.

Abstract

This chapter compares the hydration of LC³-10%(ACAC2.2,Cs) and LC³-10%(ACAC1.7,Cs), focusing on the C_3S hydration with the aim of clarifying the reasons for the delay. The experimental studies in Chapter 3 showed that the hydration of C_3S is delayed in LC³ blends incorporating ACAC1.7 (low C/A ratio CAC) and Cs. Thermodynamic modelling shows that a positive saturation index with respect to portlandite is obtained after 4 hours of hydration for LC³ with ACAC2.2 while it is only obtained after 30 hours of hydration for LC³ blended with ACAC1.7. The results suggest that a positive saturation index with respect to calcium hydroxide is needed to trigger the C_3S hydration. Due to the low C/A ratio of ACAC1.7, there is not enough calcium for ettringite precipitation, which must also take calcium from C_3S dissolution. This results in low calcium concentration in the pore solution and portlandite remains under saturated. This is confirmed by studying the effect of adding 2% of calcium hydroxide in LC³-10%(ACAC1.7,Cs), where a part of the calcium needed to form ettringite is provided by calcium hydroxide. As a result, the pore solution becomes supersaturated with respect to portlandite earlier compared to the system without initial addition. This has a beneficial impact on the rate of hydration of C_3S. However, unexpectedly, calcium hydroxide addition does not improve the early age strength and a lower strength is obtained at 1 day compared to the system without calcium hydroxide addition.

4.1　Introduction

Calcium aluminate cement (CAC) can accelerate strength development of Portland cement [47,76]. When calcium sulfate is added, the formation of metastable calcium aluminate phases is avoided. Ettringite is the main hydrate formed leading to rapid strength development [76,77]. This was used to improve the early age strength performance of LC³. In the previous chapter, it was found that the C/A ratio of the CAC used has an impact on the early age strength development of LC³-CAC blends. It particularly impacts the C_3S hydration: the C_3S dissolution was delayed when the C/A ratio of the

CAC is 1.7. This was not the case when the C/A ratio of the CAC is 2.2 and the same course of PC hydration was observed. In this chapter, reason(s) for the delay of the C$_3$S hydration are investigated.

The causes of the induction period and its end, have been intensively investigated for PC during the last decades. However, there is still a debate about the end of the induction period and the reason for the increase of the hydration rate during the acceleration period. One of the proposed reasons is that the induction period occurs because of a poisoning of calcium hydroxide nuclei by silicates. The end of the induction period has been explained as the point at which a sufficient level of supersaturation with respect to portlandite is reached to overcome this effect [78,79]. In the other hand, Odler and Dörr investigated the effect of calcium hydroxide addition on the C$_3$S hydration. They concluded that the presence of calcium hydroxide is not essential to initiate the acceleration period [80]. Other theories proposed that the induction period is governed by nucleation and growth of C-S-H. It ends when the C-S-H starts to grow [81,82]. Based on the geochemical theory, simulations performed using HydratiCa by Bullard and Flatt showed that the inhibition of the nucleation and growth of portlandite could lead to a retardation [83].

It is often reported in the literature that the addition of CAC to PC delays the C$_3$S hydration [84]. The amount of CAC added is critical. Gu and Beaudoin studied binary systems composed of CAC /PC and showed a transition from accelerating to a delaying effect of CAC at an addition of 12.5% CAC [85]. Several reasons for a delay of C$_3$S have been proposed in the past. Gu and Beaudoin attributed it to a hydrate barrier effect (mainly ettringite). It was suggested that a physical barrier did not allow a contact of water with the cement powder [85]. However, there is no evidence that ettringite is a diffusion barrier [86]. It is strongly accepted that the C$_3$S hydration is delayed due to the presence of aluminum ions. It was suggested that aluminum ions have a perturbing effect on the silicate phases reactivity [87,88]. The mechanism of aluminum ion action is still not clear and several mechanisms have been proposed. Nicoleau et al. suggested that aluminate ions covalently bind to silicate monomers present at the surface at moderate alkaline conditions. This leads to a slowing down of the C$_3$S dissolution [89]. Begarin et al. studied the hydration of alite containing aluminum. A delay of the alite hydration was observed in presence of aluminum. The authors explained the delay by the formation of C-S-H incorporating aluminum ions. It was proposed that this C-A-S-H does not act as a nuclei to C-S-H growth [90]. A delay of the C$_3$S hydration in systems composed of PC with additions of calcium sulfoaluminate cement was also observed [91]. However, the Al/Ca ratio of the C-S-H was similar to neat PC system. The hydration study of ACAC (amorphous CAC)/PC also showed a delaying effect of aluminum ions on the C$_3$S hydration [48]. Nehring et al. showed that the start of the silicate reaction in system composed of C$_3$S/CA is related to a decrease of the Al concentration and also an increase of the calcium ions concentration. It was also found that C$_3$S is also able to dissolve even at high aluminum ions concentrations [92].

Torréns-Martín et al. demonstrated that the delay of C$_3$S hydration caused by CAC addition can be avoided by adding calcium sulfate [43]. Xu et al. investigated the effect of the sulfate reactivity and its amount on the hydration of PC/CAC blends. They showed that the C$_3$S hydration delay can be counteracted by adding calcium sulfate [93]. Moreover, it was found that using anhydrite as a sulfate source leads to the formation of ettringite. Nehring et al. also found that the addition of anhydrite prevents the delay of C$_3$S hydration in CAC/PC blend. Authors suggested that aluminum ions have to be removed from the pore solution by precipitating ettringite. A sufficient amount of Cs is needed,

otherwise AFm will form and its precipitation takes more time. Once the aluminum is removed from the pore solution, alite dissolution and C-S-H formation is favored [94]. In the other hand, Lamberet observed that even in the presence of calcium sulfate the hydration of silicates phases was inhibited in ternary binders composed of PC, CAC and Cs [95]. In a more recent work, Kighelman studied the effect of adding calcium hydroxide on the kinetics of hydration of blends composed of PC/CAC/CsH$_{0.5}$ [45]. Calorimetry results showed that all hydration peaks were accelerated linearly with the calcium hydroxide content.

The aim of the present study is to provide insights into the possible reasons for the delay of the C$_3$S hydration. The effect of reducing the setting retarder content on the kinetics of hydration was investigated by isothermal calorimetry. A comparison between the hydration of LC³ blended with ACAC2.2 and ACAC1.7 at early age was made based the results from XRD-Rietveld quantification, ions concentrations in pore solution from Ion Chromatography (IC) analysis and saturation indices computed with Gibbs Energy Minimization Software (GEMS). Then, the influence of calcium hydroxide addition on the hydration and strength was studied. In addition, to the mentioned techniques, the microstructure was investigated at 1 day using Scanning Electron Microscopy- Back Scattered Electron (SEM-BSE) and SEM-Energy Dispersive spectroscopy (EDS) mapping. To understand the strength results, the porosity was assessed with Mercury Intrusion Porosimetry (MIP).

4.2   Materials and methods

4.2.1 Raw materials

In addition to materials described in Chapter 3, calcium hydroxide (CH) from Roth was used. Its Dv$_{50}$ was 4.23µm and its specific surface area using the nitrogen adsorption method is 15.66 m^2/g. Fig. 4-1 shows the particle size distribution (PSD) of CH. The particle size distribution of the other materials used are already described in Chapter 3. The physicochemical properties of PC, ACAC1.7, ACAC2.2, Cs and CClay 1 are presented in Table 3-1, Chapter 3. The phase composition of the different cements is shown in Table 3-2, Chapter 3.
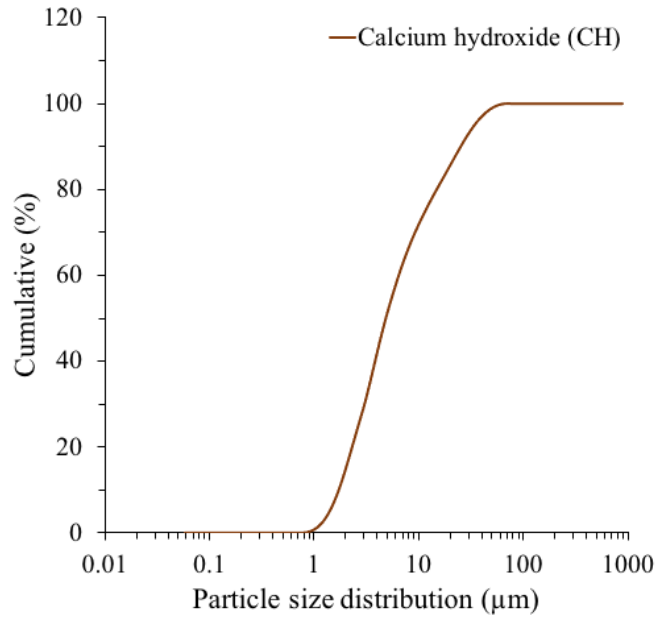
Fig. 4-1 PSD for calcium hydroxide (CH).

4.2.2 Mixture design and sample preparation

The investigated systems are PC, LC³ and LC³ with 10%(ACAC17,Cs) and 10% (ACAC2.2,Cs). To assess the effect of the setting retarder on the kinetics of hydration, its content was reduced: LC³-10%(ACAC1.7,Cs)-031ret. The effect of adding calcium hydroxide was also investigated, 2%CH was added to the LC³-10%(ACAC1.7,Cs): LC³-10%(ACAC1.7,Cs) -2%CH. The mix compositions of all the investigated systems are shown in Table 4-1. Cement pastes and mortars were prepared as already described in Chapter 3.

Table 4-1 Mix compositions of the investigated systems (wt. %).

Notation	PC	ACAC 1.7	ACAC 2.2	Cs	CClay	CsH₂	Cc	CH	Citric acid	Na₂CO₃
PC	100	-	-	-	-	-	-	-	-	-
LC³	52.66	-	-	-	25	2.34	20	-	-	-
LC³-10%(ACAC1.7,Cs)	52.15	5	-	5	24.76	2.34	9.81	-	0.33	0.61
LC³-10%(ACAC1.7,Cs) -0.31ret	52.17	5	-	5	24.76	2.34	9.81	-	0.31	0.61
LC³-10%(ACAC2.2,Cs)	52.15	-	5	5	24.76	2.34	9.81	-	0.33	0.61
LC³-10%(ACAC1.7,Cs) -2%CH	52.15	5	-	5	24.76	2.34	9.81	2	0.33	0.61

4.2.3 Methods

The heat evolution was followed by isothermal calorimetry in a TAM Air isothermal calorimeter at 20°C.

The crystalline phases were quantified at specific ages by XRD, carried-out on freshly cut slices of hardened paste. Measurements were carried-out after 4, 10, 24 and 72 hours of hydration.

In-situ XRD experiments were carried out, the sample was prepared in the same manner as described in Chapter 3.

Pore solutions of hardened samples were extracted. To prevent precipitation of solid phases, the extracted liquid was immediately filtered using a plastic syringe attached to a 0.2 µm pore size filter. A part of the extracted solutions was diluted (10x,100x, 1000x) with MilliQ water to avoid any carbonation or precipitation and stored in the fridge until the analysis date. The remaining solutions were used to measure the pH with a BlueLine 14 pH electrode (SI Anlaytics) and a Lab 850 pH meter. The electrode was calibrated with of 0.1, 0.2, 0.5 and 1M KOH solutions as described in [96]. Ion oncentrations in the pore solution of the investigated systems of Ca, Al, S, Si were determined by Ion chromatography (IC, Dionex DP series ICS-3000). The hydroxide ion concentration was calculated based on the measured pH. Extraction times for each investigated system are shown in Table 4-2.

Table 4-2 Pore solution extraction time of the investigated systems.

Sample name	Extraction time (hours)
LC^3-10%(ACAC2.2,Cs)	4,11, 17, 52
LC^3-10%(ACAC1.7,Cs)	4, 10, 30, 96
LC^3-10%(ACAC1.7,Cs)-2%CH	4, 10, 20, 96

To calculate saturation indices, thermodynamic modelling was conducted using GEMS-PSI [54]. General thermodynamic data were taken from PSI-GEMS and supplemented by the cement database Cemdata18 [55]. The thermodynamic databases were supplemented with thermodynamic data for alite from [97] based on dissolution experiment. The saturation index with respect of a phase is defined as the ratio of the (measured) ion activity product to the theoretical solubility product. In our calculations, the ion activity product is computed by GEMS using the extended Debye-Hückel equation and based on the total measured elemental concentrations as input [98]. If we consider the case of ettringite, its solubility product is K_{ett}=4.9x10^{-44} and reaction is presented in Eq.1; Its saturation index is described by Eq.2.

$$Ca_6[Al(OH)_6]_2 \cdot 3SO_4 \cdot 26H_2O \rightarrow 6Ca^{2+} + 2Al(OH)_4^- + 4OH^- + 3SO_4^{2-} + 26H_2O \quad (1)$$
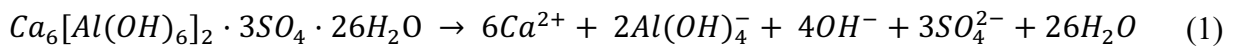
$$SI_{ettringite} = \log_{10} \frac{(a_{Ca^{2+}})^6 (a_{Al(OH)_4^-})^2 (a_{SO_4^{2-}})^3 (a_{OH^-})^4 (a_{H_2O})^{26}}{K_{ett}} \quad (2)$$

where (a$_i$) designates the activity of i.

The compressive strength of the investigated systems was tested according to the European standard EN 196-1.

The hydration of cement paste was stopped with isopropanol following the protocol in [67].

After stopping the hydration, the following experiments were carried out:

The microstructural development was investigated by SEM-BSE with an FEI Quanta 200 microscope. In addition, image analysis was carried-out, with BSE images linked to EDS mapping by the edxia platform [99]. Ratio plots of Al/Ca vs Si/Ca from EDS maps give the composition of phases present in the microstructure. Maps were collected with an accelerating voltage of 15kV and a working distance of 12.5mm. Maps were done at 1000x magnification.

The pore structure was characterized by MIP. After stopping the hydration, 4-5 small pieces of hardened pieces (~1-1.2 g) were placed in a dilatometer. A pressure up to 400 MPa was applied to intrude mercury into small porosities (~2nm). MIP measurements were monitored by assuming a contact angle of 140° between the cement paste and the mercury.

More details about isothermal calorimetry, in and ex -situ XRD and compressive strength are given in Chapter 3.

4.3   Results and discussion

4.3.1 Effect of decreasing the setting retarder content

Fig. 4-2 shows the heat release per gram of paste for PC, LC³- 10%(ACAC1.7,Cs) and -10%(ACAC1.7,Cs)-0.31 ret (decreased setting retarder amount) up to 150 hours of hydration. Calorimetry results show two well separated peaks (#1, #2). It has been demonstrated in the previous chapter that during these two events the C_3S is dissolving. It is clear that reducing the setting retarder content did not strongly impact the clinker hydration. The intensity of the first C_3S hydration peak was slightly increased (#1) and the 2nd peak was slightly accelerated (#2). This indicates that the observed delay of C_3S hydration is not primarily caused by the setting retarder.
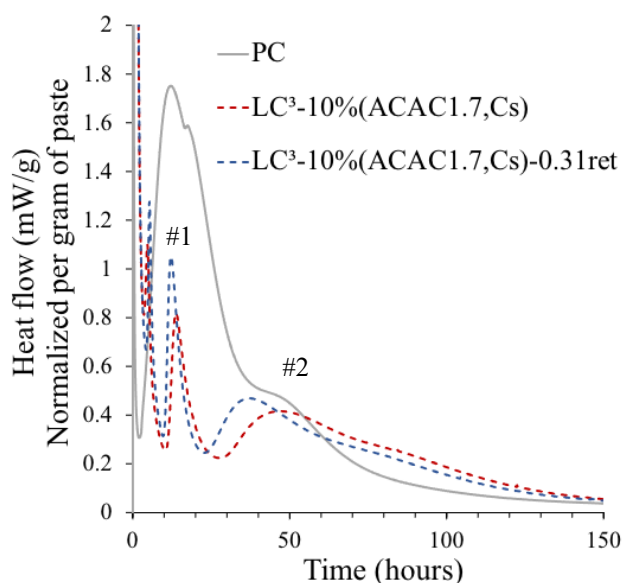
Fig. 4-2 Heat release per gram of paste for PC, LC³-10%(ACAC1.7,Cs) and -10%(ACAC1.7,Cs)-0.31ret (decreased setting retarder amount) up to 150 hours.

4.3.2 Early age hydration comparison between LC[3] blended with ACAC2.2 and ACAC1.7

4.3.2.1 Ettringite content and degree of hydration of alite

Fig. 4-3 shows the evolution of the kinetics of hydration up to 80 hours of hydration together with the degree of hydration of alite (DoH$_{C3S}$) and the ettringite (Ett) content at 4, 10, 24 and 72 hours of LC[3] blended with 10%(ACAC2.2,Cs) and 10%(ACAC1.7,Cs). The calculated degree of hydration from XRD-Rietveld quantification for the two systems is similar up to 4 hours. Following that, a lower DoH$_{C3S}$ is observed when the C/A ratio of the CAC is 1.7. At all tested ages, particularly at 10 hours of hydration, a similar ettringite amount is formed. This means that the same amount of aluminum, calcium and sulfate are consumed. As the C/A ratio of ACAC1.7 is lower, it is expected to have different elemental concentrations in the pore solution.
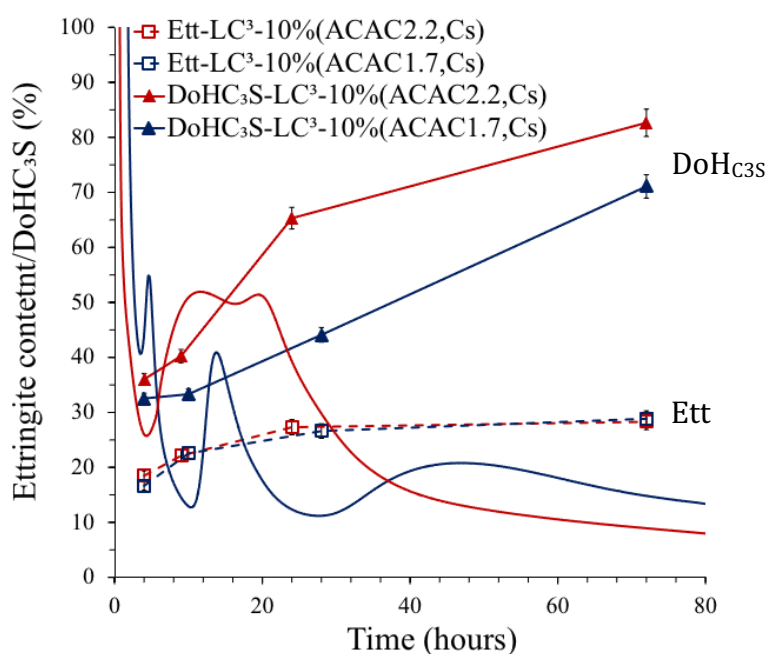
Fig. 4-3 Heat release up to 80 hours, ettringite (Ett) content and DoH$_{C3S}$ at 4, 10, 24 and 72 hours for LC[3]-10%(ACAC1.7,Cs) and LC[3]-10%(ACAC2.2,Cs).

4.3.2.2 Pore solution

Fig. 4-4(a) and (b) show the evolution of the concentrations of Ca, Al, S, Si and hydroxide for LC[3]-10%(ACAC1.7,Cs) and -10%(ACAC2.2,Cs). For both blends, at 4 hours, a high sulfate concentration is observed in the pore solution (~200mM). For ACAC1.7 blend, at 10 hours, the sulfate concentration is almost the same. Afterwards, it becomes very low. However, for ACAC2.2 blend, it strongly decreases between 4 and 10 hours. It is well known that the sulfate can adsorb on C-S-H during the acceleration period [100,101]. Since the acceleration period has already started for ACAC2.2 blend, C-S-H is forming and sulfates can adsorb on its surface. Regarding the calcium concentration, it is 40 times higher in ACAC2.2 than in ACAC1.7 blend at 4 hours (before the onset of the C$_3$S hydration peak), and a high availability of calcium has been observed to promote sulfate sorption on C-S-H

[102]. For ACAC2.2 blend, calcium concentration strongly decreases between 4 and 10 hours of hydration reaches 0.6mM at 52 hours. For ACAC1.7, the calcium concentration is very low (below 1mM) up to 10 hours. Then, it slightly increases to reach 1mM after 30 hours. On the other hand, the aluminum concentration is always lower in ACAC2.2 compared to ACAC7.7. It is 62 times lower in ACAC2.2 blend compared to ACAC1.7 blend at 4 hours. At 4 and 10 hours, the Si concentration is higher for ACAC1.7 blend compared to ACAC2.2 blend. Elemental concentrations as well as pH values of the investigated blends are detailed in the appendix of this chapter (Table 4-3).

Fig. 4-4 Elemental concentrations of Ca, Al, S, Si and hydroxide in the pore solution over time for LC³-10%(ACAC1.7,Cs) (a) and LC³-10%(ACAC2.2,Cs) (b).

4.3.2.3 Saturation indices

Fig. 4-5 shows the calculated saturation indices (SI) for LC³-10%(ACAC1.7,Cs) (a) and LC³-10%(ACAC2.2,Cs) (b) of ettringite, C-S-H, CH and alite (C₃S). Indices were calculated based on the pore solution chemistry. The saturation indices globally agree well with the XRD-Rietveld quantification results. For both systems, at 4 hours, a positive saturation index with respect to ettringite is obtained meaning that it can precipitate. However, SI_ettringite is higher for ACAC2.2 blend than for ACAC1.7 blend. This can be explained by the higher calcium concentration in the ACAC2.2 blends, as shown in Fig. 4-4(a) and (b). According to Eq.2, the activity of Ca^{2+} in the SI is to the power 6 against power 2 for $Al(OH)_4^-$, which justifies the observed differences in saturation indices. A slightly positive saturation index with respect to C-S-H is observed after 4 hours of hydration for ACAC1.7, while it is slightly negative for ACAC2.2 after 4 hours, although the difference is within the error of the method. It becomes positive afterwards. The SI_C₃S is negative at all investigated ages and for both blends, indicating that potentially C₃S should be dissolving for both blends, although this is not the case for the ACAC1.7 blend, where it is delayed. A positive saturation index with respect to portlandite is obtained after 4 hours of hydration in ACAC2.2 blend. However, it

becomes positive much later for ACAC1.7, between 10 and 30 hours of hydration. This suggests that a positive saturation index with respect to portlandite might be needed to trigger the C$_3$S hydration. To confirm this, the effect of adding 2% of calcium hydroxide on the hydration and strength was investigated.
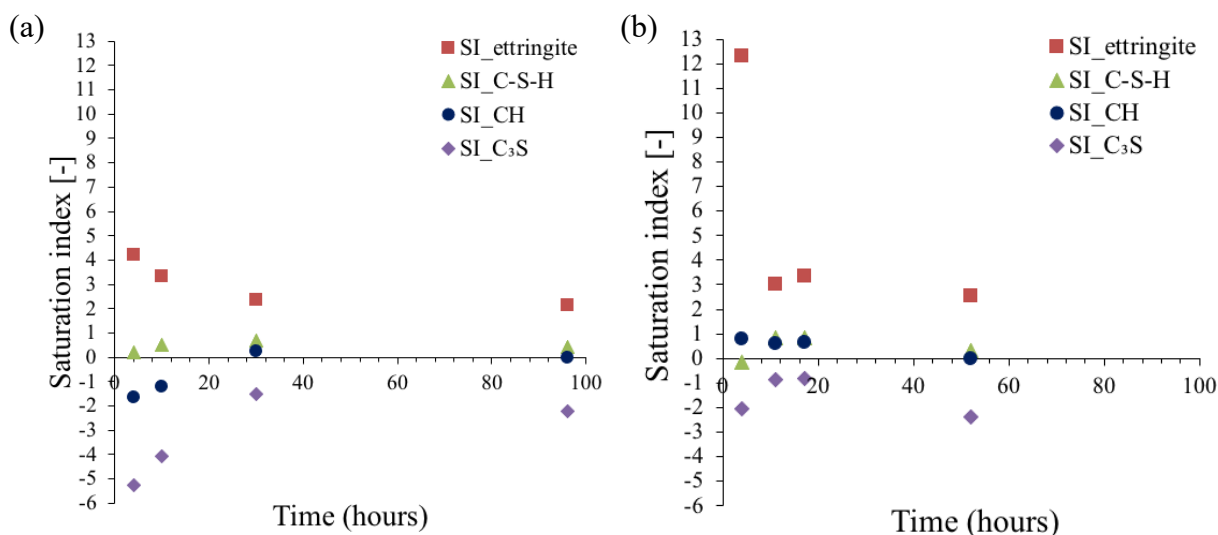
Fig. 4-5 Saturation indices of ettringite, C-S-H, CH and C$_3$S for LC^3-10%(ACAC1.7,Cs) (a) and LC^3-10%(ACAC2.2,Cs) (b).

4.3.3 Effect of calcium hydroxide addition on the hydration, microstructure and strength development of LC^3-10%(ACAC1.7,Cs) blend

4.3.3.1 In-situ XRD

Fig. 4-6 shows the phase assemblage together with the evolution of the heat flow result for LC^3-10%(ACAC1.7,Cs)-2%CH up to 10 hours Fig. 4-6(a) and up to 70 hours Fig. 4-6(b). The ettringite formation is delayed by 0.5 hour compared to the blend without calcium hydroxide addition (Chapter 3, Fig. 3-4(a)). With 2%CH blend, it starts to form after 0.8 hour. Its formation is accompanied by a peak (#2) that occurs after the introduction peak (#1). It can be seen that ettringite formation is accompanied by gypsum and calcium hydroxide consumption. Anhydrite is also consumed but it can be seen that is slowly dissolving compared to gypsum. At this step, ettringite is the sink for calcium ions. Gypsum is depleted after 3 hours. The course of gypsum depletion is similar to the system without calcium hydroxide. The added calcium hydroxide is totally consumed after 2.8 hours of hydration. The first fast dissolution of C$_3$S that was observed without calcium hydroxide addition (Chapter 3, Fig. 3-4(a)) is not observed here. In presence of 2%CH, C$_3$S is slightly dissolving during the first 10 hours of hydration. Anhydrite is faster depleted (after 6 hours of hydration) compared to the system without CH addition. A third peak (#3) is observed after 15 hours of hydration. This peak corresponds to an important C$_3$S dissolution. Portlandite is detected after 22.5 hours of hydration. It is clear that calcium hydroxide addition affects the pattern of C$_3$S hydration and the kinetics of hydration is changed. In absence of calcium hydroxide addition, it was observed in the previous chapter (Chapter 3, Fig. 3-4(b)) that the C$_3$S hydration was proceeding in two peaks and portlandite

did not form. This is not the case with calcium hydroxide addition. Only one peak is observed (#3). It can be also noted that a similar amount of ettringite forms compared to the system without calcium hydroxide (Chapter 3, Fig. 3-4(a)). This shows that the limiting factor of ettringite formation is the sulfate amount.
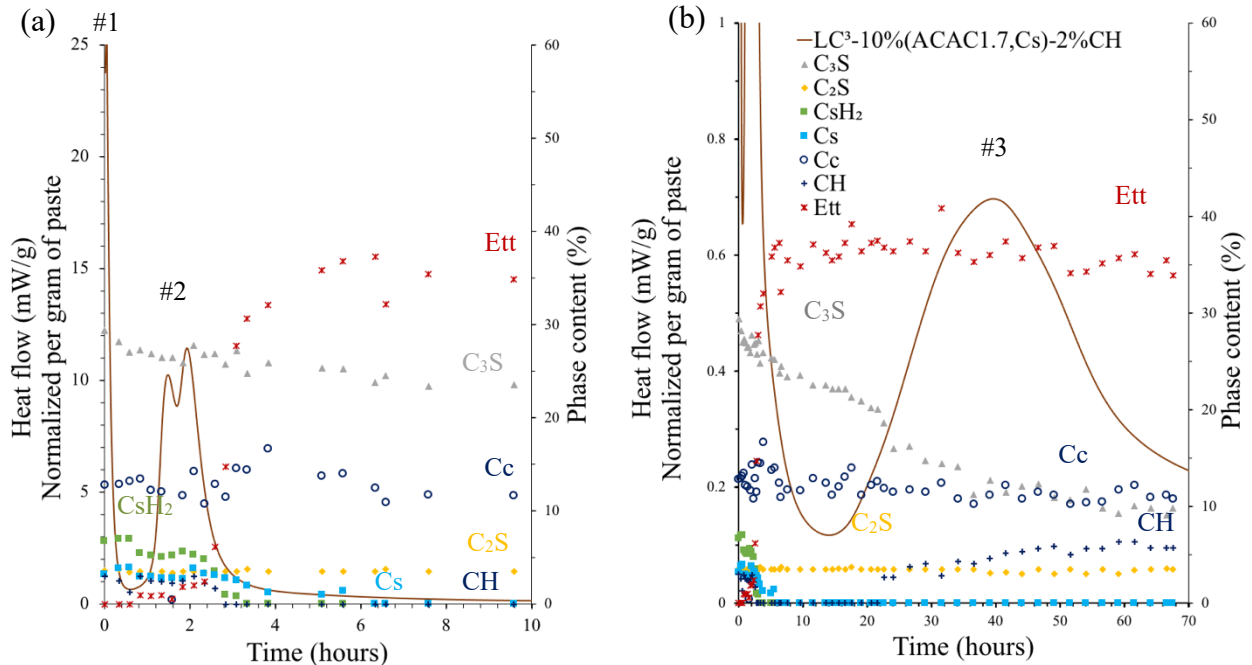
Fig. 4-6 Phase assemblage by in-situ XRD for LC³-10%(ACAC1.7,Cs)-2%CH up to 10 hours (a) and up to 70 hours (b).

4.3.3.2 Ettringite and AFm contents

To get a more reliable ettringite and AFm quantification, XRD was also carried-out on freshly-cut slices. Fig. 4-7 shows the evolution of the ettringite and AFm type phases for LC³-10%(ACAC1.7,Cs) and LC³-10%(ACAC1.7,Cs)-2%CH blends. XRD-Rietveld quantification results confirm that the addition of calcium hydroxide does not have an impact on the ettringite amount. Slightly higher AFm type phases (Hc+Mc) are formed for the 0%CH blend. The difference between the two systems is negligible. AFm phases quantification by XRD-Rietveld is very difficult. As it has a layered double hydroxide structure, many disorders can occur during the crystallization leading to a loss in crystallinity [103]. This will give a broad XRD peaks and only an approximate quantification.
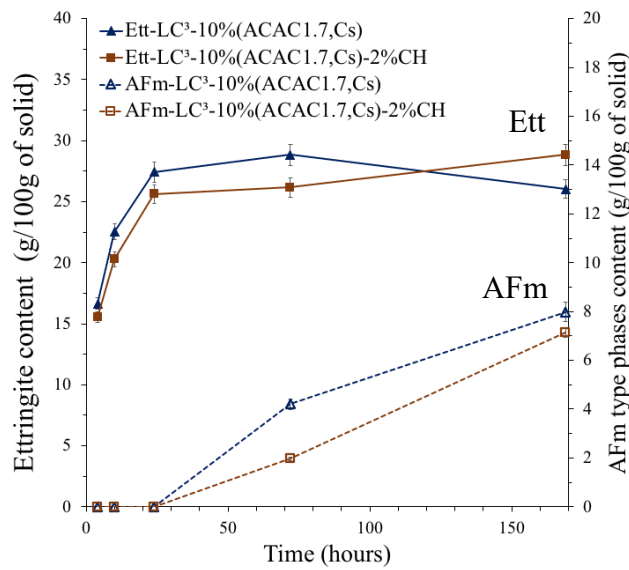
Fig. 4-7 Ettringite and AFm type phases (Hc+Mc) quantification by XRD-Rietveld for LC³-10%(ACAC1.7,Cs) and LC³-10%(ACAC1.7,Cs)-2%CH.

4.3.3.3 Degree of hydration of alite

Fig. 4-8 compares the evolution of the degree of hydration of alite (DoH$_{C3S}$) for LC³-10%(ACAC1.7,Cs) and LC³-10%(ACAC1.7,Cs)-2%CH blends at 4,10, 24, 72 and 169 hours of hydration. It can be seen that up to 10 hours of hydration similar DoH$_{C3S}$ is reached. After that, a higher DoH$_{C3S}$ is observed with 2%CH. This coincides with the C$_3$S hydration peak.
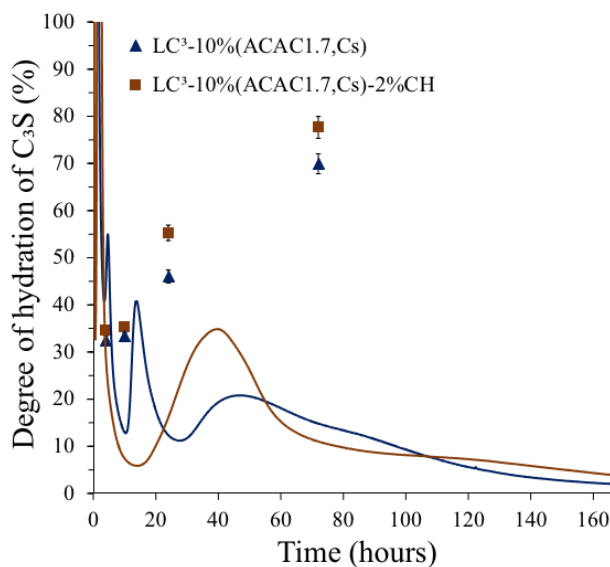
Fig. 4-8 Heat release results and degree of hydration of alite (DoH$_{C3S}$) for LC³-10%(ACAC1.7,Cs) and LC³-10%(ACAC1.7,Cs)-2%CH blends up to 170 hours.

4.3.3.4 Portlandite content

Fig. 4-9 shows the evolution of the portlandite content for LC^3-10%(ACAC1.7,Cs) and LC^3-10%(ACAC1.7,Cs)-2%CH. The results show that at 4 and 10 hours of hydration less than the initially added portlandite amount is present, indicating that calcium hydroxide is being consumed. Afterwards, it can be seen that more portlandite than the initially added amount is formed, which shows that the hydration of C$_3$S is enhanced when an extra calcium source is added. Additionally, as calcium hydroxide is an extra calcium source, less calcium is taken from C$_3$S hydration to contribute to ettringite formation. As a consequence, more calcium hydroxide will form from the hydration of C$_3$S.
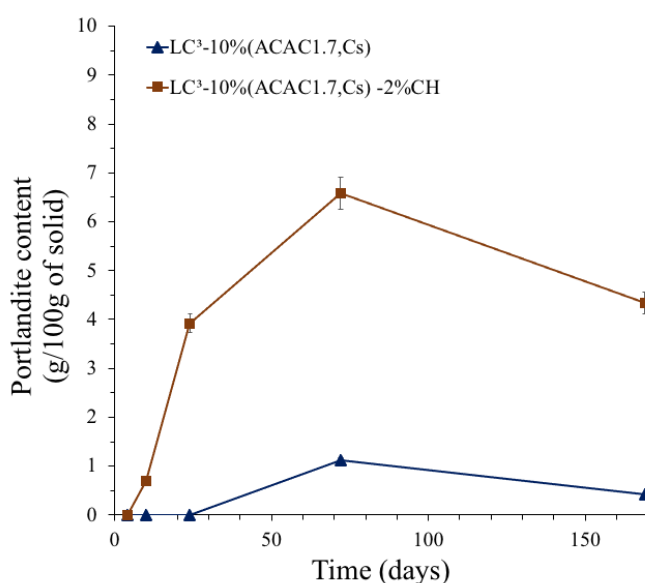
Fig. 4-9 Portlandite quantification by XRD-Rietveld for LC^3-10%(ACAC1.7,Cs) and LC^3-10%(ACAC1.7,Cs)-2%CH.

4.3.3.5 Pore solution and saturation indices

The concentrations of Ca, Al, S, Si and hydroxide are plotted in Fig. 4-10 for the 2%CH blend. At 4 hours, the sulfate concentration is high (~230mM). After that, it decreases to reach 90mM after 20 hours. At 4 hours, the calcium concentration is higher compared to the blend without CH addition (Fig. 4-4(a)). This can be explained by the extra calcium present from the dissolution of the CH addition. After that, the calcium concentration decreases and stays around 3.4mM after 20 hours. It can be also noted that although the aluminum concentration is low at 4 and 10 hours, the degree of hydration of C$_3$S was not improved compared to the system without calcium hydroxide, as shown in Fig. 4-8. This indicates that the hypothesis of an inhibiting effect of the aluminum ion in the pore solution seems to not be the reason of delaying the C$_3$S in the studied system. The silicate concentration is low at all tested ages. Elemental concentrations as well as pH values of this system are detailed in the appendix of this chapter (Table 4-3).
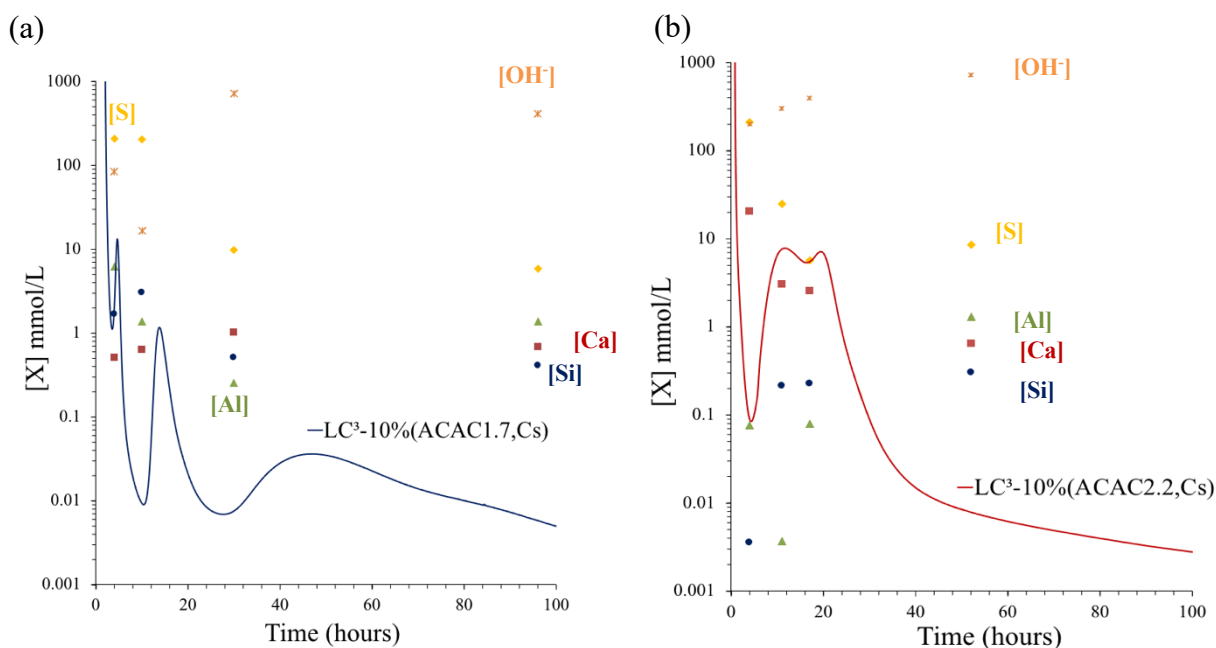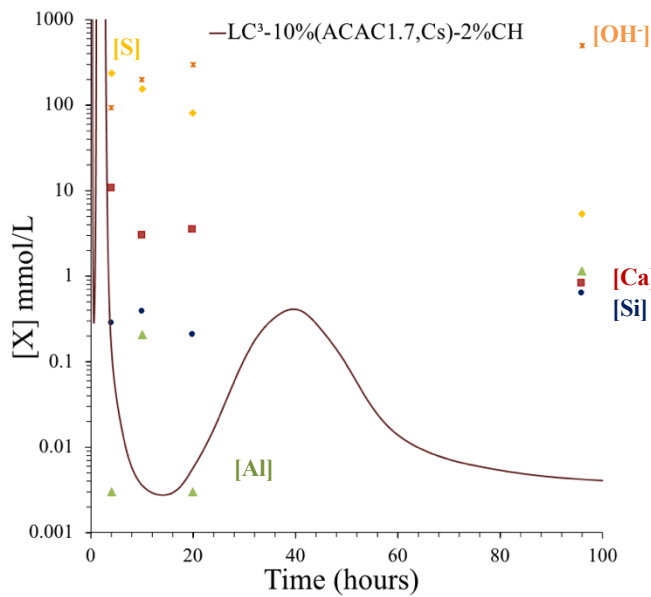
Fig. 4-10 Elemental concentrations of Ca, Al, S, Si and hydroxide in the pore solution over time for LC³-10%(ACAC1.7,Cs)- 2%CH.

Saturation indices with respect to ettringite, C-S-H, CH and C₃S are presented for LC³-10%(ACAC1.7,Cs) in Fig. 4-11(a) and for LC³-10%(ACAC1.7,Cs)-2%CH in Fig. 4-11(b). The two blends have a positive SI_ettringite, which decreases over time corresponding to the plateau in ettringite formation. A negative SI_C₃S shows that this phase could be dissolving. It is clear that for the blend with 2%CH, a positive SI_CH is obtained after 10 hours which was not the case for the blend without calcium hydroxide addition. This supports the hypothesis that the pore solution needs to be super saturated with respect to portlandite to trigger the C₃S hydration.
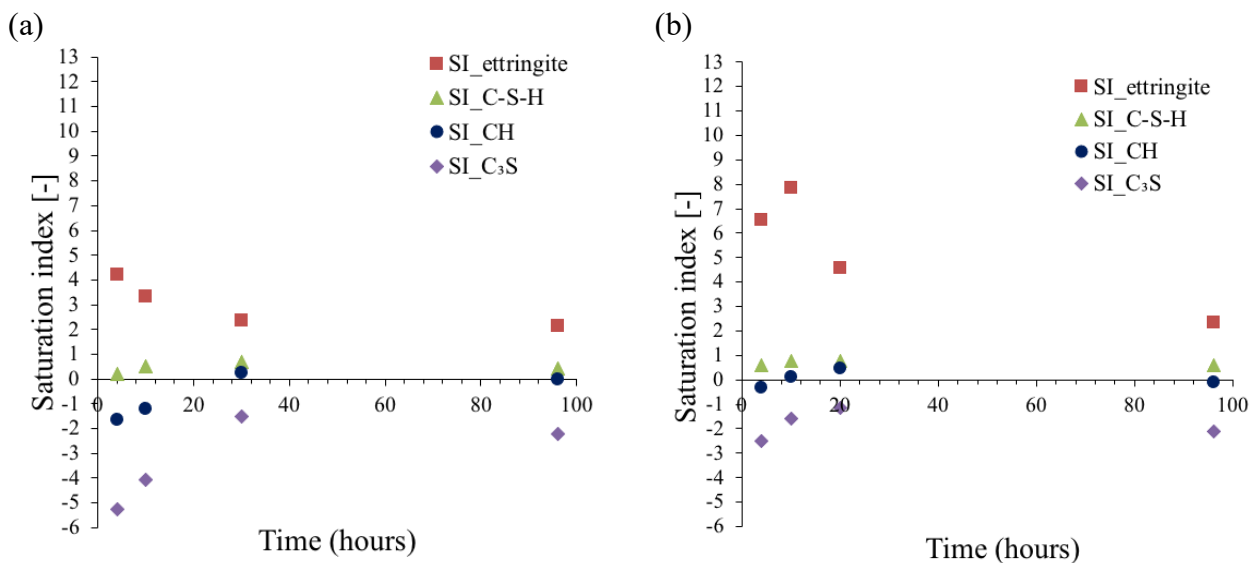
Fig. 4-11 Saturation indices of ettringite, C-S-H, CH and C₃S for LC³-10%(ACAC1.7,Cs) (a) and -10%(ACAC1.7,Cs)-2%CH (b).

4.3.3.6 Early age strength development

The compressive strength development up to 7 days for PC, LC³, LC³- 10%(ACAC1.7,Cs) and -10%(ACAC1.7,Cs)-2%CH are plotted in Fig. 4-12. Results show that a lower strength is obtained at 1 day with 2%CH addition compared to the blend without CH. This was not expected since the DoH $_{C3S}$ was enhanced at 1 day and similar ettringite content was formed. To understand the strength results the microstructure and the porosity were studied at 1 day.
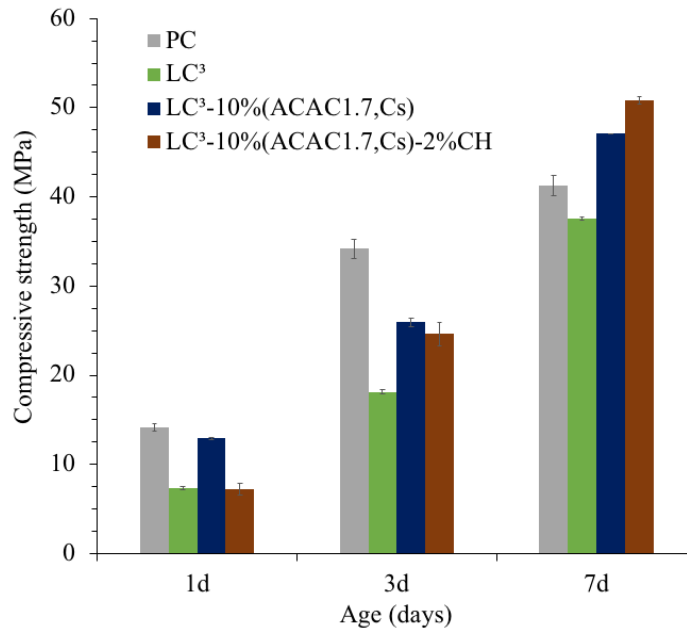
Fig. 4-12 Compressive strength development for PC, LC³, LC³- 10%(ACAC1.7,Cs) and -10%(ACAC1.7,Cs)-2%CH.

4.3.3.7 Microstructure observation at 1 day

The microstructures at 1 day for LC³- 10%(ACAC1.7,Cs) and -2%CH are shown respectively in Fig. 4-13(a) and (b). For LC³- 10%(ACAC1.7,Cs) blend, clear needles of ettringite, homogenously distributed, are observed. Portlandite is not observed. This is in agreement with portlandite quantification XRD-Rietveld result at 1 day. Although similar amounts of ettringite are reached at 1 day, it is not possible to observe it well in the blend with calcium hydroxide. However, portlandite clusters dispersed in the microstructure (indicated by red arrows) can be clearly seen. In-situ XRD quantification results in Fig. 6-6(b) showed that after full consumption of the initially added calcium hydroxide (after 2.8 hours), it starts to reform after 22.5 hours of hydration. This means that the observed portlandite is the hydration product that results from C₃S hydration. Furthermore, it is clear that the two investigated blends show a different distribution of phases. This indicates an effect of calcium hydroxide on the phase distribution. The reason is not clear.

(a)

(b)
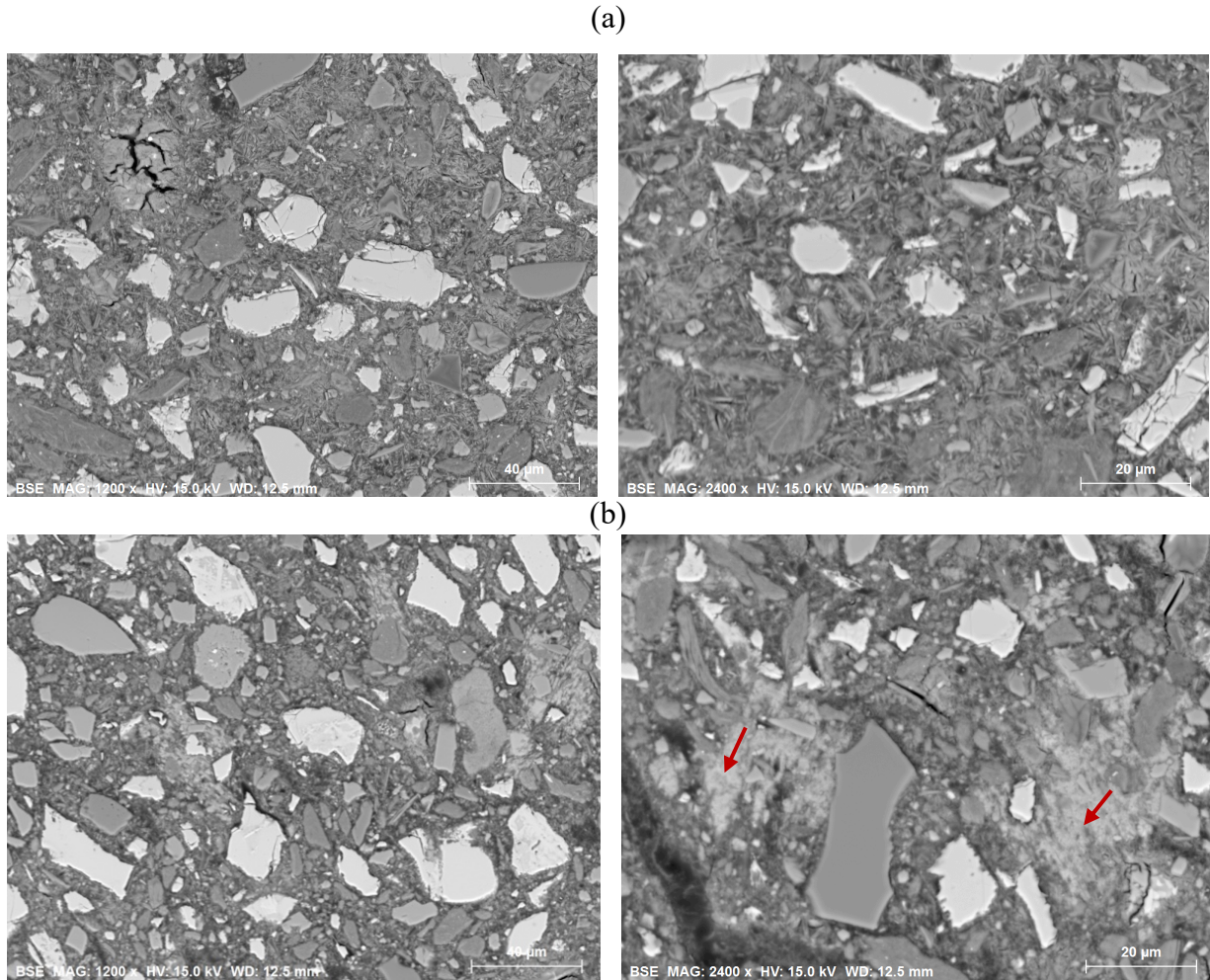
Fig. 4-13 SEM-BSE micrographs of LC³- 10%(ACAC1.7,Cs) (a) and -10%(ACAC1.7,Cs) -2%CH (b) at 1 day for 1000x and 2400x magnification.

4.3.3.8 SEM-EDS mapping

SEM-EDS mapping together with image analysis was used to see if there is any difference in the phase distribution Fig. 4-14(a) and (b) present results for LC³- 10%(ACAC1.7,Cs). As indicated on the Al/Ca and Si/Ca plot, the EDS mapping shows clusters of ettringite in Fig. 4-14(b). The blue mask selected from the ratio plots shows ettringite on the BSE image in Fig. 4-14(a). The pink mask selected from the ratio plot shows only calcite on the BSE image confirming again the absence of portlandite. Regarding the blend with 2%CH, results are shown in Fig. 4-15(a) and (b). In addition to limestone, portlandite can be seen and a small region of pure ettringite was observed.

(a) (b)
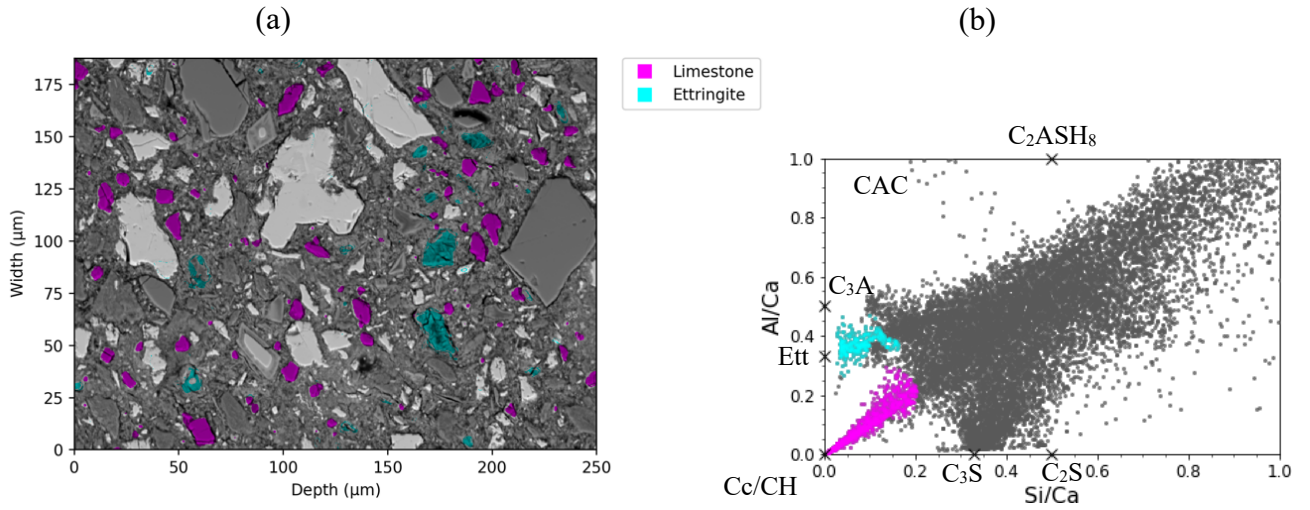
Fig. 4-14 The mask of ettringite, limestone and portlandite in SEM-BSE image of LC^3-10%(ACAC1.7,Cs) (a) and the ratio plot of Al/Ca vs. Si/Ca (b) at 1 day.

(a) (b)
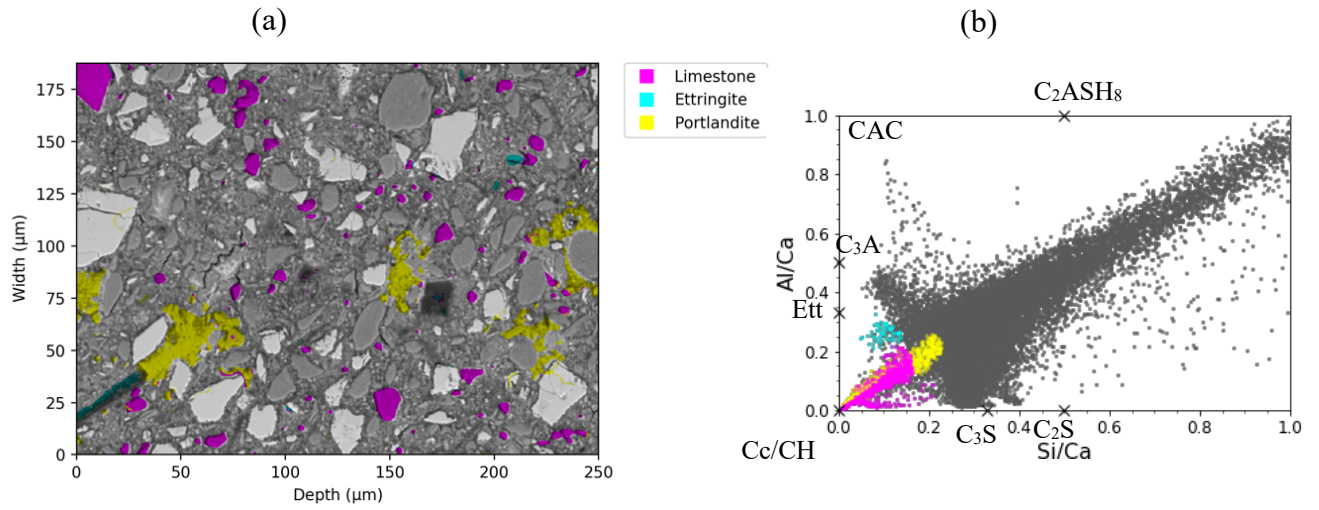
Fig. 4-15 The mask of ettringite, limestone and portlandite in SEM-BSE image of LC^3-10%(ACAC1.7,Cs)-2%CH (a) and the ratio plot of Al/Ca vs. Si/Ca (b) at 1 day.

4.3.3.9 Porosity characterization at 1 day

Fig. 4-16 shows MIP cumulative pore volumes for LC^3- 10%(ACAC1.7,Cs) and -2%CH blends after 1 day of hydration. Both systems have similar total accessible porosity by MIP. The critical pore entry diameter is smaller with 2%CH than without CH. This could be explained by the enhanced C$_3$S hydration for the blend with 2%CH. The pore fraction ranging above 0.1μm is much more important in the blend with CH addition. Although it improves the degree of hydration of C$_3$S at 1 day, calcium hydroxide addition seems to impact the phase distribution within the microstructure. This has a direct impact on the population of porosity present in the system and consequently the strength at 1 day. The reason of such an effect was not further investigated.
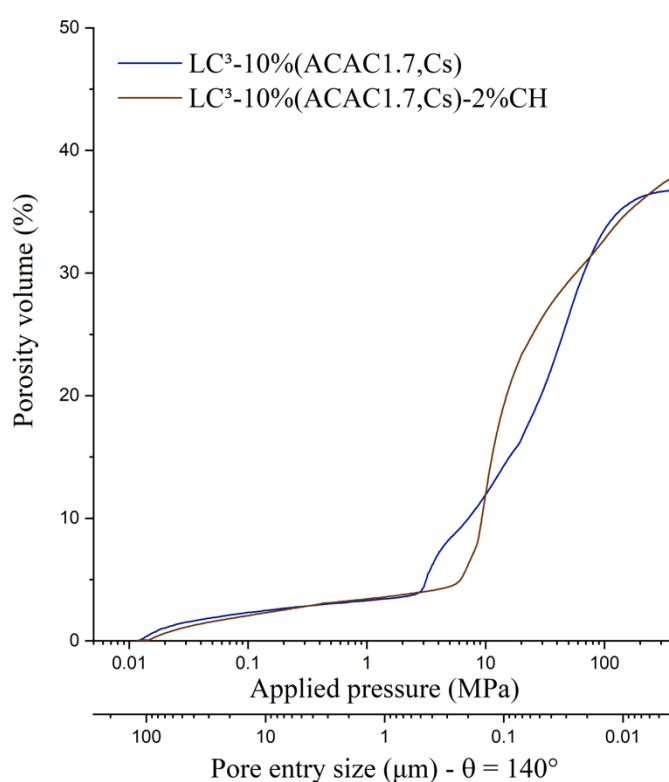
Fig. 4-16 Cumulative pore volume curves for LC^3- 10%(ACAC1.7,Cs) and -10%(ACAC1.7,Cs) -2%CH blends at 1 day.

4.4 Conclusions

This study investigates the reasons of the delay of C$_3$S hydration in LC^3-10%(ACAC1.7,Cs) blend. Based on the results presented in this chapter, the following conclusions can be drawn:

- The C/A ratio of the CAC is the key factor. The lower C/A ratio of ACAC1.7 leads to less calcium ions released from CAC dissolution in the pore solution compared to ACAC2.2.

- It seems that a critical calcium concentration in the pore solution and more precisely a positive saturation index with respect to portlandite is needed to trigger the C$_3$S hydration.

- When calcium hydroxide was added, results showed an enhancement of the degree of hydration of C$_3$S while the ettringite amount remained unchanged. Pore solution results showed an increase in the calcium concentration compared to the reference system (without CH addition). The enhancement of the C$_3$S hydration was linked to a supersaturation with respect to CH that was reached faster.

- It was also found that despite having a low aluminum concentration at 4 and 10 hours in the blend with 2%CH addition, the C$_3$S hydration was not enhanced during that time. This demonstrates that the presence of aluminum ions the pore solution is not the reason for the delay of C$_3$S hydration in the system studied.

- Although the C$_3$S hydration was enhanced and a similar amount of ettringite was formed, the strength performance at 1 day was decreased compared to the blend without CH. The CH addition impacts the distribution of hydrates within the microstructure but the reasons leading to lower strength are unclear.

4.5   Appendix

Table 4-3 The Na, K, Ca, Al, Si, SO$_4$ and hydroxide concentrations in the pore solution and pH of LC^3- 10%(ACAC2.2,Cs), -10%(ACAC1.7,Cs) and -10%(ACAC1.7,Cs-2%CH).

Sample	Extraction time (hours)	Ion concentrations (mmol/L)							pH
		Na	K	Ca	Al	Si	SO$_4$	OH-	
LC^3-10%(ACAC2.2,Cs)	4	379.50	256.28	20.38	0.1	0.004	209.39	200	13.2
	11	333.91	247.34	3.034	0.004	0.22	24.89	300	13.3
	17	353.48	284.09	2.59	0.08	0.23	5.69	400	13.5
	52	316.33	290.69	0.65	1.3	0.30	8.54	720	13.8
LC^3-10%(ACAC1.7,Cs)	4	338.66	193.36	0.51	6.2	1.68	207.44	80	12.9
	10	351.58	265.45	0.63	1.4	3.03	205.08	170	13.2
	30	391.71	325.64	1.02	0.3	0.51	9.72	720	13.8
	96	325.67	289.51	0.68	1.4	0.41	5.87	410	13.5
LC^3-10%(ACAC1.7,Cs)-2%CH	4	323.91	215.15	10.72	0.004	0.28	234.34	100	12.8
	10	378.26	248.24	2.99	0.21	0.39	155.46	200	13.3
	20	337.59	238.44	3.49	0.004	0.21	80.95	300	13.4
	96	271.18	218.52	0.08	1.15	0.62	5.39	490	13.6
	140	198.33	145.87	0.55	3.77	0.81	4.93	290	13.4

Chapter 5   Understanding the late age strength of LC³-CAC blends

5.1   Introduction

In Limestone calcined clay cement (LC³), it is known that neither clinker nor metakaolin completely react at late ages (w/b=0.4) [63]. Recently, Briki et al. showed that neither the lack of portlandite nor aluminum in the pore solution are responsible for the slowing down of the metakaolin reaction at late age [104]. Relative humidity measurements of LC³ at 28 days showed that above a pore radius of 13nm pores are empty. This is one of the reasons which explains the limited further reaction at late age.

The use of alkali is known to improve the early age strength of LC³, but has a negative impact on the late age strength [28]. In Chapter 3, it was shown that the incorporation of CAC and Cs improved the strength of LC³ at all ages. The higher early age strength in LC³-CAC blends was linked to the ettringite formation during the first hours of hydration.

This chapter focuses on understanding the late age strength of LC³-CAC blends. The hydration over longer periods of time (up to 1 year) was investigated. Powerful techniques, such as X-Ray diffraction (XRD), scanning electron microscopy (SEM), mercury intrusion porosimetry (MIP), relative humidity (RH) measurements and transmission electron microscopy (TEM) were used. Thermodynamic modelling with Gibbs energy minization software (GEMS) was also used to determine the phase assemblage.

5.2   Materials and methods

5.2.1 Raw materials

Same materials to those detailed in Chapter 3 are used.

5.2.2 Mixture deisgn and sample preparation

The mix compositions of the investigated systems are shown in Table 5-1. Cement paste samples were used to study hydration by X-ray diffraction (XRD), scanning electron microscopy (SEM), mercury intrusion porosimetry (MIP) and transmission electron microscopy (TEM). Pastes were prepared with two water to binder ratios w/b = 0.4 and 0.3. A high-speed mixer was used to mix the cement paste for 2 minutes at 1600rpm. Samples were cast in a 50mL cylindrical polyethylene containers (diameter: 35mm), which were sealed with parafilm and a lid. Samples were stored until

365 days of hydration in a controlled temperature room (20°C). At a specific testing age, two slices of 2-3mm thickness were cut from the hardened cement paste using a diamond saw and water as lubricant.

Mortar samples were prepared according to the European EN196-1 standard. The water to binder ratios were: 0.5 and 0.35. Mixing was carried out at room temperature. Mortars were cast in steel moulds, then, demolded after 1 day. Prisms were cut to 4x4x4cm cubes and were kept in plastic bags in a humidity chamber ($\sim$ 95%) until the required testing age.

For blends with low water content, a w/b=0.3 (paste) and 0.35 (mortar), polycarboxylate superplasticizer (Mapei Dynamon SP914) was used. The amount required depends on the workability of the blend, the maximum used content is 2% of total solid mass.

Table 5-1 Mix compositions of the investigated systems (wt. %).

Notation	PC	CAC	Cs	CClay	CsH$_2$	Cc	Citric acid	Na$_2$CO$_3$
PC	100	-	-	-	-	-	-	-
LC³	52.66	-	-	25	2.34	20	-	-
LC³-10%(ACAC1.7,Cs)	52.15	5	5	24.76	2.34	9.81	0.33	0.61
LC³-10%(ACAC2.2,Cs)	52.15	5	5	24.76	2.34	9.81	0.33	0.61

5.2.3 Methods

Compressive strength tests were carried out according to EN196-1. Strengths were measured at 7, 28, 90 and 365 days with a loading rate of 2.4kN/s. Three cubes were tested for each age. Compressive strength tests were carried on mortars at two w/b: 0.35 and 0.5.

XRD was carried out on fresh slices to characterize the crystalline phases after the hydration. More details can be found in Chapter 3.

The phase assemblage at 28 days with a w/b=0.4 was calculated with GEMS-PSI software [54] with the Cemdata18 database [55] using the CSHQ model to represent C-S-H. The degree of hydration of anhydrous phases, limestone, anhydrite and gypsum from XRD Rietveld and the degree of reaction of metakaolin at 28 days (determined in chapter 3) were used as input for the calculation. Amorphous CAC was assumed to completely react in these simulations. The volume fraction (%) of the present phases was calculated based on the phase mass given by GEMS. The C-S-H water content was corrected according to A.C.A. Müller et al. (Ca$_z$ (Si$_y$, Al$_{(1-y)}$) O$_{(z+1/2y+3/2)}$ (H$_2$O)$_x$) with H$_2$O/Ca=2.8) [105] and the bulk density of C-A-S-H was 1.95 g/cm³ [105]. The remaining water volume fraction was estimated by subtracting the water volume consumed for all hydrates (ettringite, C-A-S-H, AFm phases, portlandite, etc.) from the initial water volume. Empty pores (voids) form during hydration reactions. The volume of empty pores (due to chemical shrinkage) was calculated by subtracting the initial volume (clinker, calcined clay, limestone and water, etc.) from the final volume (hydrates, unreacted clinker, unreacted calcined clay, unreacted limestone and pore solution).

The hydration was stopped with isopropanol as it is the best method to conserve the microstructure [67].

After stopping the hydration, the following experiments were carried out:

Scanning electron microscope analysis (SEM) was carried-out using a FEI Quanta 200 equipped with Bruker XFlash 4030 EDS detector. Back scattered electron (BSE) images were linked to EDS mapping by the edxia platform [99]. Based on ratio plots of Al/Ca vs. Si/Ca and S/Ca vs. Al/Ca obtained from EDX maps, representative points were attributed to the present phases. This allows the distribution of the main hydrates to be observed within the microstructure of LC³-CAC blends and to compare it with the microstructure of LC³. Maps were collected with an accelerating voltage of 12kV, a working distance of 12.5mm and at 1000x magnification. SEM samples were prepared as follows: a small piece of sample was impregnated in epoxy resin and a hardener (EpoTek 3018OZ). After hardening for 1 day, samples were polished with diamond particles of 9, 3 and 1μm. More details about SEM samples preparation can be found in Chapter 3.

Mercury intrusion porosimetry (MIP) was used. A pressure up to 400 MPa was applied to intrude mercury into small porosities (~2nm). The contact angle between the cement paste and the mercury was assumed to be of 140°.

Internal relative humidity (RH) measurements were conducted on cement paste at 28 days, with water activity probes from Rotronic. The device has 3 channels each one has its own water activity and temperature sensor. To maintain the temperature constant at 20°C, water was circulated around each channel. RH data were collected at 28 days every 5 minutes. K_2SO_4, K_2NO_3, KCl and NaCl saturated solutions were used to calibrate the sensors before every experiment. Cement paste samples were cast according to 5.2.2. At 28 days, cement pastes were crushed into small pieces (~5mm) and were introduced into plastic cylinders. Then, plastic containers were placed inside the channel. To ensure an accurate measurement, every sample was measured 3 times.

The decrease of the RH during hydration is due to the desaturation of pores due to chemical shrinkage (RH_k) and to the increase of dissolved salt in the pore solution (RH_s). RH can be expressed according to Eq.1 [106].

$$RH = RH_k . RH_s \qquad (1)$$

In order to determine the RH_s needed to calculate RH_k, the pore solution was extracted after 28 days. Pore solutions were collected by a mechanical press at 800kN. To make sure that there are no small particles, solutions were filtered using a 0.2 μm pore size filter. Relative humidity measurement of the pore solution was monitored for 3 days for an accurate RH_s determination.

From the internal RH measurement of the cement paste (RH) and of the pore solution (RH_s), the radius of the largest capillary pore filled with water was calculated according to Eq. 2. A detailed explanation is provided in [106].

$$r = \frac{2M\gamma}{ln\left(\frac{RH}{RH_s}\right)\rho RT} \qquad (2)$$

Where M is the molar weight of water (0.01802 kg/mol), γ is the surface tension of water (0.073 N/m). ρ is the density of water (1000 kg/m³). R is the ideal gas constant (8.314 J/mol K) and T is the absolute temperature (293.15K, 20°C). RH is the measured internal relative humidity of the cement paste at 28 days of hydration.

Transmission electron microscopy (TEM) was used to observe the morphology of hydrates particularly the C-A-S-H morphology. A FEI Tecnai Osiris was used (CIME, EPFL) with an XFEG source. The EDS detector was used. In the scanning mode (STEM) mode, images are formed using the bright field (BF) and the high annular dark field (HAADF) detectors. To avoid beam damage a small spot size with a low accelerating voltage (80kV) were used. Several zones of interest were identified and quantified with EDS to obtain their composition. For TEM observations, TEM lamellae were prepared as follows: Samples were embedded in a hard resin (Gatan G2) and cut to slices of 2x2x0.7mm³ size using a diamond saw. Following that, a mechanical polishing using the Tripod method was used. Then, Focused ion beam (FIB) technique using a Zeiss NVision 40 dual-beam microscope was used to obtain a several thin regions (100-150nm) in the same embedded sample.

The cement paste study was done with a w/b 0.4. Only MIP was carried out on cement paste at both a w/b of 0.4 and 0.3.

5.3   Results and discussion

5.3.1   Late age compressive strength

Fig. 5-1 shows the compressive strength result for PC, LC³, LC³-10%(ACAC2.2,Cs) and -10%(ACAC1.7,Cs) at 7, 28, 90 and 365 days, w/b=0.5. The results show an increase of the compressive strength of LC³-CAC blends between 7 and 28 days. Afterwards, the compressive strength keeps slowly increasing to reach 68 MPa and 71 MPa after 365 days respectively for LC³-10%(ACAC2.2,Cs) and -10%(ACAC1.7,Cs). This suggests that the hydration is continuing in LC³-CAC blends. For LC³ blend, the strength increases up 54 MPa at 90 days and then slightly decreases at 365 days. At 365 days, the maximum strength reached for PC and LC³ is respectively ~13% and ~25% lower compared to LC³-CAC blends.
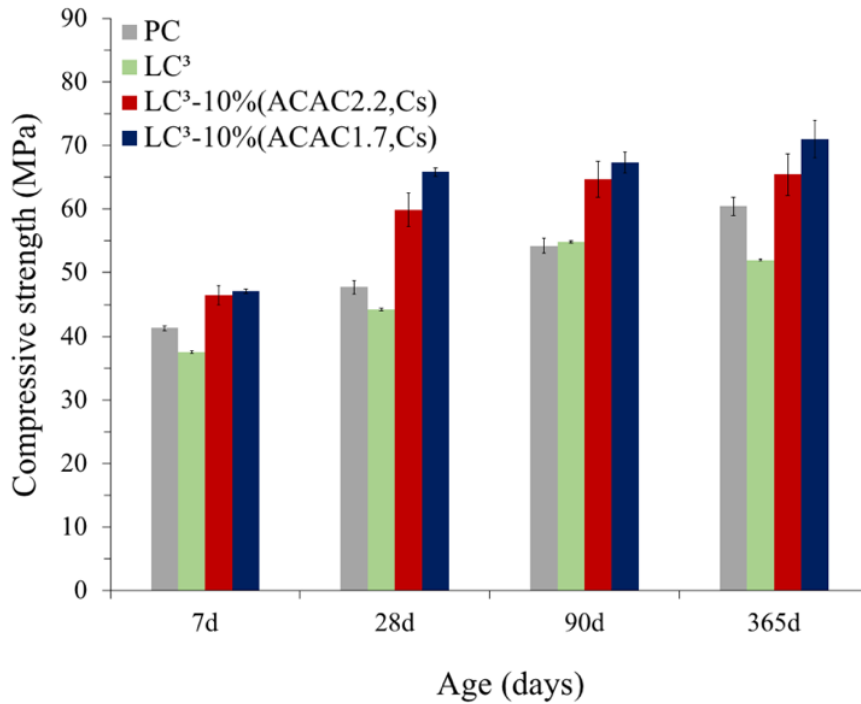
Fig. 5-1 Compressive strength development for PC, LC³, LC³-10%(ACAC2.2,Cs) and -10%(ACAC1.7,Cs) at 7, 28, 90 and 365 days, w/b=0.5.

5.3.2 Understanding the late age strength

5.3.2.1 Phase mass and volume fraction

Phase assemblages of LC³, LC³-10%(ACAC2.2,Cs) and -10%(ACAC1.7,Cs) at 28 days of hydration with a w/b=0.4 were calculated. The results are shown in Fig. 5-2(a). For the investigated systems, the thermodynamic calculations predict the formation of C-S-H and ettringite as the main hydrates. Portlandite and AFm phases are also predicted but in lower amounts. Less unreacted clinker and a higher amount of C-S-H is observed in LC³ compared to LC³-CAC blends. A higher ettringite amount is calculated to be present in LC³-CAC blends than LC³. This is in agreement with the quantification from XRD-Rietveld. Based on these predictions, free water (gel and/or capillary water) is still present at 28 days in all the investigated blends. The volume fraction of the phases was calculated and the results are shown in Fig. 5-2(b). C-S-H, ettringite and AFm phases occupy 49% of the total volume in LC³ while they occupy 54% and 56% of the total volume respectively in LC³-ACAC2.2 and -ACAC1.7 blends. This shows that the increase of strength in LC³-CAC blends comes from a higher volume of hydrates. Also, it can be seen that ettringite fills twice the volume in LC³-CAC blends compared to LC³.
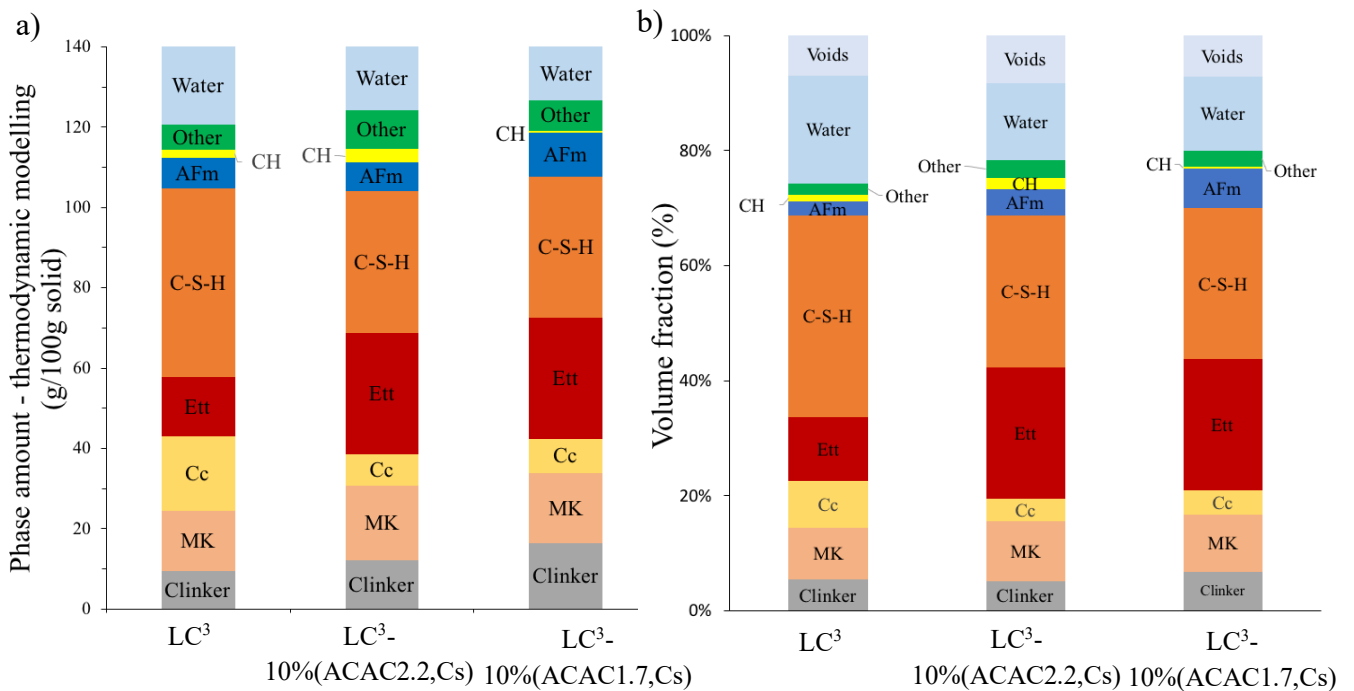
Fig. 5-2 Phase mass from thermodynamic modelling (a) and calculated volume fraction of predicted phases (b) at 28 days for LC³, LC³- 10%(ACAC2.2,Cs) and -10%(ACAC1.7,Cs): MK (metakaolin),Cc (calcite), AFm (Hc+Mc), CH (portlandite), Ett (ettringite), Other (brucite + hydrogarnet), w/b= 0.4.

5.3.2.2 Phase distribution

Fig. 5-3 shows the EDS mapping results together with BSE images for LC³ (a), LC³- 10%(ACAC2.2,Cs) (b) and -10%(ACAC1.7,Cs) (c) at 28 days. For all systems, it can be seen that AFm (Hc and Mc) phases forms in the space of reacted cement grains. For LC³ blend, a very small area of C-S-H/AFt intermixing is observed. LC³-CAC blends show extended intermixed regions of C-S-H and ettringite (tens of micron length areas). Due to its good space filling, it can be seen that ettringite is well distributed within the microstructure. It is also more present in LC³-CAC than in LC³.

a)

b)

c)
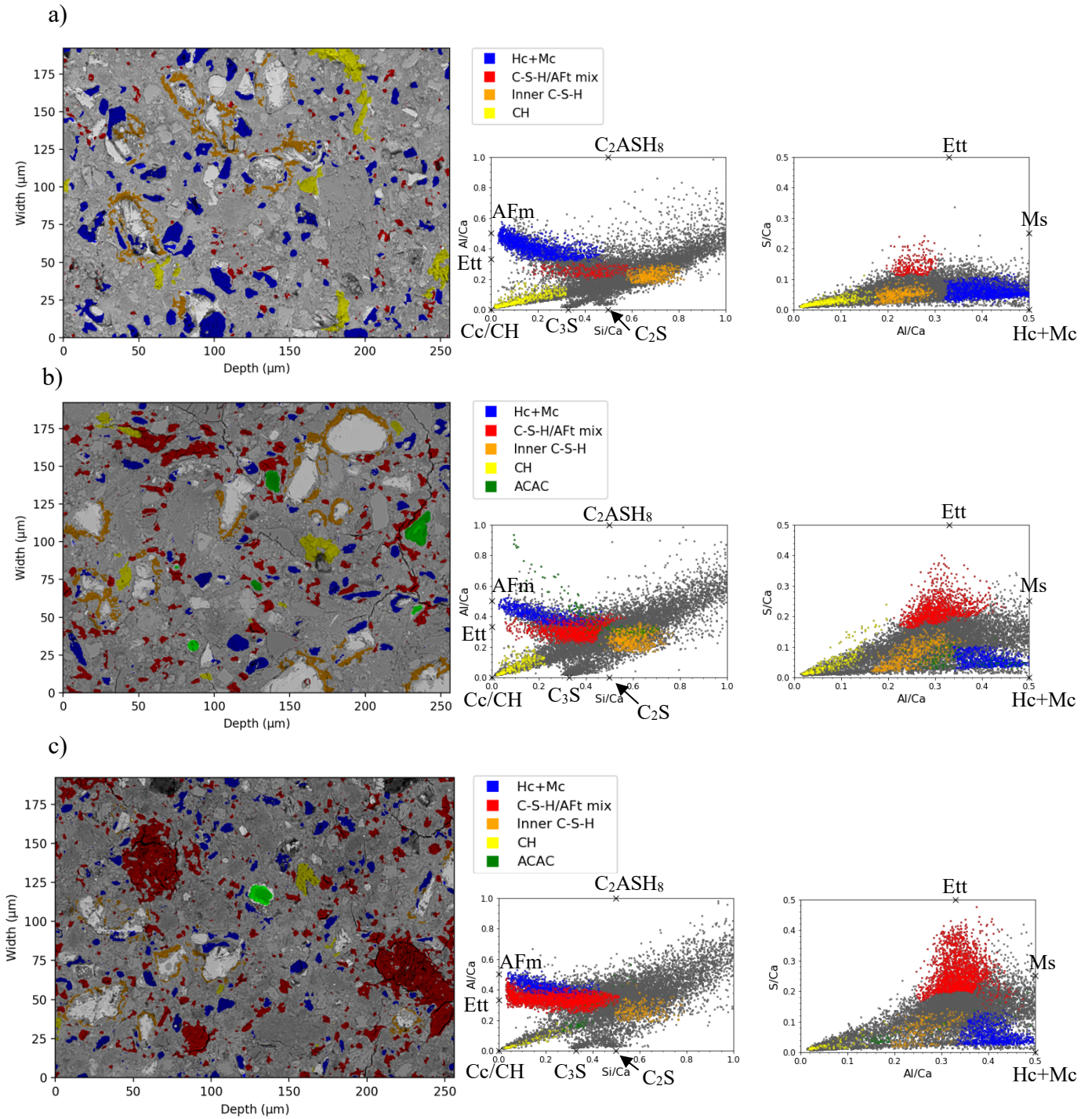
Fig. 5-3 Identification of Hc+ Mc, C-S-H/AFt mix, inner C-S-H, CH and ACAC using BSE images, Al/Ca vs. Si/Ca and S/Ca vs. Al/Ca for LC³ (a) LC³-10%(ACAC2.2,Cs) (b) and -10%(ACAC1.7,Cs) (c).

5.3.2.3 Correlation between total porosity vs. strength

Fig. 5-4 shows MIP results at 28 days for w/b =0.4 (a) and w/b=0.3 (b) for PC, LC³, LC³-10%(ACAC2.2,Cs) and 10%(ACAC1.7,Cs). The total porosity of the investigated systems is shown in Table 5-2. Results show that LC³-CAC blends have a lower total porosity than PC and LC³ either with a w/b= 0.4 or 0.3.
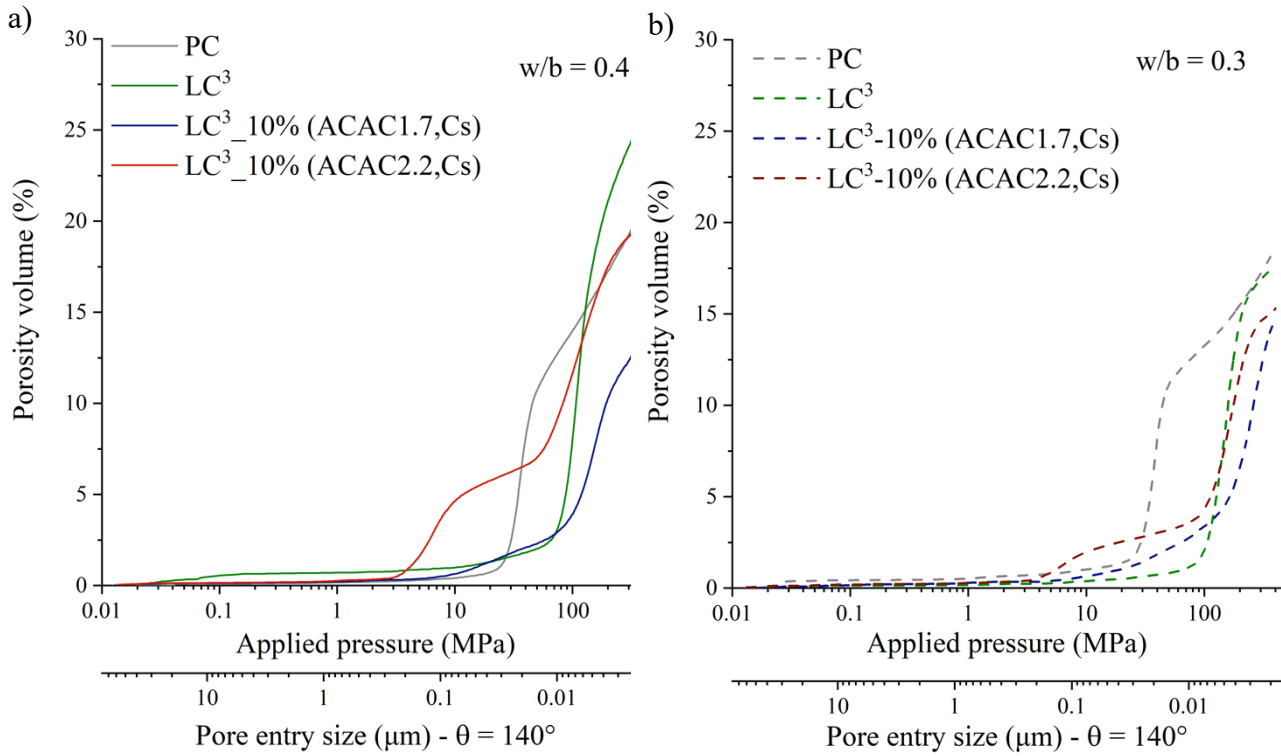
Fig. 5-4 Cumulative pore volume curves for PC, LC³ and LC³-10%(ACAC2.2,Cs) and 10%(ACAC1.7,Cs) at 28 days, w/b=0.4 (a) and w/b=0.3 (b).

Table 5-2 Total porosity for all the investigated systems at 28 days.

Sample	w/b	Total porosity (%)
PC	0.4	21
LC³	0.4	26
LC³-10%(ACAC1.7,Cs)	0.4	13
LC³-10%(ACAC2.2,Cs)	0.4	20
PC	0.3	19
LC³	0.3	18
LC³-10%(ACAC1.7,Cs)	0.3	15
LC³-10%(ACAC2.2,Cs)	0.3	15

Fig. 5-5 shows the relationship between the total porosity from MIP, the porosity from GEMS including voids and the compressive strength of LC³, LC³-10%(ACAC2.2,Cs) and -10%(ACAC1.7,Cs) at 28 days of hydration. Overall, the strength is linearly correlated with the total porosity. This shows that it is possible to explain the compressive strength by the the total porosity. A better correlation between the compressive strength and the porosity from GEMS+voids is obtained.
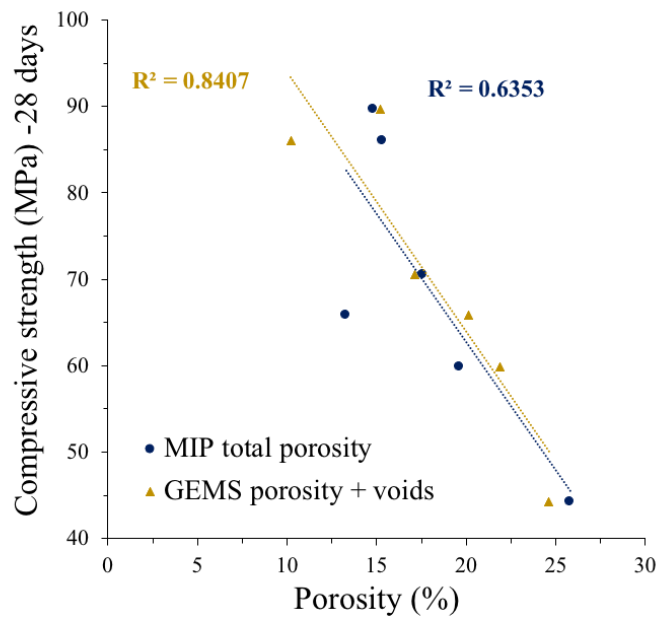
Fig. 5-5 Compressive strength vs. total porosity from MIP and GEMS porosity+voids for PC, LC³, LC³-10%(ACAC2,2,Cs) and -10%(ACAC1.7,Cs).

5.3.3 Saturation limit of water filled pores

The limit pore radius between empty and filled pores with water was estimated from RH measurements. The data collected from cement paste measurements of PC, LC³ and LC³-10%(ACA2.2,Cs) with w/b=0.4 are ploted in Fig. 5-6. The measured RH is assumed to be stable after 40 hours of measurement. The average value after 40 hours is around 82.3, 80.6, 75.4% respectively for PC, LC³ and LC³-10%(ACA2.2,Cs). The RH_s from the measurement of the relative humidity of the pore solution extracted at 28 days, is 95.6, 96.4, 96.5% respectively for PC, LC³ and LC³-10%(ACA2.2,Cs). The RH_k, caused by desaturation of pores, was calculated by dividing RH_k to RH_s according to Eq.1. The pore radius of the largest capillary pore filled with water at 28 days, calculated according to Eq.2, is 6.8, 5.9, 4.3 nm respectively for PC, LC³, LC³-10%(ACA2.2,Cs). Above this limit, pores are filled with vapor and air instead of water.
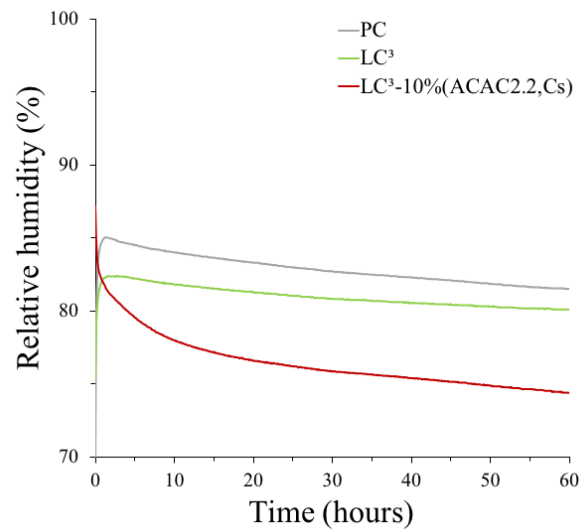
Fig. 5-6 Relative humidity of cement paste at 28 days for PC, LC³ and LC³-10%(ACAC2.2,Cs).

Fig. 5-7 shows the cumulative pore volume curves at 28 and 90 days for PC, LC³ and LC³-10%(ACA2.2,Cs) with w/b=0.4. For all the investigated systems, at 28 days, it can be seen that the critical pore entry radius is higher than the calculated limit pore radius above which there is no more water. The comparison of the MIP data at 28 days with those at 90 days shows that for PC and LC³ the critical entry radius remains the same. For LC³- ACAC2.2 blend, where the critical pore entry radius is larger than the calculated pore limit radius, the critical pore entry radius is reduced at 90 days. Recently, Zunino et al. suggested that in pores bigger than the limit pore size hydration and precipitation continues in the pore solution film that covers the surface [107]. In our case as metakaolin is still available, the increase of metakaolin reaction can explain this refinement of porosity.
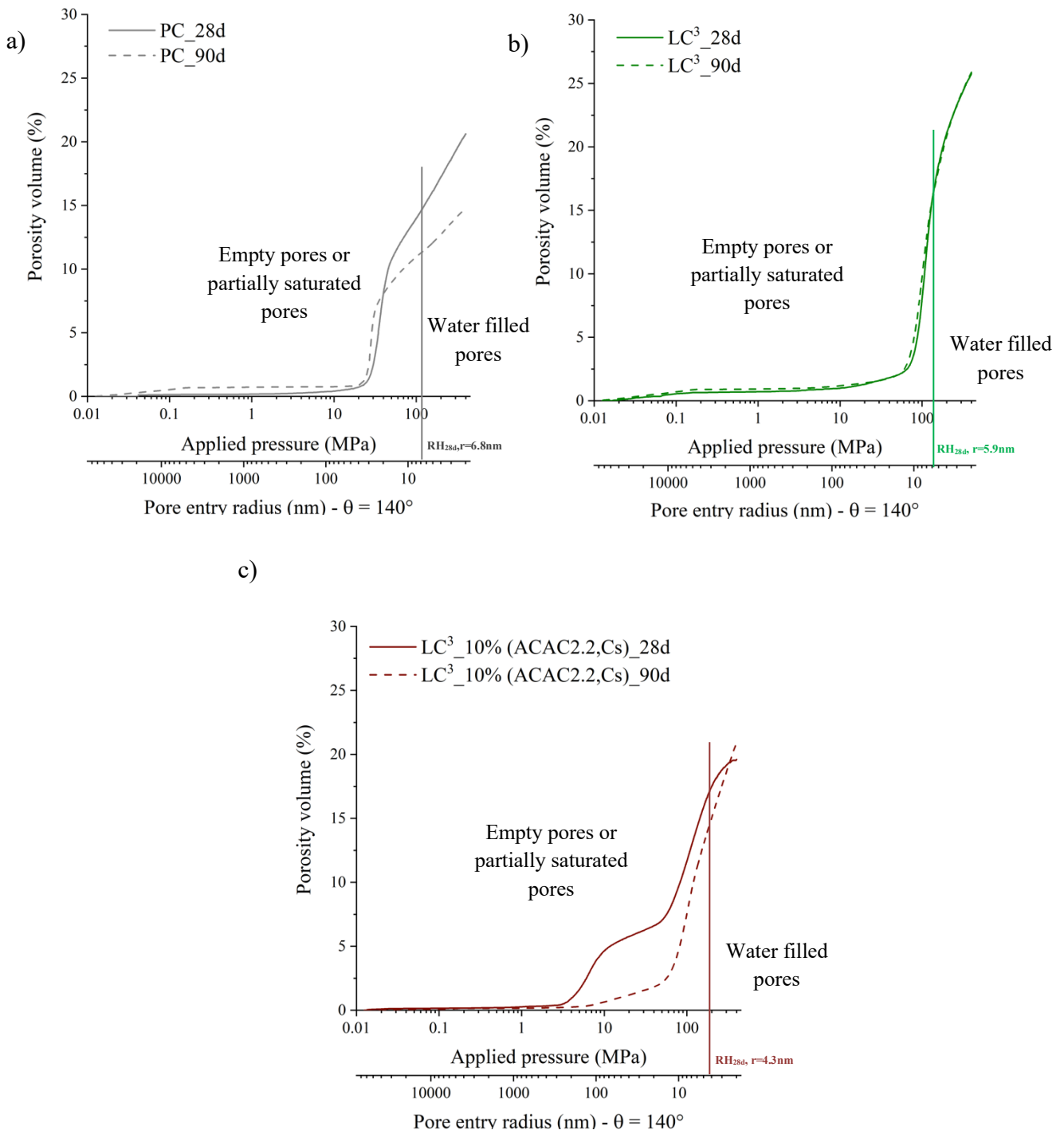
Fig. 5-7 Cumulative pore volume curves for PC, LC³ and LC³-10%(ACAC2.2,Cs) at 28 and 90 days, w/b= 0.4.

5.3.4 CA-S-H morphology

The microstructure of LC³ from [108] is shown in Fig. 5-8(a). The microstructure LC³-10%(ACAC2.2,Cs) at 28 days of hydration in bright field mode (BF) and high angle annular dark field (HAADF) mode is shown in Fig. 5-8(b). A fibrillar C-A-S-H morphology is observed in both

blends showing that there is no influence of CAC and Cs incorporation on the morphology of C-A-S-H. Ettringite (AFt) is also observed in LC³-10%(ACAC2.2,Cs).

a)

b)
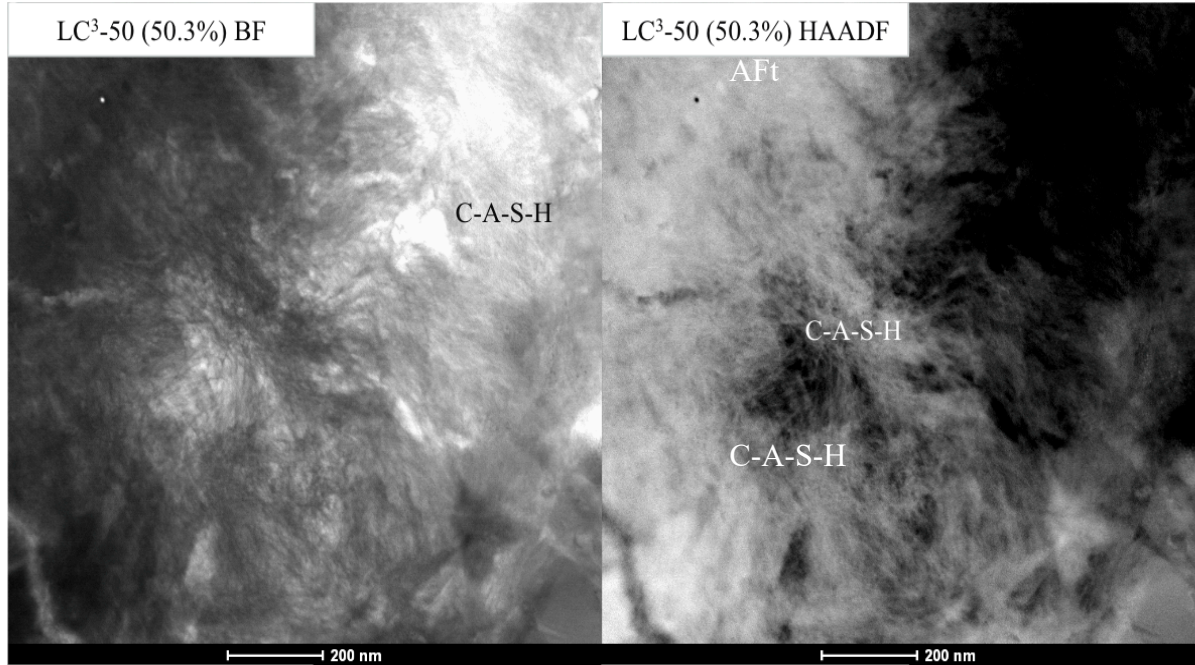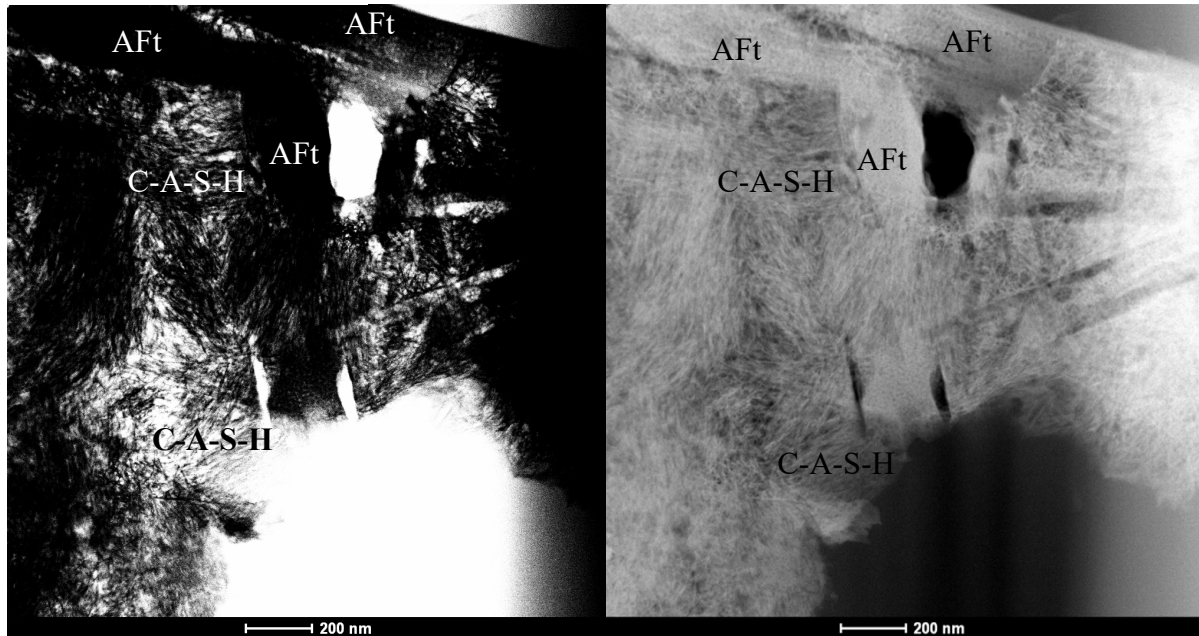
Fig. 5-8 Microstructure of LC³ from [108] and LC³-10%(ACAC2.2,Cs) at 28 days in bright field (BF) and high angle annular dark (HAADF) modes.

5.4   Conclusions

This ongoing study focuses on understanding the high late age strength of LC³-CAC blends. Based on the results the following preliminary conclusions can be drawn:

- Thermodynamic predictions showed that a higher ettringite amount is present in LC³-CAC blends than LC³ which agrees well with XRD-Rietveld results (Chapter 3, Fig. 3-5 and Fig. 3-11). Predictions also showed that free water was still present at 28 days in all the investigated mixes.

- The calculated volume fraction of the predicted phases from thermodynamic modelling showed that the main hydrates (ettringite, C-S-H and AFm) occupy 49% of the total volume in LC³ while they occupy around 55% of the total volume in LC³-CAC blends. This explains the high strength of LC³-CAC blends. Additionally, ettringite occupies twice the volume in LC³-CAC blends compared to LC³. This was confirmed by SEM-EDS mapping which showed that ettringite is well distributed and highly intermixed with C-S-H in LC³-CAC blends.

- A good correlation was observed between the strength and the porosity. This shows once again that the increase of strength comes from the reduction of porosity due to the higher volume of hydrates.

- Relative humidity measurements showed that, for LC³-ACAC2.2 blend, the critical pore radius was further refined between 28 and 90 days, although the critical pore radius was higher than the calculated saturated pore limit. This demonstrates that the hydration is continuing in LC³-CAC blend. The key question is why for PC and LC³ the long-term strength is limited while it is not the case for LC³-CAC blends.

- Regarding the morphology of the C-A-S-H, TEM images showed a fibrillar morphology for both LC³ and LC³-ACAC2.2 systems. So, there is no influence of the CAC and Cs on the C-A-S-H morphology.

Chapter 6   Durability properties of LC^3-CAC blends

Note: This chapter is based on an article in preparation for submission to a peer reviewed journal

Contribution of the doctoral candidate: conceptualization, methodology, experiments, analysis and writing of the first manuscript draft.

Abstract

In the following chapter, the chloride and carbonation resistance of PC, LC^3 and LC^3-CAC blends are investigated. The mini-migration test method shows that LC^3-CAC blends have excellent results in terms of resistance to chloride ingress. Although they have higher CO_3-AFm content, less chemical binding in LC^3-CAC blends is observed compared to PC. A lower physically bound chloride in LC^3-CAC blend is obtained compared to PC and LC^3. The reason of the observed improvement seems to be related to the porosity refinement induced by CAC and Cs addition. However, the refinement of pores is not proportional to the degree of enhancement.

The natural carbonation study shows that LC^3 and LC^3-CAC blends have a lower carbonation resistance compared to PC. Among the investigated systems, LC^3-ACAC2.2 blend has the highest carbonation coefficient. The microstructure observation of LC^3 and LC^3-ACAC2.2 blends, shows a more porous network induced by carbonation. On the other hand, carbonation of PC is observed to lead to a less porous microstructure. Furthermore, compressive strength carried-out on mortar cubes after 6 months of forced carbonation shows that the carbonation of PC leads to an enhancement of strength. On the other hand, carbonation of LC^3 and LC^3-CAC blends leads to a decrease in strength. Despite the decrease of strength due to carbonation, LC^3-CAC blends still have at least similar strength to the non-carbonated specimen of PC.

6.1   Introduction

The durability of concrete is defined as its ability to resist to weathering and chemical attack without losing the required engineering properties. The main durability concerns for concrete infrastructure are corrosion of steel reinforcement due to the ingress of chlorides and carbon dioxide (CO_2) in concrete.

Chloride ions from de-icing salts or sea water can penetrate the reinforced concrete structure and can cause a depassivation of the steel reinforcement. The rate of the transport of chloride ions, generally, depends on the pore structure of concrete, the chloride binding capacity and the pore solution. Chloride can be chemically bound to AFm phases, where it readily displaces hydroxide, sulfate and carbonate in the AFm structures [109]. Limestone addition leads to ettringite stabilization and mono- and hemi- carboaluminates are formed instead of mono-sulfoaluminate. In this case, carboaluminate hydrates convert to Friedel's salt or to AFm phases containing chloride, carbonate and hydroxide [110]. In addition to chemical binding, chloride can physically adsorb on C-A-S-H [111]. The extent of adsorption depends on the C-A-S-H composition. It was found that higher Ca/Si ratio leads to higher chloride adsorption [112].

The replacement of a fraction of cement by Supplementary Cementitious Materials (SCMs) significantly contributes to lowering the CO_2 emissions and costs related to cement production [3]. SCMs incorporation generally enhances the chloride resistance of blends due to the porosity refinement of blended cements [113]. It has been reported that blends containing metakaolin are known to have a good capacity to bind chloride which is attributed to the chemical binding of chloride ions in Friedel's salt [114,115] and the physical binding into C-A-S-H [116]. Recently, Wilson et al. explained the improvement of the resistance to chloride ingress by a reduction of the pore connectivity and /or the pore solution conductivity [117].

To evaluate the chloride penetration, the bulk diffusion test is the most common approach. This method consists in fully immersing a specimen in a chloride source [118]. The penetration is unidirectional since the specimen is coated with epoxy resin except its surfaces. One of the limitations of this method is that it takes a long time (months to years).

Recently, a chloride mini-migration method has been proposed as a simple and fast method to estimate the effective diffusion coefficient (D_{eff}) at the cement paste scale [117]. The effective diffusion coefficient is estimated based on the chloride flow through the sample. This method can be supplemented by additional techniques to explain the obtained D_{eff} of the investigated systems.

In the case of carbonation, CO_2 from the air penetrates into the cement matrix and dissolves in the pore solution. As a result, carbonic acid (H_2CO_3) is formed that in turn dissociates into $HCO_3^-{}_{(aq)}$ and $CO_3^{2-}{}_{(aq)}$ according to Eq.1 and Eq.2.

$$CO_{2(g)} + H_2O_{(aq)} \rightarrow H_2CO_{3(sd)} \rightarrow H^+ + HCO^-_{3(aq)} \tag{1}$$

$$HCO^-_{3(aq)} \rightarrow H^+ + CO^{2-}_{3(aq)} \tag{2}$$
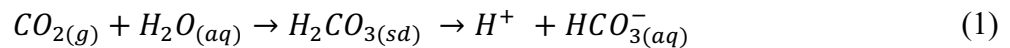
With sd: solid and aq: aqueous.

Aqueous carbon dioxide reacts with hydration products such as C-S-H, portlandite and ettringite to form carbonated phases [119,120]. In Portland cement, the main hydration products are C-S-H and portlandite. It is well known that portlandite buffers the pH to 12.5. This is ensured by releasing hydroxyl ions in solution. The reaction of CO_2 with portlandite in this system is the most important and leads to a reduction in alkalinity. The reaction proceeds in two steps: First portlandite dissolves (Eq.3). Then, calcite precipitates (Eq.4).

$$Ca(OH)_{2(s)} \rightarrow Ca^{2+}_{(aq)} + 2OH^-_{(aq)} \tag{3}$$

$$Ca^{2+}_{(aq)} + CO_3^{2-} \rightarrow CaCO_{3(sd)} \tag{4}$$
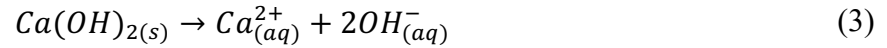
Carbonation of C-S-H seems to occur in parallel [121]. However, from a thermodynamical point of view carbonation of CH occurs first [122]. The decalcification of C-S-H leads to silica gel formation and calcite according to Eq.5 [123].

$$(CaO)_x.(SiO_2)_y.(H_2O)_z + xCO_2 \rightarrow xCaCO_3 + ySiO_2.(H_2O)_t + (z - yt)H_2O \tag{5}$$
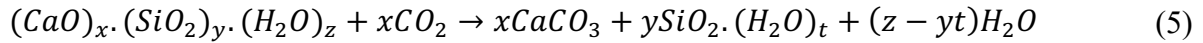
Apart from C-S-H and CH, ettringite can carbonate according to Eq.6. As a result, gypsum and alumina gel are formed [119].

$$3CaO.Al_2O_3.3CaSO_4.32H_2O + CO_2 \rightarrow 3CaCO_3 + 3(CaSO_4.2H_2O) + Al_2O_3.xH_2O + (26 - x)H_2O \tag{6}$$
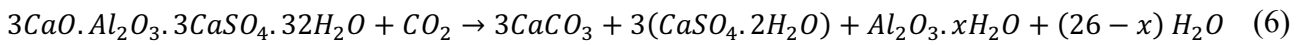
When carbonated the pH of the pore solution of hydrated cement is reduced. It goes from about 12.5 to below 9 [124]. It is well known that, at low pH, the protective oxide layer surrounding steel rebars breaks down and corrosion is initiated [125]. Blended cements with pozzolanic materials contain much less portlandite as it is consumed by the pozzolanic reaction of metakaolin and synergetic reactions (between calcined clay and limestone) [21,60,126]. As a consequence, higher carbonation depth is obtained at low calcium hydroxide blends.

Carbonation changes the pore structure and strength performance [127,128]. For ordinary Portland cement, it is well known that carbonation of phases in natural or accelerated conditions leads to a small decrease in porosity [129,130] and results in strength improvement [131]. This is explained by the positive difference in terms of molar volume between portlandite and calcite, which is the main carbonated hydrate. However, in blended cements, due to the lower calcium hydroxide content, carbonation of other hydrates also takes place and leads to a coarsening of the pore structure and an increase of the total porosity [130]. Table 6-1 shows the variation of the solid volume (%) calculated based on the density of the main hydrates from [55]. For example, the carbonation of portlandite and $C_{1.67}SH_{2.1}$ leads respectively to an increase of 11% and 8% of the solid volume. However, the carbonation of $C_{1.33}SH_{2.2}$ and ettringite leads respectively to a decrease of 5% and 48% of the solid volume.

Table 6-1 Properties of portlandite, C-S-H, ettringite and calcite from [16,55].

Mineral	Molar volume (cm³/mol)	Variation of solid volume (%)
Portlandite	33	+11
C-S-H ($C_{1.67}SH_{2.1}$)	78	+8
C-S-H ($C_{1.33}SH_{2.2}$)	76	-5
Ettringite	707	-48
Calcite	37	-

The carbonation rate varies with the relative humidity (RH). Moisture content is a critical factor that determines the phase composition and pore structure [132]. From 50 to 75% of RH, the carbonation

rate is at its highest level. For RH < 50%, there is not enough pore solution for CO_2 to dissolve and carbonation does not occur. For RH>75%, the diffusivity of CO_2 is slowed down due to the high-water content [133,134].

The resistance of Limestone calcined clay cement (LC³) to chloride ingress [116,135,136] and to carbonation [128,137,138] have been investigated. LC³ blends are known to have a better chloride resistance and a lower resistance to carbonation than PC.

This chapter focuses on assessing both the chloride and carbonation resistance of PC, LC³ and LC³-CAC blends. LC³ incorporating two types of CACs (ACAC1.7 and ACAC2.2) are studied. The chloride resistance was assessed by using the mini-migration test. The effective diffusion coefficient was calculated based on simplified Nernst-Planck equation. The diffusion process of chloride is affected by factors such as its binding into C-S-H and AFm phases. In this study, chemically bound chloride in AFm phases was quantified with X-Ray Diffraction (XRD)-Rietveld method. The estimated C-A-S-H content using the Gibbs free energy minimization software (GEMS) and the Cl/Ca atomic ratio of C-A-S-H from Scanning Electron Microscopy - Energy Dispersive X-Ray spectroscopy (SEM-EDX) measurements allowed to get a rough estimation of the physically bound chloride on C-S-H.

The influence of carbonation under natural and accelerated conditions was investigated. The carbonation depth was estimated using an acid-base color indicator. For natural carbonation study, SEM and XRD were used to track the microstructural and phase changes. In addition to that, the effect of forced carbonation on the strength performance of PC, LC³ and LC³-CAC blends was studied.

6.2   Materials and methods

6.2.1 Raw materials

The raw materials used in this study are the same detailed in Chapter 3. The physicochemical properties are shown in Table 6-2. Cements phase compositions from XRD-Rietveld analysis are shown in Table 6-3.

Table 6-2 Physicochemical properties of PC, ACAC1.7, ACAC2.2, Anhydrite (Cs) and CClay1.

(wt.%)	PC	ACAC1.7	ACAC2.2	Cs	CClay1
Al_2O_3	4.56	45.71	40.12	-	31.74
SiO_2	20.08	4.75	4.55	0.18	62.91
CaO	63.59	43.68	49.36	42.00	0.07
Fe_2O_3	3.18	1.74	1.90	0.01	1.15
MgO	1.85	0.90	0.48	1.14	0.19
K_2O	0.95	0.26	0.23	-	0.42
Na_2O	0.16	0.07	0.06	-	0.00
P_2O_5	0.18	0.13	0.11	0.01	0.05
SO_3	3.27	0.10	0.04	56.62	-
TiO_2	0.35	2.21	1.78	-	1.50
Cr_2O_3	0.01	0.13	0.04	-	0.02
MnO	0.04	0.07	0.03	0.00	0.01
SrO	0.06	0.00	0.04	0.13	-
ZnO	0.00	0.00	0.00	0.02	0.00
LOI*	1.65	0.10	0.12	-	2.3
SSA* (m^2/g)	1.41	0.50	0.70	0.97	17.24
$D_{v\,50}$ (µm)	13.67	11.75	12.7	5.20	7.31

LOI* Loss of ignition, SSA Specific surface area

Table 6-3 Cements phase composition from XRD-Rietveld analysis.

Phase (wt.%)	PC	ACAC1.7	ACAC2.2
C_3S	70.4	-	-
C_2S	7.8	-	-
C_4AF	8.5	-	-
C_3A	6.3	-	-
Dolomite	0.9	-	-
CsH_2	2.4	-	-
Cs	0.3	-	-
Cc*	2.6	-	-
CA	-	7	-
C_2AS	-	0.15	-
CFT*	-	1	-
$C_{12}A_7$	-	0.45	7.3
Magnetite	-	-	-
Periclase	0.5	-	-
Quartz	0.3	-	-
Amorphous	-	91.40	92.7

*Cc: $CaCO_3$, CFT: Perovskite

6.2.2   Mixture design and sample preparation

6.2.2.1   Mixture design

Mix compositions of the investigated systems is shown in Table 6-4.

Table 6-4 Mix compositions of the investigated systems (wt. %).

System	PC	CAC	Cs	CClay	CsH_2	Cc	Citric acid	Na_2CO_3
PC	100	-		-	-	-	-	-
LC³	52.66	-	-	25	2.34	20	-	-
LC³-10%(ACAC1.7,Cs)	52.15	5	5	24.76	2.34	9.81	0.33	0.61
LC³-10%(ACAC2.2,Cs)	52.15	5	5	24.76	2.34	9.81	0.33	0.61

6.2.2.2   Sample preparation for mini-migration tests

The water to binder ratio (w/b) was 0.4. Dry mixes were mixed with deionized water using a mixer at 1600 rpm for 2 minutes. To remove air bubbles trapped within the cement paste, a mixing under vacuum was carried out at 450 rpm for 1 minute. Cement paste was then introduced in a plastic cylinder and sealed with parafilm and a lid. Hardened cement paste was demolded after being stored for 1 day at 20°C. Following that, samples were cured until 28 days in water in presence of small pieces of hardened cement of the same specimen. The aim is to provide a pore solution curing and avoid ion leaching.

6.2.2.3   Sample preparation for carbonation tests

Two exposure conditions were selected in this study:

For natural carbonation, the water to binder ratio (w/b) was 0.4. Dry powder was mixed with deionized water then placed in cylindrical plastic containers. Samples were demolded after 24 hours and were then cured for 3 days in a humid chamber. To have unidirectional carbonation, all surfaces were coated with epoxy resin and covered with aluminum tape as shown in Fig. 6-1(a). Paste samples were exposed to natural carbonation for 4, 7 months and 1 year for PC, LC³ and LC³-CAC blends. The RH of the room is ~ 60-65%.

Forced carbonation was studied on mortar cubes using the same protocol for mortars preparation for compressive strength test (Chapter 3). After demolding, prisms were cut to 40x40x40mm cubes. Cubes were cured for 7 days in a humid chamber. After that, a part of the cubes was stored in a glove box saturated with CO_2 and RH ~ 75%. The glove box was filled every two weeks with CO_2. The RH was maintained ~ 75% using sodium nitrate. The forced carbonation set-up is presented in Fig. 6-1(b). Some of the cubes were stored in the humid chamber until the testing age. It is worth noting that the aim of the forced carbonation experiments is to study the impact on the strength and not the carbonation rate.

a)   b)
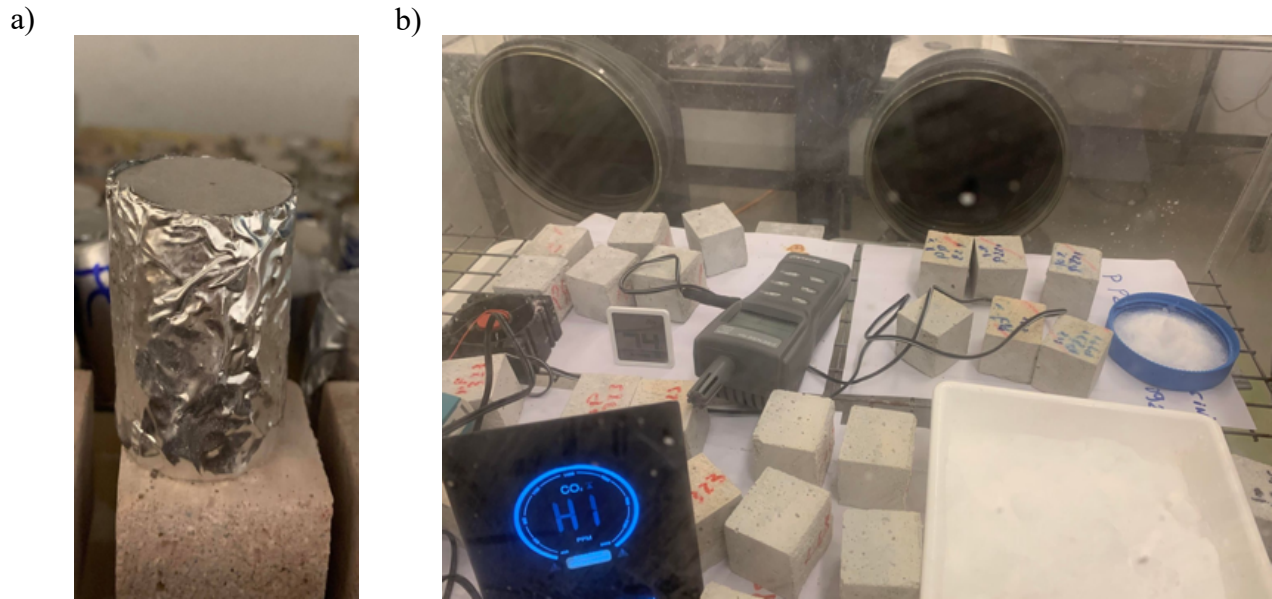
Fig. 6-1 Exposed cement paste to natural carbonation (a) and mortar cubes to forced carbonation (b).

6.2.3 Methods

6.2.3.1 Mini-migration test

After pore solution curing for 28 days, cylindrical specimens of 10 mm thickness and 35 mm diameter were cut. Sand paper was used to give a flat contact surface on both sides. Dust was removed by cleaning the sample in ultrasonic bath for 30 seconds, then they were mounted in a plastic ring with silicon. Samples were stored in a humid room for 3 hours to let the silicon dry. Samples were then immersed in NaOH (0.3M) for 48 hours under a small vacuum. Afterwards, upstream and downstream cells were attached to each other with the sample in between and two rubber rings. One rubber ring for each side. The upstream and downstream reservoirs were filled at the same time with different solutions. The upstream solution is NaOH (0.3M) and NaCl (0.5M). The downstream solution is NaOH (0.3M). The mini-migration setup is shown in Fig. 6-2. The applied voltage determines the duration of the experiment. An appropriate voltage was selected for each system. The aim is to obtain an initial current between 5-25mA. Table 6-5 shows the applied voltage for PC, LC^3 and LC^3-CAC blends. The current was continuously recorded during the experiment using a logging instrument (Squirrel Data Logger). The current curve enables to identify the interesting region to calculate D$_{eff}$.
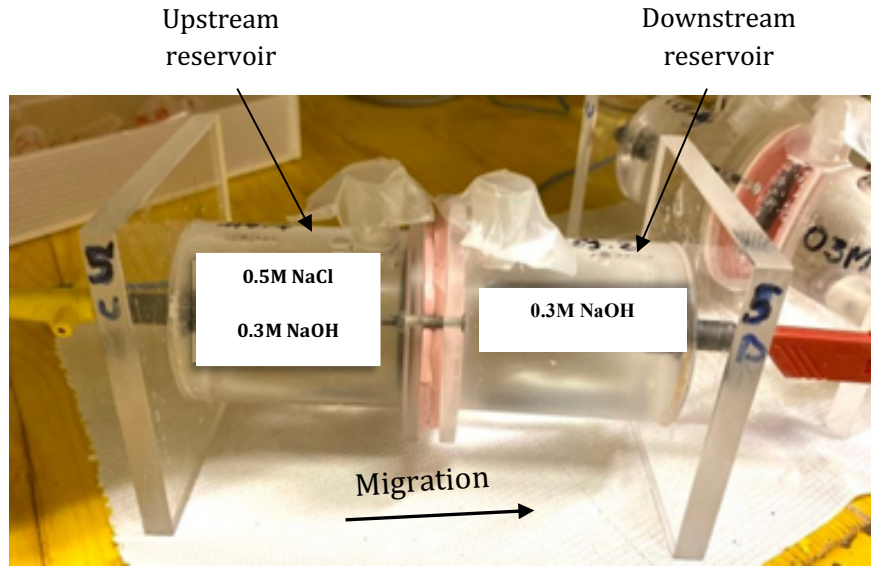
Fig. 6-2 Mini-migration test setup

Table 6-5 Applied voltage for PC, LC³ and LC³-CAC blends.

	Notation	Applied voltage (V)
PC	PC	5
LC³	LC³	12
LC³-CAC	LC³-10%(ACAC1.7,Cs)	12
	LC³-10%(ACAC2.2,Cs)	10

The effective chloride diffusion coefficient (D$_{eff}$) was calculated using a simplified Nernst-Planck equation for transport in solution according to Eq.7.

$$D_{eff} = \frac{J_{down}}{C_{up}} \frac{RT}{F} \frac{l}{\Delta E} \tag{7}$$

C$_{up}$ is the chloride concentration in the upstream reservoir (mol/m³), R is the gas constant, T is the temperature (K), F is the Faraday constant, l is the sample thickness and ΔE is the difference between the initial and final voltage in solution. J$_{down}$ is the chloride flux through the specimen (mol/m²s). It is expressed according to Eq.8.

$$J_{down} = \frac{1}{A} \frac{\dot{m}_{Cl^-}}{M_{wCl^-}} \tag{8}$$

A is the surface area of the specimen (m²), M$_{wCl^-}$ is the molar mass of chlorine (g/mol), $\dot{m}_{Cl^-}$ (g/s) is the chloride slope mass from the titration of chloride of the downstream cell. For 14 days, every 2-4 days, 5mL were taken from the downstream cell. To maintain the same total solution volume, the taken solution was replaced with 5mL of fresh NaOH (0.3M). To obtain the evolution of the chloride mass over time (days), the sampling solutions (collected every 2-4 days) from the downstream reservoir were titrated with AgNO₃ (0.05M) using TitroLine ® 5000. The instrument is calibrated

with a standard solution of NaCl (0.1M). Titration results of the downstream cell of PC as a function of time is shown in Fig. 6-3. The time needed for chloride to pass from the upstream reservoir to the downstream reservoir is t_0. Following that, as long as the change in the concentration in the downstream cell is negligible, a constant migration regime is observed (~ 14 days). The slope of the chloride mass as a function of time gives the chloride flow that is used to calculate the D_{eff}.

PC

$$mCl- = 0.0234t - 0.041$$
$$R^2 = 0.997$$
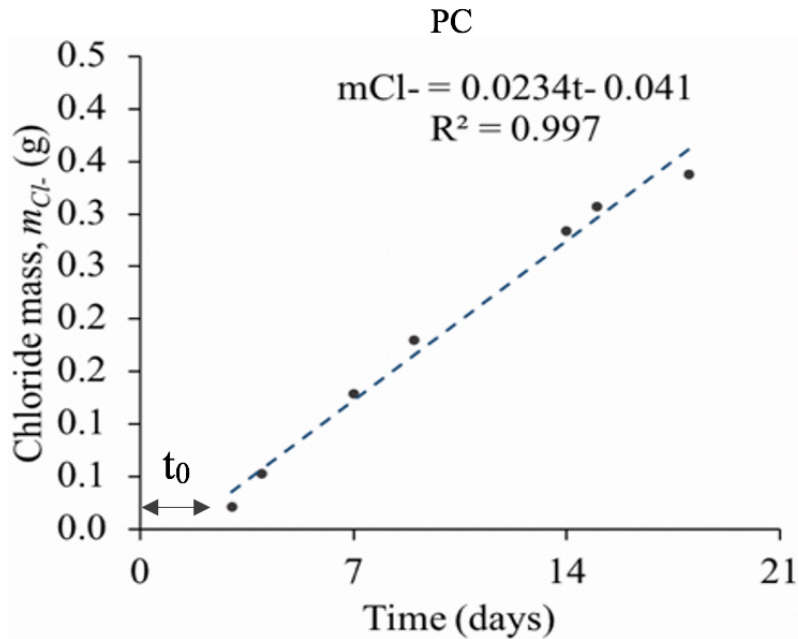
Fig. 6-3 Evolution of chloride mass m_{Cl-} in the downstream cell from titration as a function of time (days).

Cement paste samples were analyzed by XRD after 28 days of hydration and after running the mini-migration test. A solid solution between Friedel's salt and Hemicarboaluminate (Hc) was considered to quantify the chemically bound chloride in all blends. The quantification of the ettringite, Friedel's salt solid solution and CO_3-AFm content was conducted by XRD-Rietveld refinement method using the High Score Plus Software.

After stopping the hydration using the solvent exchange drying method [67], the following experiments were conducted.

SEM-EDX was used to determine the elemental composition (Al/Ca, Si/Ca and Cl/Ca) of C-A-S-H after the chloride ingress. The aim is to quantify the physically bound chloride. It was assumed that using the solvent exchange method will not remove the physically bound chloride on C-A-S-H. SEM samples were prepared according to [67].

Additionally, image analysis by element distribution maps were carried-out. BSE images were linked to EDX mapping with the edxia platform [99]. Based on ratio plots of Al/Ca vs. Si/Ca and Cl/Ca vs. Al/Ca obtained from EDX maps, representative points were attributed to C-S-H and CO_3-AFm and Friedel's salt solid solution phases. To observe the distribution of these phases after chloride ingress in the microstructure, masks were created from the regions identified in the ratio plots. This allows to observe these phases in the microstructure phases after the exposure to chloride.

Thermodynamic modelling was carried out with GEMS to determine the phase assemblage after 28 days of hydration and particularly the C-A-S-H content. The multiplication of the Ca content in C-A-S-H by the Cl/Ca ratio will allow to estimate the amount of physically bound chloride to C-A-S-H.

Pore structure was characterized by MIP. Experiments were performed using a Porotec 140 and 440 devices. The contact angle between mercury and paste is 140°. Samples were tested after 28 days of hydration to assess the pore network.

6.2.3.2 Carbonation tests

For both natural and forced carbonation tests, to observe the extent of CO_2 ingress, the carbonation depth was measured after cutting the paste cylinders and mortar cubes into two equally pieces. Measurements were made after 4, 7 months and 1 year of natural carbonation exposure and after 6 months of forced carbonation exposure. Thymolphthalein was used as an acid-base indicator color. Depending on the pH, this color indicator changes from colorless to blue. Below a pH of 9.3-10.5, it is colorless. Above this pH, it gives a blue color. From the measurement of the carbonation depth as a function of time, the carbonation coefficient can be estimated. It represents the slope of the regression curve of the carbonation as a function of the square root of time.

XRD together with Rietveld refinement was used to quantify the transformation of crystalline phases to carbonated products. The amorphous part was determined using the external method.

To characterize the changes in the microstructure due to the difference in the molar volume of hydrates and carbonated phases, SEM-BSE micrographs were taken. The effect of natural carbonation on the chemical composition of C-S-H was also investigated with SEM-EDX. Around 150 points C-S-H points were analyzed each time from a non-carbonated region and a carbonated region. The aim is to see if there is any difference in the C-S-H composition and if decalcification of C-S-H occurs.

The effect of natural carbonation on the porosity was investigated with MIP. The purpose is to compare the pore structure between a carbonated and a non-carbonated region.

To assess the effect of forced carbonation on the strength, compressive strength was performed after 6 months on both the exposed and non-exposed samples to CO_2.

More details about XRD, SEM, MIP can be found in the previous chapters.

6.3 Results and discussion

6.3.1 Mini-migration study

6.3.1.1 Effective diffusion coefficient (D_{eff})

The effective diffusion coefficient of chloride for PC, LC³, LC³-10%(ACAC2.2,Cs) and -10%(ACAC1.7,Cs) was calculated according to Eq.7. For all the investigated systems, the mini-migration test was performed twice. The D_{eff} values shown in Fig. 6-4 are the average value of two replicates. A significant reduction of D_{eff} is observed for LC³ and LC³-CAC blends compared to PC system. The incorporation of CAC and Cs shows a further improvement of chloride resistance compared to LC³. Among all the investigated systems, LC³ blended with 10%(ACAC2.2,Cs) has the lowest D_{eff}. To understand these results additional characterization techniques were used.
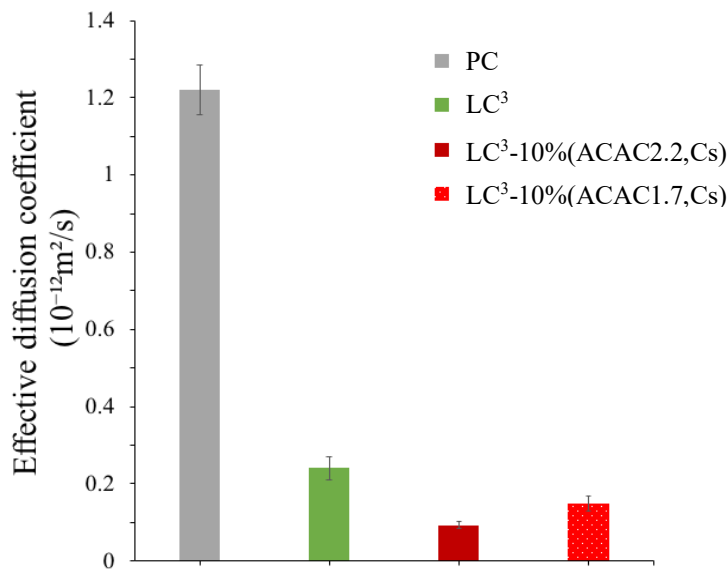
Fig. 6-4 Effective chloride diffusion coefficients measured from chloride flows in mini-migration tests for PC, LC³, LC³ with 10%(ACAC2.2,Cs) and -10%(ACAC1.7,Cs).

6.3.1.2 Chemical binding of chloride

Fig. 6-5 shows Friedel's salt (Fs), Friedel's salt solid solution (SS), CO_3-AFm (Hc+Mc) and the ettringite content for PC, LC³, LC³-10%(ACAC2.2,Cs) and -10%(ACAC1.7,Cs) before and after the mini-migration test. A solid solution between Friedel's salt (Fs) and Hc was considered, as a peak shift occurred between Hemicarboaluminates (Hc) and Fs for all the investigated systems, as shown in Fig. 6-6. This is in agreement with previous studies [30,109] where a solid solution between Fs and Hc was observed in blends containing limestone. The results presented in Fig. 6-5 show that a more chemical binding of chloride is observed with LC³ compared to PC. This is in agreement with previous studies where it was reported that aluminate rich SCM's such as calcined clay contribute to the increase of chemical chloride binding thanks to the formation of additional Friedel's salt.

However, for blended systems a non-negligible amount of carboaluminates remained after the test. For LC³ -CAC blends, although they had an important CO₃-AFm content, the binding capacity was not improved compared to LC³ and even less chloride is chemically bound to CO_3-AFm phases compared to PC. William et al. showed that in systems with a relatively high sulfate contents ions compete for incorporation/ adsorption in aluminous hydrates [139]. The smaller chemical binding of Cl in LC³-CAC blends compared to PC can be attributed to the higher sulfate content of these mixes (Chapter 5, Fig. 5-3). It is also worth noting that in addition to the solid solution of Friedel's salt, a small amount of pure Friedel's salt was detected in all the investigated systems.
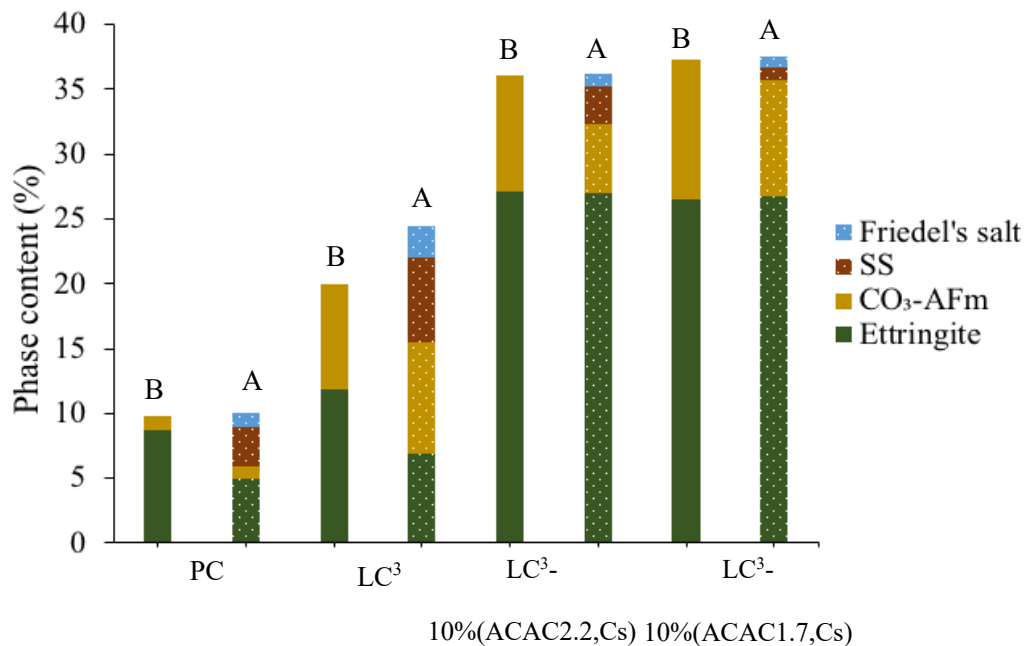
Fig. 6-5 Friedel's salt, Friedel's salt solid solution (SS), CO₃-AFm (Hc+Mc) and ettringite content before (B) and after (A) mini-migration test for PC, LC³, LC³-10%(ACAC2.2,Cs) and LC³-10%(ACAC1.7,Cs).
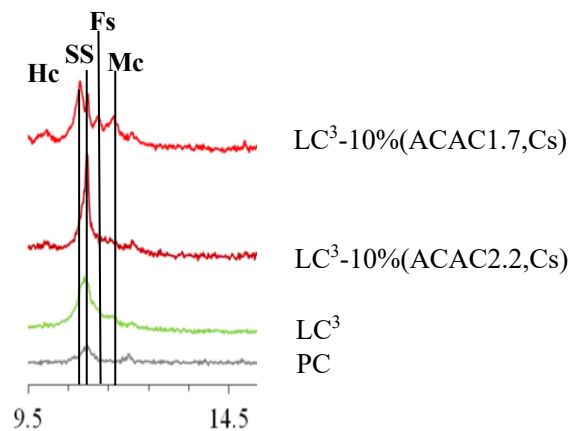
Fig. 6-6 Hemicarboaluminates (Hc), Friedel's salt (Fs), Friedel's salt solid solution (SS) and Monocarboaluminates (Mc) XRD peaks for PC, LC³, LC³-10%(ACAC2.2,Cs) and -10%(ACAC1.7,Cs) after the mini-migration test.

6.3.1.3 Physical binding of chloride

The physical binding of chloride to C-A-S-H was also investigated. The average C-A-S-H composition was determined from the plot of Al/Ca vs. Si/Ca atomic ratios. Fig. 6-7 shows C-A-S-H composition for PC, LC³ and LC³-10%(ACAC2.2,Cs). Based on the selected Al/Ca of the C-A-S-H, the Cl/Ca ratio of the C-A-S-H was determined from the plot of Cl/Ca vs. Al/Ca. Table 6-6 gives the Al/Ca, Si/Ca and Cl/Ca atomic ratios obtained by SEM-EDX. The variation inside the same system is larger than between the different systems. The high error in the determination of the Cl/Ca ratio is related to the EDX detector. As chloride is a light element, it is not well quantified.
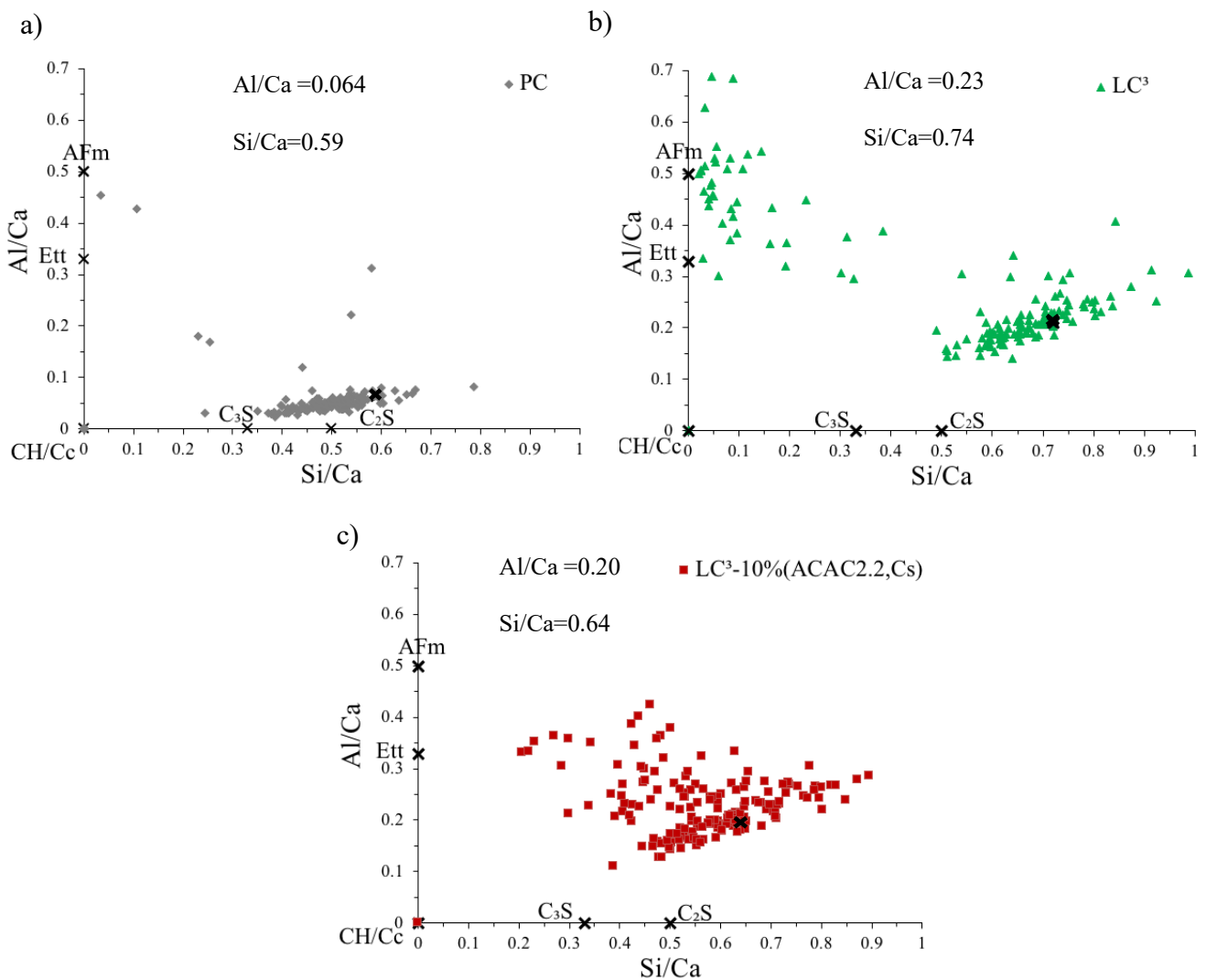
Fig. 6-7 Al/Ca atomic ratio as a function of Si/Ca atomic ratio after chloride ingress determined by SEM-EDX for PC (a), LC³ (b) and LC³-10%(ACAC2.2,Cs) (c).

Table 6-6. Al/Ca and Si/Ca atomic ratios of C-A-S-H after chloride ingress by SEM-EDX.

	Al/Ca	Si/Ca	Ca/Si	Cl/Ca
PC	0.064±0.015	0.59±0.01	1.69±0.01	0.018±0.011
LC^3	0.23±0.01	0.74±0.01	1.74±0.01	0.009±0.008
LC^3-10%(ACAC2.2,Cs)	0.20±0.02	0.64±0.01	1.56±0.01	0.011±0.014

The amount of bound chloride into C-S-H was calculated by multiplying the Cl/Ca ratio by the total amount of Ca in C-A-S-H. Results, shown in Table 6-7, indicate that a higher amount of C-A-S-H is formed with LC^3 compared to PC and LC^3-10%(ACAC2.2,Cs). The lower C-A-S-H content using the ACAC2.2 compared to LC^3 can be explained by the slightly lower degree of reaction of metakaolin in this system (Chapter 3, Fig. 3-15(b)). Regarding the amount of Cl physically bound to C-A-S-H, it can be seen that PC system has a high chloride binding compared to LC^3 and LC^3-CAC blends. A previous study showed that an increase of the Si/Ca ratio is responsible for decreasing the binding capacity. This was explained by the increase of deprotonated silanol group at the surface of C-A-S-H and a reduced availability of calcium that forms a net positive charge on C-A-S-H responsible for promoting chloride binding [140]. Incorporation of aluminum is also found to reduce the chloride binding for same Ca/(Si+Al) [140]. The incorporation of aluminum decreases the number of total adsorption sites in C-A-S-H. In our case, higher Si/Ca and Al/Ca ratios are obtained in blended systems. This can explain the lower content of physically bound chloride to C-A-S-H.

Table 6-7 C-A-S-H content determined using thermodynamic modelling and the amount of chloride chemically bound to C-A-S-H for PC, LC^3 and LC^3-10%(ACAC2.2,Cs).

	C-A-S-H content from GEMS (g/100g of solid)	Cl in C-A-S-H (mg/g pate)
PC	40.8	1.80
LC^3	49.6	0.99
LC^3-10%(ACAC2.2,Cs)	36.8	0.95

6.3.1.4 Pore structure at 28 days

To understand the reason why LC^3-CAC blends show a better chloride resistance compared to LC^3 and LC^3-CAC blends, the pore structure was characterized after 28 days of hydration. Results are plotted in Fig. 6-8. A reduction in the total porosity of LC^3-CAC blends compared to PC and LC^3 systems is observed. The total porosity is around 20% and 13% respectively for LC^3-10%(ACAC2.2,Cs) and -10%(ACAC1.7,Cs) against 23% and 22% respectively for PC and LC^3. The reduction in porosity of LC^3-CAC is attributed to the additional ettringite formation and its good capacity to fill space. On the other hand, it can be seen that ACAC1.7 has the smallest critical pore entry size followed by ACAC2.2 blend. The peak indicating the existence of coarse porosity in ACAC2.2 blend is unexpected and could be due to a possible bad packing in this system. It is worth noting that the decrease in the total porosity or in the critical pore entry size is not proportional to the enhancement of the chloride resistance. Furthermore, ACAC1.7 blend has a lower total porosity and

smaller critical pore entry size compared to ACAC2.2 but a higher chloride diffusion coefficient compared to ACAC2.2.
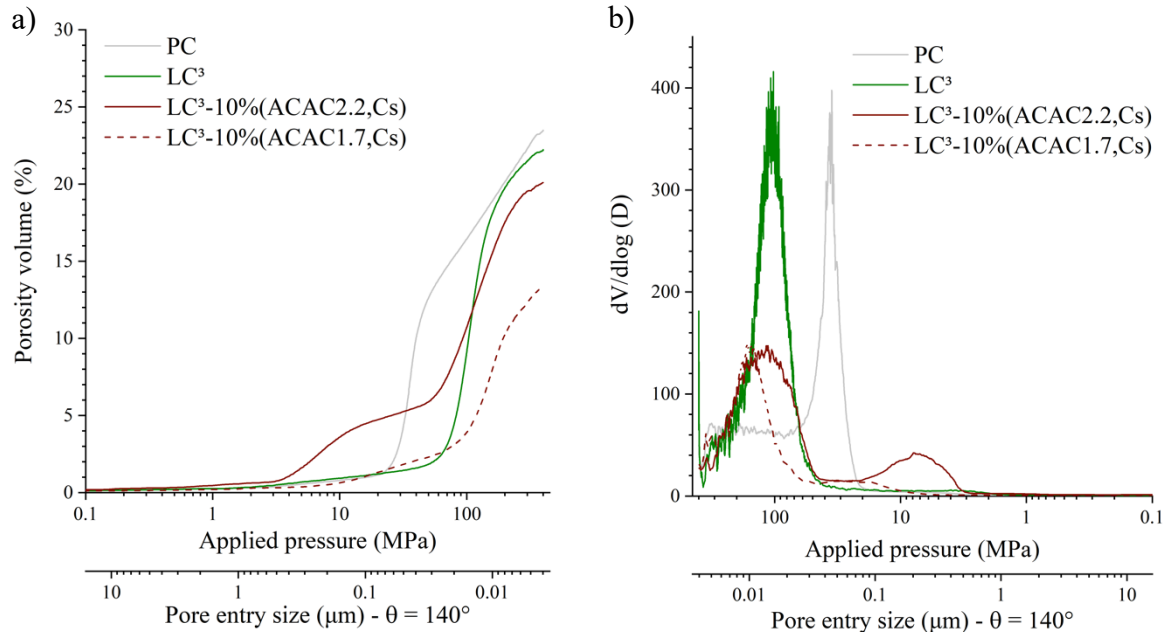
Fig. 6-8 Cumulative pore volume curves (a) and their first derivative (b) for PC, LC³ and LC³-CAC blends at 28 days.

6.3.2 Natural Carbonation study

6.3.2.1 Carbonation depth

Fig. 6-9 shows the carbonation depth as a function of the square root of time for PC, LC³, LC³-10%(ACAC2.2,Cs) and -10%(ACAC1.7,Cs). The carbonation depth increases with the increase of exposure. LC³-CAC blends have a higher carbonation depth compared to LC³. Among all the tested systems, PC, where most CaO is available, has the lowest carbonation depth.
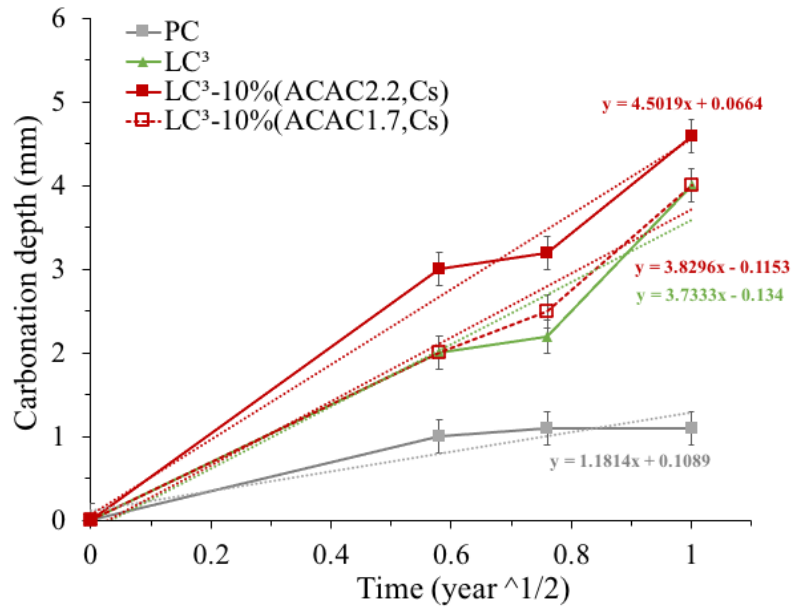
Fig. 6-9 Carbonation depth for PC, LC³, LC³ -10%(ACAC2.2,Cs) and -10%(ACAC1.7,Cs) determined using Thymolphthalein.

6.3.2.2 Carbonation coefficient

The estimated carbonation coefficients for PC, LC³, LC³-10%(ACAC2.2,Cs) and -10%(ACAC1.7,Cs) are shown in Fig. 6-10. Results show that PC has the lowest carbonation coefficient. LC³ has a higher carbonation coefficient than PC. Blending LC³ with CAC shows even higher carbonation coefficient compared to LC³. However, within the CAC blends, LC³-ACAC2.2 blend has the highest carbonation coefficient.
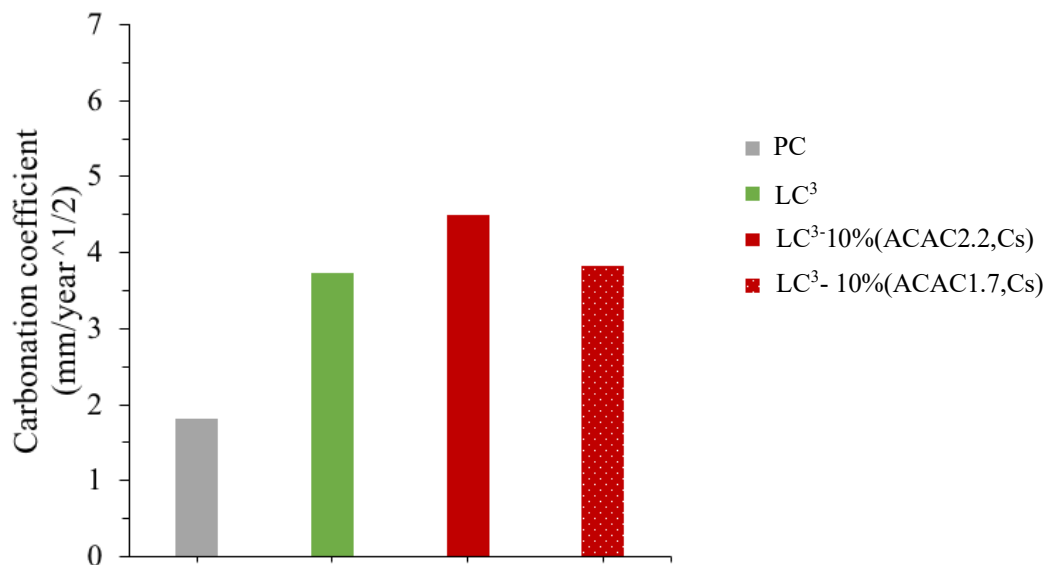
Fig. 6-10 Carbonation coefficient for PC, LC³, LC³-10%(ACAC2.2,Cs) and -10%(ACAC1.7,Cs) of natural carbonation on cement paste cured for 3 days before exposure.

6.3.2.3 Phase assemblage

XRD-Rietveld quantification results after 4 and 7 months of exposure (C) and non-carbonated (NC) samples are shown in Fig. 6-11. After 4 months of hydration, all NC systems have portlandite, ettringite and CO_3-AFm as crystalline hydration products. After 7 months of hydration, same hydrates are observed in the NC systems, except portlandite that is not present in LC³-10%(ACAC1.7,Cs). In carbonated specimens, it can be seen that portlandite is depleted except in PC system where portlandite is still present even after 7 months of natural carbonation. It can be also seen that in all samples, carbonation of ettringite, CO_3-AFm phases and portlandite is taking place and calcium carbonate is formed. Only calcite is formed for PC reference. However, different polymorphs of calcium carbonate (vaterite, aragonite and calcite) are present in LC³ and LC³-CAC blends. Contrary to PC, further hydration of C_3S and C_2S was observed in LC³ and LC³-CAC blends. The amorphous part includes C-S-H, non-reacted calcined clay, silica and alumina gel and possibly other minor phases. It is also important to note that although the high portlandite content in the non-carbonated sample of LC³-ACAC2.2 blend compared to LC³-ACAC1.7 blend. LC³-ACAC2.2 blend has a higher carbonation coefficient.
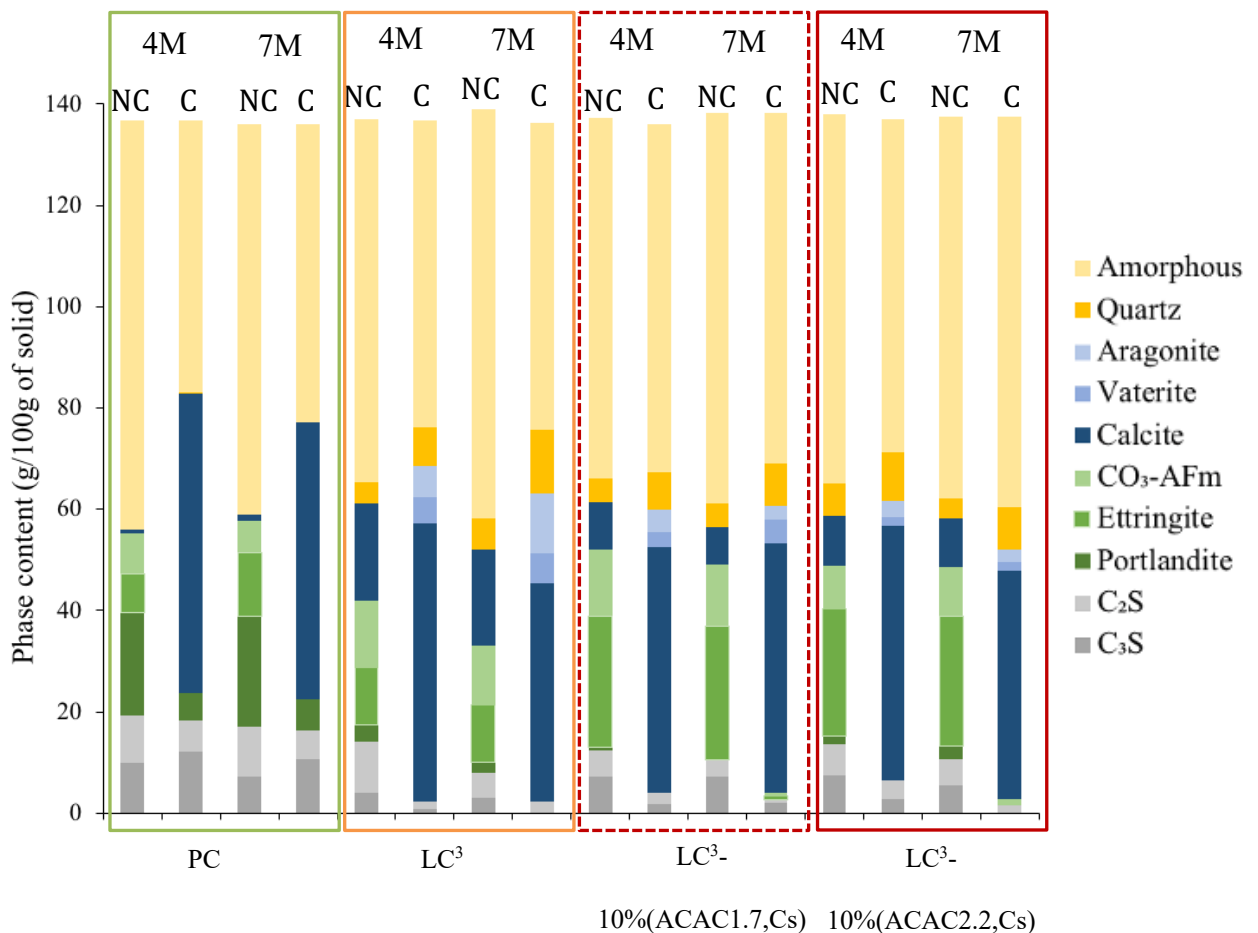
Fig. 6-11 Phase assemblage by XRD-Rietveld analysis for PC, LC³, LC³- 10%(ACAC1.7,Cs) and -10%(ACAC2.2,Cs) after 4 and 7 months of exposure.

6.3.2.4 Microstructure observation

SEM-BSE images of carbonated and non-carbonated regions of PC, LC^3 and LC^3-10%(ACAC2.2,Cs) are presented in Fig. 6-12. It is clear that carbonation leads to a change in the microstructure. No portlandite is observed in any of the carbonated systems (C). Carbonation of LC^3 and LC^3-ACAC2.2 blends leads to a more porous microstructure, which can be explained by the difference in molar volume of the hydrates and the carbonated phases. This in agreement with previous studies [128,141]. Additionally, two rims of C-S-H (dark inner rim and outer bright rim) are observed in blended systems. Similar observation was made by Shah et al. [128], who explained the darker rim by the further hydration during the exposure period. The outer brighter rim corresponds to the inner rim formed before the exposure to CO$_2$.
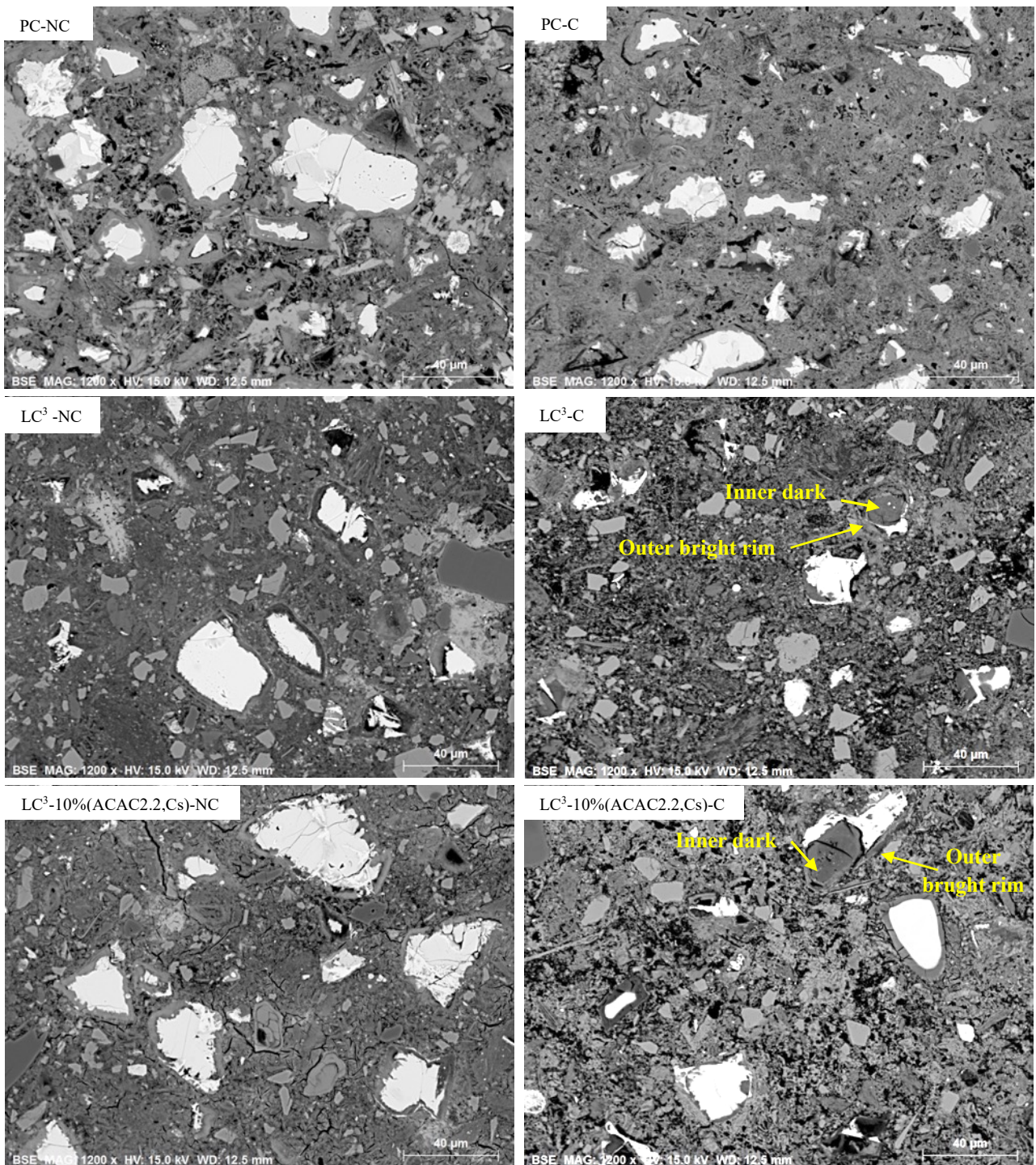
Fig. 6-12 SEM pictures of PC, LC³ and LC³-10%(ACAC2.2,Cs) of a non-carbonated (NC) and carbonated (C) front after 7 months of exposure.

6.3.2.5 C-S-H chemical composition

The effect of natural carbonation on the C-S-H chemical composition was investigated. Fig. 6-13 shows the atomic plots of Al/Ca vs. Si/Ca of measurements performed on C-S-H from the carbonated region (both inner dark rim and outer bright rim) and on C-S-H rims from a non-carbonated region. For PC system, Fig. 6-13(a) shows that C-S-H selected in carbonated regions has a lower Si/Ca ratio. This could be due to its intermixing with calcium carbonate. LC³ and LC³-10%(ACAC2.2,Cs) results respectively presented in Fig. 6-13(b) and (c) show that the dark C-S-H_C (d) has a high Si/Ca and Al/Ca ratios confirming the decalcification of C-S-H and the formation of silica and alumina gel. For LC³ and LC³-CAC, the bright C-S-H (outer C-S-H rim in the carbonated region) has a chemical composition very close to the C-S-H in the non-carbonated region (C-S-H_NC).
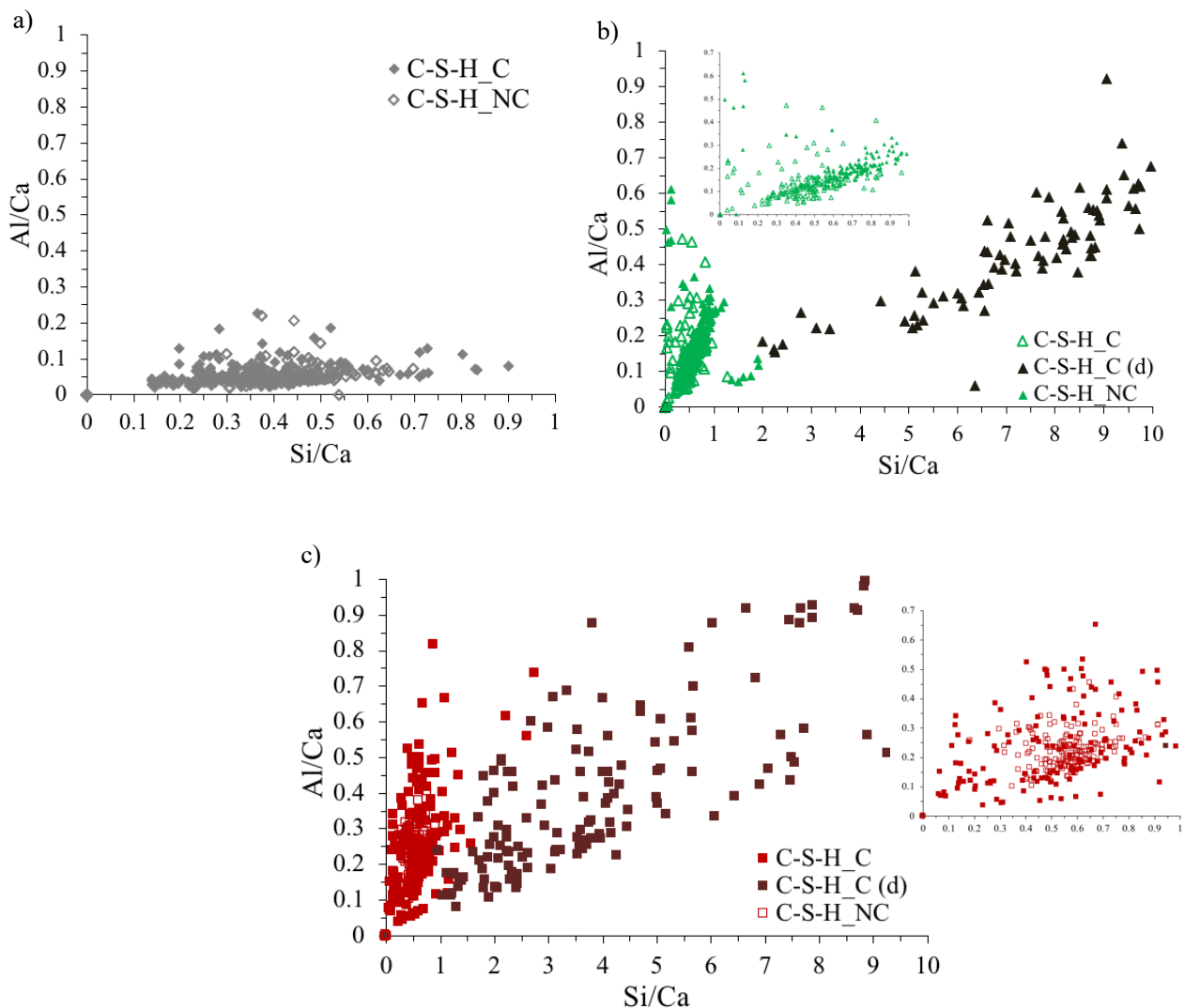
Fig. 6-13 Al/Ca vs. Si/Ca atomic ratios of C-S-H_ C: bright outer rim in a carbonated region, C-S-H_C (d): dark inner rim in a carbonated region and C-S-H_ NC: inner C-S-H in a non-carbonated region from SEM-EDX measurements for PC (a), LC³ (b) and LC³-10%(ACAC2.2,Cs) (c) after 7 months of exposure.

6.3.2.6 Porosity characterization

Fig. 6-14 compares the pore structure for PC (a), LC³ (b) and LC³-10%(ACAC2.2,Cs) (c) each time of a non-carbonated and carbonated samples after 7 months of exposure. For PC system, a slightly higher total porosity and coarser pores are obtained with the carbonated system. As portlandite is the main carbonated phase in PC system, the formation of calcium carbonate was expected to lead to an increase in the total solid volume of 11% (as shown in Table 6-1). However, XRD-Rietveld quantification results presented in Fig. 6-11 showed that carbonation of other hydrates (ettringite and CO_3-AFm phases) that have a higher molar volume than calcite is also taking place in the PC system. This can explain the slight increase and coarsening of porosity. For LC³ and LC³-10%(ACAC2.2,Cs), the carbonation does not significantly impact the total porosity but leads to an important coarsening of pores. This can be explained by the change in the solid volume. Due to the low portlandite content in these blends, carbonation of AFt and CO_3-AFm phases is more important compared to PC. As shown in Table 6-1, the carbonation of AFt (ettringite: a main hydrate in these blends) leads to a decrease of 48% of the solid volume. In our case, this led to a slightly higher total porosity and more importantly to a coarsening of the porosity.
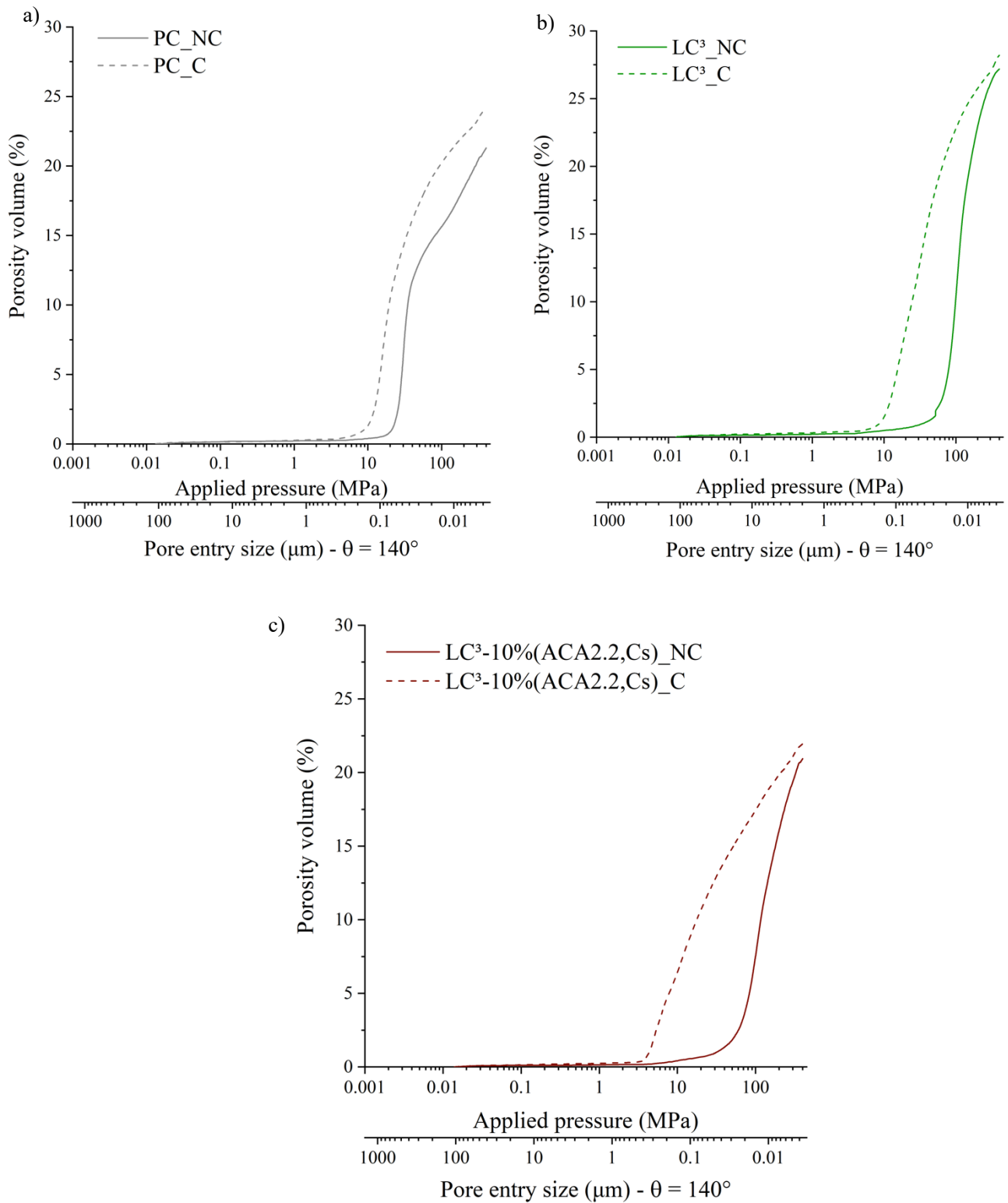
Fig. 6-14 Cumulative pore volume curves for PC (a), LC³ (b) and LC³-10%(ACAC2.2,Cs) (c) carbonated: C and non carbonated: NC blends after 7 months of exposure.

6.3.3 Forced carbonation

6.3.3.1 Carbonation depth

To assess the carbonation depth of PC, LC^3 and LC^3-CAC blends, mortar specimens were split and sprayed with Thymolphthalein. Results after 6 months of forced carbonation are shown in Fig. 6-15. It can be seen that CO$_2$ can ingress from all directions. Estimated carbonation depth of the investigated systems is shown in Table 6-8. PC has the smallest carbonation depth. LC^3 and LC^3-10%(ACAC2.2,Cs) are fully carbonated. Although the portlandite content is the lowest in the non-carbonated specimen of LC^3-10%(ACAC1.7,Cs), as shown in Fig. 6-11(a) and (b), it carbonates slower than LC^3 and LC^3-10%(ACAC2.2,Cs) blends. This result is in agreement with the natural carbonation study on paste where LC^3 blended with ACAC1.7 was also carbonating slower than LC^3 blended with ACAC2.2. This suggests that not only portlandite availability and the amount of total CaO are key factors in carbonation process. In addition also the pore structure plays an important role and the slightly higher and coarser porosity observed before carbonation (see Fig. 6-8) could be responsible for lower carbonation depth observed for LC^3-10%(ACAC2.2,Cs).

a)   b)

c)   d)
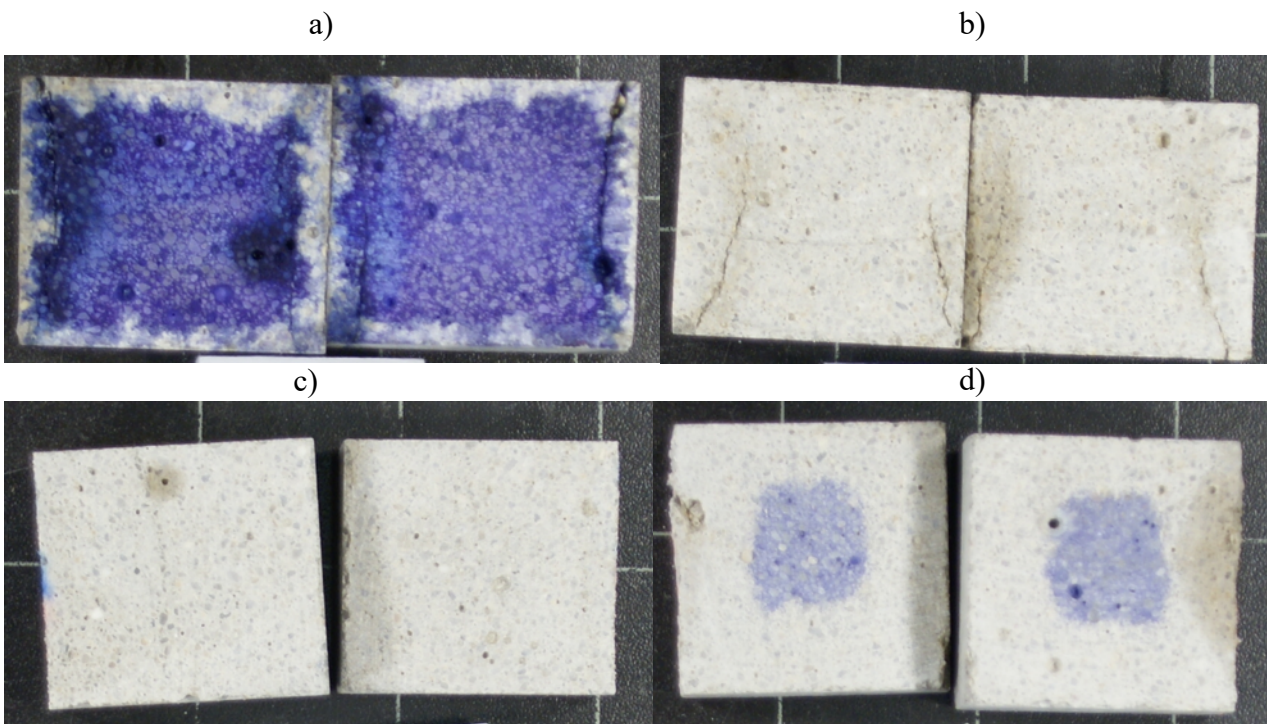
Fig. 6-15 Mortar specimens split and sprayed with Thymolphthalein to measure the carbonation depth for PC (a), LC^3 (b), LC^3-10%(ACAC2.2,Cs) (c) and LC^3-10%(ACAC1.7,Cs) (d).

Table 6-8 Carbonation depth for PC, LC³, LC³-10%(ACAC2.2,Cs) and LC³-10%(ACAC1.7,Cs).

Sample name	Carbonation depth (cm)
PC	0.47 ±0.08
LC³	fully carbonated
LC³-10%(ACAC2.2,Cs)	fully carbonated
LC³-10%(ACAC1.7,Cs)	1 ± 0.15

6.3.3.2 Compressive strength

The compressive strength results of PC, LC³, LC³-10%(ACAC2.2,Cs and -10%(ACAC1.7,Cs) mortar cubes exposed and non-exposed to forced carbonation for 6 months are shown in Fig. 6-16. Results show that the carbonated specimen of PC has a higher strength compared to the non-carbonated specimen. The full carbonation of LC³ and LC³-ACAC2.2. blends lead to a reduction in the strength. However, comparable strength to the non-carbonated PC sample is obtained in presence of ACAC2.2. Interestingly, the carbonation of LC³-10%(ACAC1.7,Cs) blend did not decrease the compressive strength significantly.
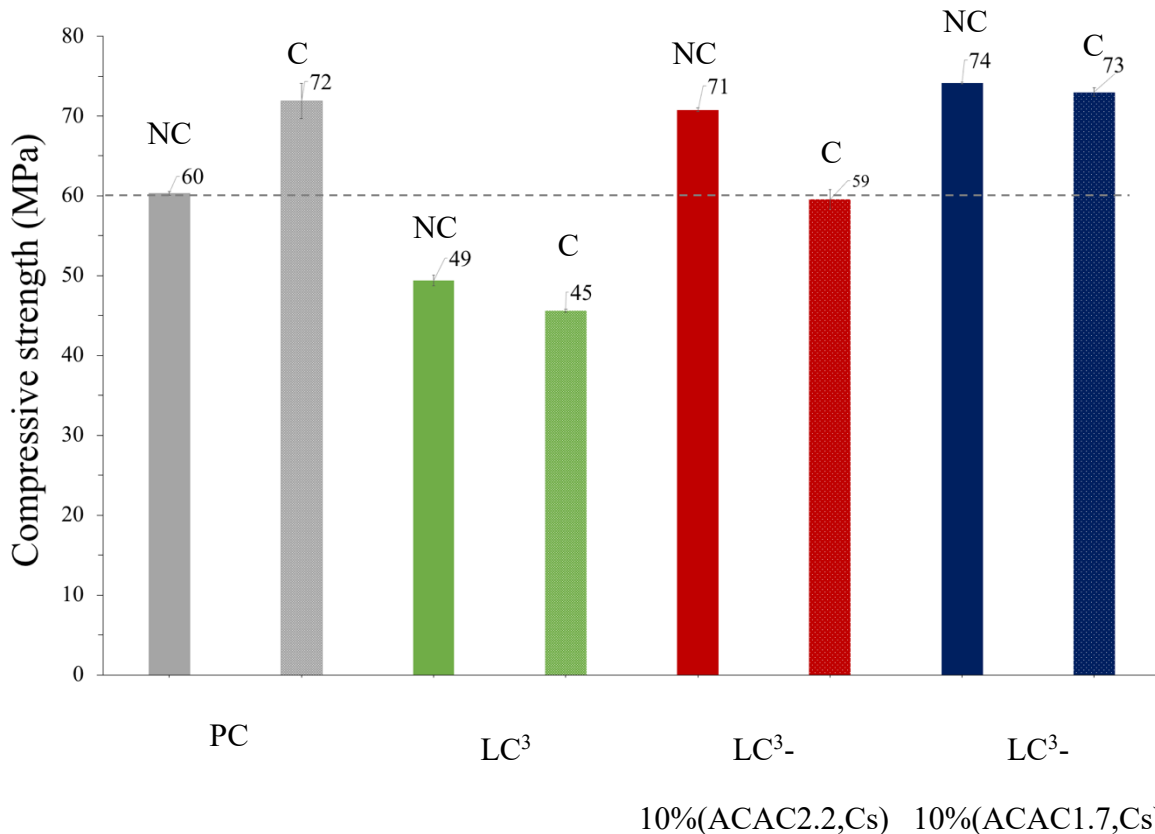
Fig. 6-16 Compressive strength development for PC, LC³, LC³-10%(ACAC2.2,Cs) and LC³-10%(ACAC1.7,Cs) each time for non-carbonated (NC) and carbonated (C) specimens.

6.4 Conclusions

This study focused on investigating the durability properties of LC³-CAC blends and on comparing them to PC and LC³.

Chloride resistance of the investigated blends was assessed with the mini-migration test method. This method was supplemented with other techniques to explain the obtained effective diffusion coefficients (D_{eff}).

- Results showed that LC³-CAC blends have better chloride resistance compared to PC and LC³. The effective chloride diffusion coefficient follows this order: LC³-10%(ACAC2.2,Cs) < LC³-10%(ACAC1.7,Cs) < LC³ < PC.

- The chemical binding of chloride in LC³-CAC blends was reduced compared to PC and LC³ systems. This can be explained by the relatively high sulfate content in these blends. Sulfate ions can compete with chloride ions and thus less chloride will incorporate CO_3-AFm phases.

- Lower physically bound chloride in LC³-ACAC2.2 blend was observed in comparison with PC. In LC³-ACAC2.2 blend, the formed C-A-S-H has a higher Al/Ca ratio and Si/Ca ratio. The decrease of available calcium in C-S-H lowers the chloride binding.

- Pore structure characterization at 28 days showed that in addition to reducing the critical pore entry radius compared to PC, CAC and Cs incorporation led to a more important decrease of the total porosity in comparison with LC³. This porosity refinement can explain the lower chloride diffusion coefficients. However, the porosity refinement was not proportional to the degree of improvement of chloride resistance. Other factors such as chloride incorporation/adsorption into ettringite could explain the enhancement of chloride resistance in LC³-CAC blends but this was not explored in this study.

Carbonation was tested in both natural and accelerated conditions:

- The natural carbonation study showed that LC³-CAC blends have a higher carbonation rate compared to PC.

- XRD-Rietveld results showed that except for PC, different polymorphs of calcium carbonate (vaterite, aragonite and calcite) were formed from carbonation of hydrates. For PC, portlandite is the main carbonated hydrate. For LC³ and LC³-ACAC2.2 blend, due to the lack of portlandite, all hydrate carbonate and the hydration of C_3S and C_2S was enhanced due to exposure.

- It was found that although the high portlandite content in the non-carbonated LC³- ACAC2.2 blend compared to the LC³-ACAC1.7 blend, LC³-ACAC2.2 blend was observed to have a lower carbonation resistance than LC³-ACAC1.7 blend. This was not expected.

- Microstructure observation of the carbonated region of LC^3 and LC^3-10%(ACAC2.2,Cs) blend showed two rims of C-S-H (a dark inner rim and a bright outer rim). SEM-EDS measurements, showed that the bright outer rim has a composition close to inner C-S-H in the non-carbonated region. The dark rim is silica and alumina gel that raises from decalcification of the C-S-H formed during the exposure.

- The pore structure network was impacted by carbonation. The coarsening of the porosity was more important in LC^3 and LC^3-ACAC2.2 blend in comparison with PC. This is explained by solid volume changes. The lack of portlandite in these systems led to an important carbonation of AFt and CO$_3$-AFm phases. These phases have a higher molar volume than calcium carbonate.

- The study of specimens exposed to forced carbonation is in agreement with the natural carbonation study: LC^3-ACAC2.2 blend is less resistant to carbonation compared to LC^3-ACAC1.7. The carbonation of PC lead to an improvement of strength. This is due to an increase of the total solid volume due to calcium carbonate formation from portlandite carbonation. Due to the decrease of the total solid volume induced by carbonation, the opposite was observed for LC^3 and LC^3-CAC blends. Although the reduction of strength due to carbonation, LC^3-ACAC2.2 blends still have at least similar strength to the non-carbonated specimen of PC.

Chapter 7   Conclusions and Perspectives

7.1   Conclusions

The work elaborated in this thesis was focused on two main aspects: the first aspect is the study of the hydration and strength of a fixing mortar formulation with/without calcined clay. The second one explored the feasibility of substituting limestone in LC^3 with CAC and Cs in terms of hydration and properties.

7.2   Interactions between calcined clay, PC, CAC, Cs and calcined clay in a fixing mortar formulation

To isolate the hydration mechanisms taking place in a fixing mortar formulation, simple systems were studied. The study covered two simple systems composed of:

1- PC with an increasing amount of (CAC+ Cs)
2- PC incorporating 20% calcined clay and with an increasing amount of (CAC + Cs)

Following that, a fixing mortar formulation with various calcined clay content was investigated. The main findings of this study can be summarized as follows:

- Increasing the CAC and Cs substitution in a PC system led to a higher ettringite formation and a lower portlandite content. This is because portlandite is involved in the ettringite formation. However, the pozzolanic reaction of metakaolin was not impacted.

- Increasing the CAC and Cs content in PC with 20% calcined clay was observed to lead to slightly lower degrees of hydration of C$_3$S.

- In PC systems with CAC, Cs and calcined clay, the formation of strätlingite in addition to monosulfate was observed. This was not the case for PC alone with calcined clay nor PC alone with CAC and Cs.

- Compressive strength results showed the feasibility of using calcined clay as clinker substitute in the studied fixing mortar formulation. Strength was reduced at early age due to the lower amount of reacted C$_3$S at higher CClay dosage. From 7 days onwards, at least similar strength to the reference was observed. This was explained by the calcined clay reaction that is taking place.

7.2.1 Effect of incorporating CAC and Cs in an LC^3 blend

- Strength results showed that the incorporation of CAC+Cs in an LC^3 blend as limestone substitue was observed to give same or higher 1 day strength as/than PC reference.

  - The early age strength performance of LC^3-CAC blends depends on the C/A ratio as well as the CAC content.

  - The ettringite content was found to be independent of the C/A ratio of the CAC used, depending on the amount of Cs present. Consequently, increasing the CAC and Cs content was observed to lead to a higher ettringite content.

  - Using a CAC with a C/A ratio of 1.7 "ACAC1.7" hindered the C$_3$S hydration. Increasing the amount added intensified this effect and led to a decrease in the early age strength. However, using a CAC with a C/A ratio of 2.2 "ACAC2.2" did not produce such an effect on the C$_3$S hydration. Here, increasing the amount increases the strength.

  - The incorporation of CAC and Cs was observed to slightly decrease the degree of reaction of metakaolin.

- The substitution of 10% of the overall LC^3 by ACAC2.2 and Cs also showed equivalent strength to PC at 1 day and higher strength from 7 days onwards.

7.2.2 Reasons of delaying alite hydration in LC^3 incorporating low C/A ratio CAC

- The lower C/A ratio of CAC led to less calcium ions being released from CAC.

- To trigger the C$_3$S hydration, a critical calcium concentration seems to be needed in the pore solution and particularly a supersaturation with respect to portlandite.

- Calcium hydroxide addition enhanced the degree of hydration of C$_3$S. The pore solution results showed a higher calcium concentration than its reference system.

7.2.3 Long-term properties

LC^3-CAC blends have a high late age strength compared to PC and LC^3.

- Thermodynamic predictions showed that a higher ettringite amount is present in LC^3-CAC blends than LC^3. Additinally, predictions also showed that free water was present at 28 days in all the investigated mixes.

- The calculated volume fraction of the predicted phases from thermodynamic modelling showed that C-S-H and ettringite occupy 49% of the total volume in LC^3 while they occupy around 55% of the total volume in LC^3-CAC blends. This explains the high strength of LC^3-CAC blends.

- A good correlation was observed between the strength and the porosity. This demonstrates that the high late age strength comes from the reduction of porosity due to the higher volume of hydrates.

- Relative humidity measurements showed that, for LC^3-ACAC2.2 blend, although the critical pore radius was higher than the calculated saturated pore limit, the critical pore entry was refined. This shows that the hydration is continuing in LC^3-CAC blend.

- TEM images showed that CAC and Cs incorporation did not have an influence on the C-S-H morphology.

The durability properties with respect to chloride ingress and carbonation resistance were investigated.

- LC^3-CAC blends showed better resistance to chloride ingress than PC and LC^3. The effective diffusion coefficients of LC^3-CAC blends calculated from the mini-migration method were around ~9x lower than PC and ~1.8x lower than LC^3.

- The chloride binding was found to be lower in LC^3-CAC blends than in PC. The reason behind the observed improvement seems to be related to the porosity refinement compared to PC, and to the decrease of the total porosity compared to LC^3.

- The natural carbonation study showed a higher carbonation rate of LC^3-CAC blends than PC. LC^3- ACAC2.2 blend with a higher portlandite content than LC^3-ACAC1.7 showed a lower carbonation resistance compared to LC^3-ACAC1.7. This was not expected as LC^3-ACAC2.2 was observed to have a higher portlandite content.

- Porosity characterization results showed that contrary to PC the carbonation of LC^3-ACAC2.2 blend induced an important coarsening of porosity. This is explained by the important carbonation of phases other than portlandite (ettringite and CO$_3$-AFm phases). The carbonation of ettringite is known to lead to a decrease of the total solid volume (-48%). However, the carbonation of portlandite (main carbonated phase in PC) is known to lead to an increase of the solid volume (+11%).

- The effect of carbonation on the compressive strength was assessed after exposing mortar samples to forced carbonation conditions. Similar to the natural carbonation study, the LC^3-ACAC 2.2 blend is less resistant to carbonation than LC^3-ACAC1.7 blend. The carbonation of PC led to an improvement of strength. However, the carbonation of LC^3 and LC^3-CAC blends led to a decrease in strength. The reason is mainly due to the volume changes induced by carbonation as explained above. Strength results also showed that LC^3-CAC blends still exhibit at least similar strength to the non-carbonated PC reference system.

7.3   Perspectives

7.3.1 Adjusting the mix design

For the fixing mortar formulation and in LC³-CAC blends, a part of the unreacted metakaolin could be replaced by limestone. This would improve the rheology, reduce the admixtures content and therefore reduce the cost of these two systems.

More work is needed to study the feasibility of reducing the CAC and Cs content together with the admixtures content in LC³-CAC formulations. An optimization of the CAC, Cs and admixtures content could lead to reducing costs. Therefore, it is interesting to better understand the effect of admixtures on the hydration of LC³-CAC blends and explore if costs can be further reduced.

The influence of substituting the overall LC³ by CAC and Cs should be further investigated. This would allow to further reduce costs compared to the investigated LC³-CAC blends.

7.3.2 Assessment of metakaolin reactivity

The degree of reaction of metakaolin was computed using GEMS based on the portlandite content. In LC³-ACAC1.7, the portlandite content was quite low such that only a minimum reaction degree could be quantified, which was associated with a high error. In addition to the thermodynamic simulation, ^{27}Al-NMR or ^{29}Si-NMR could be used to quantify the reaction degree of metakaolin.

7.3.3   Long term properties

Regarding the chloride ingress, bulk diffusion would be an interesting method for comparison with the mini-migration method. The bulk diffusion test would require a significant amount of time for a measurement (6 months or more). Because of time constraints, it was not possible to run this experiment. Indeed, using this method in the future would allow to measure chloride profiles after a specific exposure time (months to years). The apparent diffusion (D_{app}) coefficient could be calculated for each system. It combines the binding of chloride and the chloride diffusion.

Some other properties could be investigated to validate the use of LC³-CAC blends in specific environment. The interesting properties include the resistance to alkali silica reaction (ASR), the resistance to sulfate attack and the corrosion resistance to chemicals.

It is known that mixes containing calcined clay exhibit very good resistance to alkali silica reaction. This was attributed to the high aluminum ions concentration in these blends that could reduce the silica dissolution and the ASR gel formation [142]. The presence of CAC in LC³-CAC blends is responsible for a higher aluminum ions concentration in the pore solution which means that it would take years to be able to study the ASR products and to identify the mechanisms taking place. For this reason, investigating ASR using highly reactive aggregates would allow to study the ASR products in a shorter period of time. In addition, the lower pH present in the LC³-CAC blends would also strongly slow down ASR reaction [143].

7.3.4 Further perspectives

It would be interesting to do a life cycle assessment (LCA) to this new LC^3-CAC blends. This would alow to find a balance between mechanical performance, costs and CO_2 footprint.

From an application point of view, it would be also important to implement LC^3-CAC blends in the European standards.

Appendix

Effect of the curing temperature on the strength and hydration

The influence of decreasing the curing temperature was investigated. Two tememperatures were compared: 5 and 20°C.

- Compressive strength

Fig. 8-1 shows the compressive strength for PC, LC^3 and LC^3 with 10%(ACAC1.7,Cs) and -10%(ACAC2.2,Cs) up to 90 days, at 5 and 20°C. For all the investigated blends, the strength is decreased by decreasing the curing temperature. At 5°C, PC and LC^3 systems show very low strength at 1 day. On the other hand, incorporating rather ACAC2.2 or ACAC1.7 in LC^3 blends significantly improves the strength at 5°C. At 90 days, contrary to PC and LC^3, the curing temperature has no effect on the strength of LC^3-CAC blends.
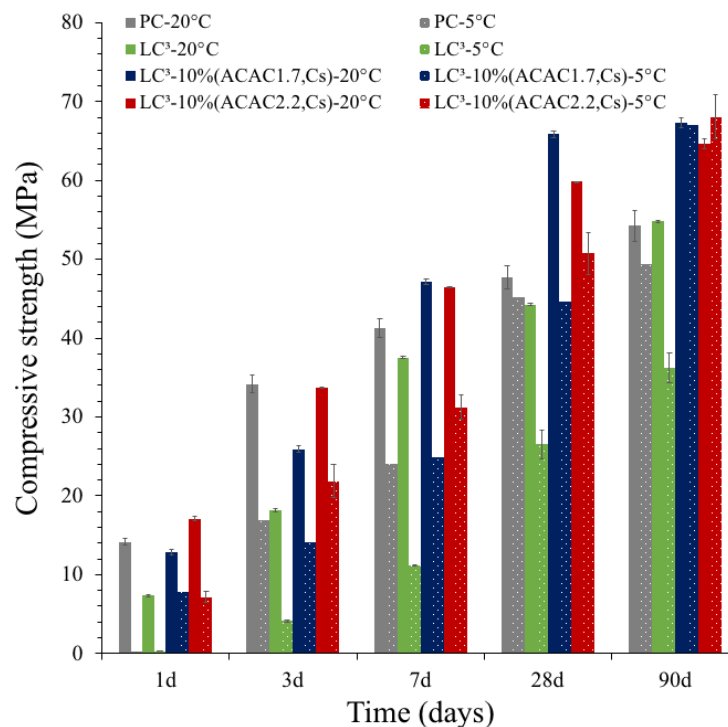
Fig. 8-1 Compressive strength development for PC, LC^3 and LC^3-CAC blends cured at 5 and 20°C.

- Degree of hydration of clinker

To understand the strength results XRD-Rietveld analysis was carried-out up to 90 days. Fig. 8-2 shows the evolution of the degree of hydration of clinker for PC, LC^3 and LC^3 with 10%(ACAC1.7,Cs) and -10%(ACAC2.2,Cs) up to 90 days of hydration. Results show that by decreasing the curing temperature to 5°C the clinker hydration is slowed down for all the investigated

blends. At late age, except for PC, the effect of the curing temperature is reduced and almost a similar degree of hydration of clinker is reached for a same system at 5 and 20°C.
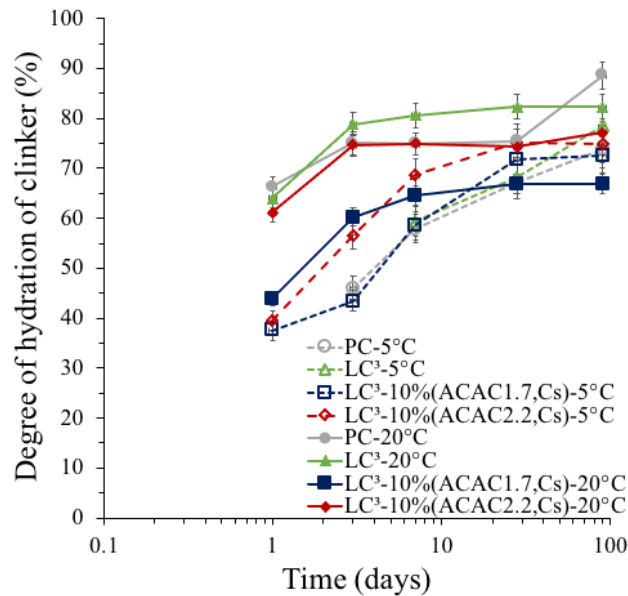
Fig. 8-2 Degree of hydration of clinker for PC, LC^3 and LC^3-CAC blends cured at 5 and 20°C.

- ▪ Ettringite and AFm phases content

Fig. 8-3(a) shows the ettringite content for PC, LC^3 and LC^3 with 10%(ACAC1.7,Cs) and -10%(ACAC2.2,Cs) up to 90 days of hydration. It is clear that decreasing the curing temperature to 5°C leads to a low ettringite content at early age compared to 20°C. For LC^3-CAC blends, the ettringite amount is still high at 5°C and a similar ettringite amount is reached compared to systems cured at 20°C from 7 days onwards. This explains the good strength of LC^3-CAC blends at early age. For all the investigated blends, at 5°C, the AFm type phases (Ms+Hc+Mc) formation is also delayed as shown in Fig. 8-3(b). It starts to form from 7 days onwards at 5°C. These results explain the low compressive strength obtained at 5°C compered to 20°C.
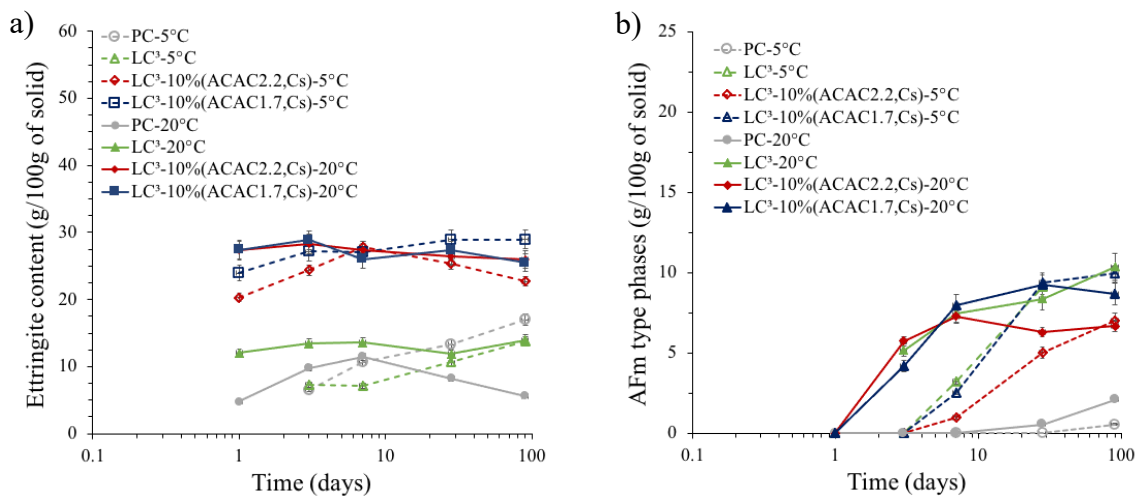
Fig. 8-3 Ettringite and AFm type phases (Ms+Hc+Mc) Rietveld quantification results for PC, LC^3 and LC^3-CAC blends at 5 and 20°C.

- Microstructure observation at 7 days

Fig. 8-4 shows SEM-BSE images of PC, LC^3 and LC^3 blended with 10%(ACAC2.2,Cs) and -10%(ACAC1.7,Cs) at 7 days at a curing temperature of 5°C. Qualitatively, a less porous microstructure is observed in presence of CAC and Cs.
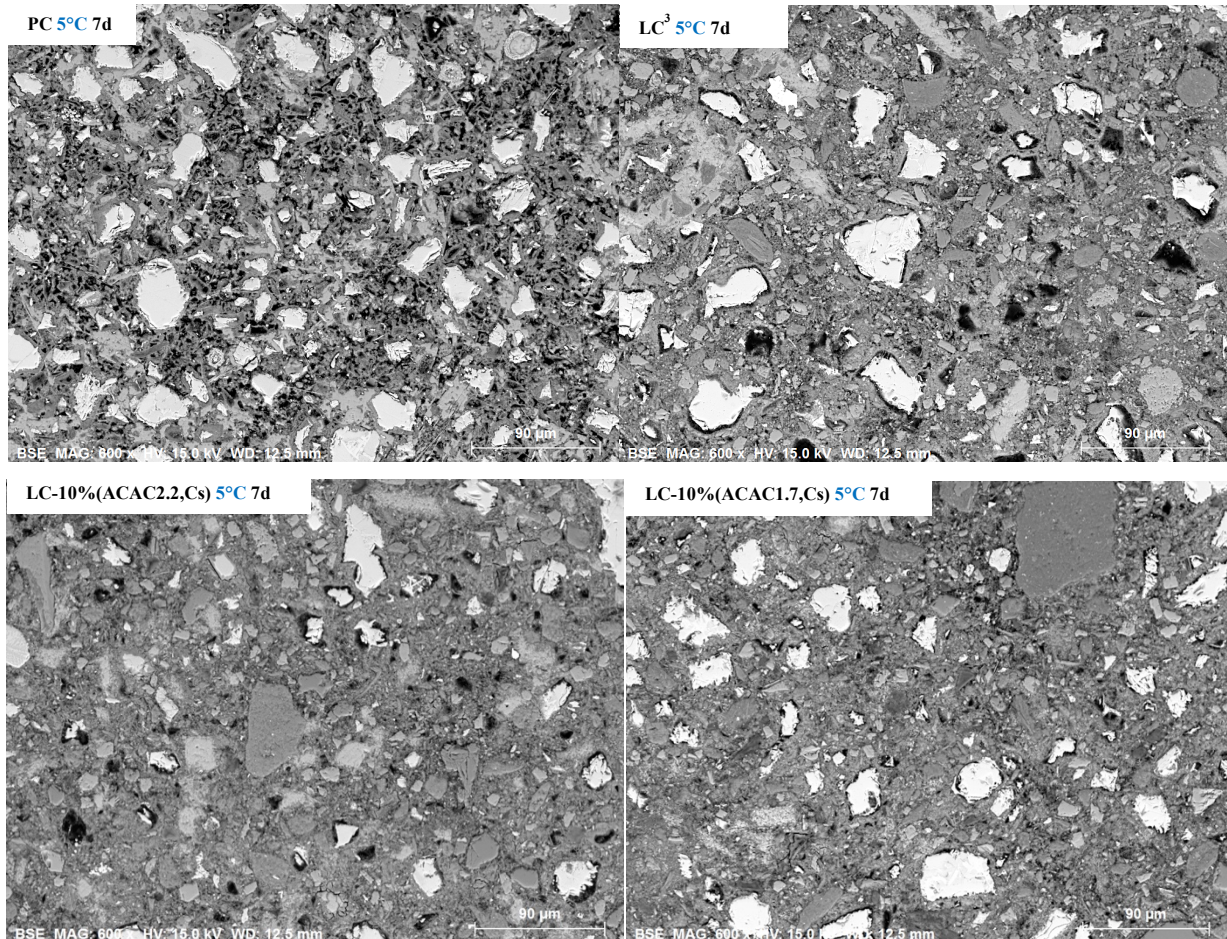
Fig. 8-4 SEM pictures of PC, LC^3, LC^3-10%(ACAC2.2,Cs) and -10%(ACAC1.7,Cs) after 7 days of hydration cured at 5°C.

LC^3-CAC blends keep showing a higher strength performance than PC and LC^3 at 5°C. The decrease of the compressive strength performance of the investigated systems is explained by the slowing down of the kinetics of the clinker hydration, the early ettringite formation and the AFm type phases formation.

References

[1]   J.H.I. Ideker, K.L. Scrivener, H. Fryda, B. Touzo, Lea' s Chemistry of Cement and Concrete : Chapter 13, Fifth edition, 2019. http://www.dbpia.co.kr/view/ar_view.asp?arid=1536305.

[2]   P.G. Hammond, C. Jones, E.F. Lowrie, P. Tse, A BSRIA guide: Embodied Carbon The Inventory of Carbon and Energy (ICE), 2011. www.bath.ac.uk/mech-eng/sert/embodied/. (accessed April 14, 2022).

[3]   International Energy Agency, Technology Roadmap - Low-Carbon Transition in the Cement Industry, (2018) 66. www.wbcsdcement.org.

[4]   Global Cement and Concrete Association, Net CO2 emissions-Weighted average, (2019). https://gccassociation.org/gnr/ (accessed April 15, 2022).

[5]   E. Gartner, H. Hirao, A review of alternative approaches to the reduction of CO2 emissions associated with the manufacture of the binder phase in concrete, Cement and Concrete Research. 78 (2015) 126–142. https://doi.org/10.1016/J.CEMCONRES.2015.04.012.

[6]   J.H.A. Rocha, R.D. Toledo Filho, N.G. Cayo-Chileno, Sustainable alternatives to CO2 reduction in the cement industry: A short review, Materials Today: Proceedings. (2022). https://doi.org/10.1016/J.MATPR.2021.12.565.

[7]   K.L. Scrivener, V.M. John, E.M. Gartner, Eco-efficient cements: Potential economically viable solutions for a low-CO2 cement-based materials industry, Cement and Concrete Research. 114 (2018) 2–26. https://doi.org/10.1016/j.cemconres.2018.03.015.

[8]   A. Nonat, L'hydratation des ciments, in: La Durabilité Des Bétons, 2008: pp. 25–50.

[9]   J.W. Bullard, H.M. Jennings, R.A. Livingston, A. Nonat, G.W. Scherer, J.S. Schweitzer, K.L. Scrivener, J.J. Thomas, Mechanisms of cement hydration, Cement and Concrete Research. 41 (2011) 1208–1223. https://doi.org/10.1016/J.CEMCONRES.2010.09.011.

[10]   H.F.W. Tylor, Cement chemistry, 2nd edition, Thomas Telford Publishing, 1997. https://doi.org/10.1680/cc.25929.

[11]   C. Hea, B.Osbzckb, E.Makovicky, Pozzolanic reactions of six principal clay minerals: activation, reactivity assemments and technological effects, Cement and Concrete Research. 25 (1995) 1691–1702.

[12] A. Shvarzman, K. Kovler, G.S. Grader, G.E. Shter, The effect of dehydroxylation/amorphization degree on pozzolanic activity of kaolinite, Cement and Concrete Research. 33 (2003) 405–416. https://doi.org/10.1016/S0008-8846(02)00975-4.

[13] R. Fernandez, F. Martirena, K.L. Scrivener, The origin of the pozzolanic activity of calcined clay minerals: A comparison between kaolinite, illite and montmorillonite, Cement and Concrete Research. 41 (2011) 113–122. https://doi.org/10.1016/j.cemconres.2010.09.013.

[14] K.L. Konan, C. Peyratout, A. Smith, J.P. Bonnet, S. Rossignol, S. Oyetola, Comparison of surface properties between kaolin and metakaolin in concentrated lime solutions, Journal of Colloid and Interface Science. 339 (2009) 103–109. https://doi.org/10.1016/j.jcis.2009.07.019.

[15] E. Berodier, K. Scrivener, Understanding the filler effect on the nucleation and growth of C-S-H, Journal of the American Ceramic Society. 97 (2014) 3764–3773. https://doi.org/10.1111/JACE.13177.

[16] B. Lothenbach, K. Scrivener, R.D. Hooton, Supplementary cementitious materials, Cement and Concrete Research. 41 (2011) 1244–1256. https://doi.org/10.1016/J.CEMCONRES.2010.12.001.

[17] M. Zajac, A. Rossberg, G. le Saout, B. Lothenbach, Influence of limestone and anhydrite on the hydration of Portland cements, Cement and Concrete Composites. 46 (2014) 99–108. https://doi.org/10.1016/J.CEMCONCOMP.2013.11.007.

[18] B. Lothenbach, G. le Saout, E. Gallucci, K. Scrivener, Influence of limestone on the hydration of Portland cements, Cement and Concrete Research. 38 (2008) 848–860. https://doi.org/10.1016/J.CEMCONRES.2008.01.002.

[19] Olga Chowaniec, Limestone Addition in Cement, Ecole Polytechnique Fédérale de Lausanne , 2012. https://doi.org/10.5075/epfl-thesis-5335 (accessed June 28, 2022).

[20] T. Matschei, B. Lothenbach, F.P. Glasser, The role of calcium carbonate in cement hydration, Cement and Concrete Research. 37 (2007) 551–558. https://doi.org/10.1016/J.CEMCONRES.2006.10.013.

[21] A. Tironi, M.A. Trezza, A.N. Scian, E.F. Irassar, Assessment of pozzolanic activity of different calcined clays, Cement and Concrete Composites. 37 (2013) 319–327. https://doi.org/10.1016/J.CEMCONCOMP.2013.01.002.

[22] A.S. Silva, A. Gameiro, J. Grilo, R. Veiga, A. Velosa, Long-term behavior of lime-metakaolin pastes at ambient temperature and humid curing condition, Applied Clay Science. 88–89 (2014) 49–55. https://doi.org/10.1016/j.clay.2013.12.016.

[23] M. Antoni, J. Rossen, F. Martirena, K. Scrivener, Cement substitution by a combination of metakaolin and limestone, Cement and Concrete Research. 42 (2012) 1579–1589. https://doi.org/10.1016/j.cemconres.2012.09.006.

[24] F. Zunino, K. Scrivener, The reaction between metakaolin and limestone and its effect in porosity refinement and mechanical properties, Cement and Concrete Research. 140 (2021) 106307. https://doi.org/10.1016/J.CEMCONRES.2020.106307.

[25] H. Huang, X. Li, F. Avet, W. Hanpongpun, K. Scrivener, Strength-promoting mechanism of alkanolamines on limestone-calcined clay cement and the role of sulfate, Cement and Concrete Research. 147 (2021) 106527. https://doi.org/10.1016/J.CEMCONRES.2021.106527.

[26] J.P. Perez, A. Nonat, S. Pourchet, M. Garrault, C. Canevet, Why TIPA leads to an increase in the mechanical properties of mortars whereas TEA does not, ACI Materials Journal. 217 (2003) 583–594.

[27] F. Zunino, K. Scrivener, Assessing the effect of alkanolamine grinding aids in limestone calcined clay cements hydration, Construction and Building Materials. 266 (2021) 121293. https://doi.org/10.1016/J.CONBUILDMAT.2020.121293.

[28] W. Hanpongpun, Investigation of the use of Limestone Calcined Clay Cement (LC3) applied to Thailand, Ecole Polytechnique Fédérale de Lausanne, 2019. https://doi.org/10.5075/EPFL-THESIS-9005.

[29] S. Sui, F. Georget, H. Maraghechi, W. Sun, K. Scrivener, Towards a generic approach to durability: Factors affecting chloride transport in binary and ternary cementitious materials, Cement and Concrete Research. 124 (2019). https://doi.org/10.1016/J.CEMCONRES.2019.105783.

[30] S. Sui, W. Wilson, F. Georget, H. Maraghechi, H. Kazemi-Kamyab, W. Sun, K. Scrivener, Quantification methods for chloride binding in Portland cement and limestone systems, Cement and Concrete Research. 125 (2019). https://doi.org/10.1016/J.CEMCONRES.2019.105864.

[31] V. Shah, S. Bishnoi, Carbonation resistance of cements containing supplementary cementitious materials and its relation to various parameters of concrete, Construction and Building Materials. 178 (2018) 219–232. https://doi.org/10.1016/J.CONBUILDMAT.2018.05.162.

[32] J. Khunthongkeaw, S. Tangtermsirikul, T. Leelawat, A study on carbonation depth prediction for fly ash concrete, Construction and Building Materials. 20 (2006) 744–753. https://doi.org/10.1016/J.CONBUILDMAT.2005.01.052.

[33] K. Scrivener, Calcium aluminate cements, 2003. https://doi.org/10.1016/B978-075065686-3/50278-0.

[34]   K.Y. Ann, C.G. Cho, Corrosion resistance of calcium aluminate cement concrete exposed to a chloride environment, Materials. 7 (2014) 887–898. https://doi.org/10.3390/ma7020887.

[35]   A. Macias, A. Kindness, F.P. Glasser, Corrosion behaviour of steel in high alumina cement mortar cured at 5, 25 and 55 °C: chemical and physical factors, Journal of Materials Science. 31 (1996) 2279–2289.

[36]   H.A. Khan, A. Castel, M.S.H. Khan, A.H. Mahmood, Durability of calcium aluminate and sulphate resistant Portland cement based mortars in aggressive sewer environment and sulphuric acid, Cement and Concrete Research. 124 (2019) 105852. https://doi.org/10.1016/J.CEMCONRES.2019.105852.

[37]   K. Nakagawa, I. Terashima, K. Asaga, M. Daimon, A study of hydration of amorphous calcium aluminate by selective dissolution analysis, Cement and Concrete Research. 20 (1990) 655–661. https://doi.org/10.1016/0008-8846(90)90108-A.

[38]   S.M. Park, J.G. Jang, H.M. Son, H.K. Lee, Stable conversion of metastable hydrates in calcium aluminate cement by early carbonation curing, Journal of CO2 Utilization. 21 (2017) 224–226. https://doi.org/10.1016/J.JCOU.2017.07.002.

[39]   M. Chavda, J. Provis, M.A. Chavda, H. Kinoshita, J.L. Provis, Modification of a calcium aluminate cement system to prevent conversion to cubic hydrates and minimise corrosion of encapsulated aluminium metal: 32nd Cement and Concrete Science Conference, Queen's University Belfast, 17-18 September, in: 2012. https://www.researchgate.net/publication/251572196 (accessed April 9, 2022).

[40]   H.M. Son, S. Park, H.Y. Kim, J.H. Seo, H.K. Lee, Effect of CaSO4 on hydration and phase conversion of calcium aluminate cement, Construction and Building Materials. 224 (2019) 40–47. https://doi.org/10.1016/J.CONBUILDMAT.2019.07.004.

[41]   P.C. Hewlett, M. Liska, Lea's chemistry of cement and concrete, Elsevier, 2019. https://doi.org/10.1016/C2013-0-19325-7.

[42]   J. Nehring, J. Neubauer, S. Berger, F. Goetz-Neunhoeffer, Acceleration of OPC by CAC in binary and ternary systems: The role of pore solution chemistry, Cement and Concrete Research. 107 (2018) 264–274. https://doi.org/10.1016/j.cemconres.2018.02.012.

[43]   D. Torréns-Martín, L. Fernández-Carrasco, M.T. Blanco-Varela, Conduction calorimetric studies of ternary binders based on Portland cement, calcium aluminate cement and calcium sulphate, Journal of Thermal Analysis and Calorimetry. 114 (2013) 799–807. https://doi.org/10.1007/s10973-013-3003-9.

[44]   J. Bizzozero, Hydration and dimensional stability of calcium aluminate cement based systems, Ecole Polytechnique Fédérale de Lausanne, 2014. https://doi.org/10.5075/epfl-thesis-6336 (accessed June 28, 2022).

[45]   J. Kighelman, Hydration and Structure Development of Ternary Binder System as Used in Self-Levelling Compounds, Ecole Polytechnique Fédérale de Lausanne, 2007. https://doi.org/10.5075/epfl-thesis-3777 (accessed June 28, 2022).

[46]   L. Xu, P. Wang, G. Zhang, Calorimetric study on the influence of calcium sulfate on the hydration of Portland cement-calcium aluminate cement mixtures, Journal of Thermal Analysis and Calorimetry. 110 (2012) 725–731. https://doi.org/10.1007/s10973-011-1920-z.

[47]   L. Amathieu, T. Bier, K. Scrivener, Mechanisms of set acceleration of Portland cement through CAC addition, International Conference on Calcium Aluminate Cements. (2001) 303–317.

[48]   G. le Saoût, B. Lothenbach, A. Hori, T. Higuchi, F. Winnefeld, Hydration mechanism of quick hardening cement based on OPC blended with an amorphous calcium aluminate, Proceedings of the 18th International Conference on Building Materials (Ibausil), Weimar. (2012).

[49]   H.J. Yang, K.Y. Ann, M.S. Jung, Development of strength for calcium aluminate cement mortars blended with GGBS, Advances in Materials Science and Engineering. 2019 (2019). https://doi.org/10.1155/2019/9896012.

[50]   J. Bizzozero, K.L. Scrivener, Limestone reaction in calcium aluminate cement-calcium sulfate systems, Cement and Concrete Research. 76 (2015) 159–169. https://doi.org/10.1016/j.cemconres.2015.05.019.

[51]   L. Fernández-Carrasco, E. Vázquez, Reactions of fly ash with calcium aluminate cement and calcium sulphate, Fuel. (2009) 1533–1538. https://doi.org/10.1016/j.fuel.2009.02.018.

[52]   J. Astoveza, R. Trauchessec, S. Migot-Choux, R. Soth, Y. Pontikes, Iron-rich slag addition in ternary binders of Portland cement, aluminate cement and calcium sulfate, Cement and Concrete Research. 153 (2022) 106689. https://doi.org/10.1016/J.CEMCONRES.2021.106689.

[53]   J. Astoveza, R. Trauchessec, R. Soth, Y. Pontikes, Properties of calcium aluminate blended cement incorporating iron-rich slag: Evolution over a curing period of 1 year, Construction and Building Materials. 282 (2021). https://doi.org/10.1016/J.CONBUILDMAT.2021.122569.

[54]   D.A. Kulik, T. Wagner, S. v. Dmytrieva, G. Kosakowski, F.F. Hingerl, K. v. Chudnenko, U.R. Berner, GEM-Selektor geochemical modeling package: revised algorithm and GEMS3K numerical kernel for coupled simulation codes, Computational Geosciences 2012 17:1. 17 (2012) 1–24. https://doi.org/10.1007/S10596-012-9310-6.

[55]   B. Lothenbach, D.A. Kulik, T. Matschei, M. Balonis, L. Baquerizo, B. Dilnesa, G.D. Miron, R.J. Myers, Cemdata18: A chemical thermodynamic database for hydrated

Portland cements and alkali-activated materials, Cement and Concrete Research. 115 (2019) 472–506. https://doi.org/10.1016/J.CEMCONRES.2018.04.018.

[56]   W. Hummel, U. Berner, E. Curti, F.J. Pearson, T. Thoenen, Nagra / PSI Chemical Thermodynamic Data Base 01/01; Nagra technical report 02-16, 813 (2002) 805–813.

[57]   K.L. Scrivener, J.L. Cabiron, R. Letourneux, High-performance concretes from calcium aluminate cements, Cement and Concrete Research. 29 (1999) 1215–1223. https://doi.org/10.1016/S0008-8846(99)00103-9.

[58]   E.C. Industry, I. Bat, " Best available techniques " For the cement industry, 1999.

[59]   R. Snellings, Assessing, Understanding and Unlocking Supplementary Cementitious Materials, RILEM Technical Letters. 1 (2016) 50. https://doi.org/10.21809/rilemtechlett.2016.12.

[60]   A.S. Silva, A. Gameiro, J. Grilo, R. Veiga, A. Velosa, Long-term behavior of lime–metakaolin pastes at ambient temperature and humid curing condition, Applied Clay Science. 88–89 (2014) 49–55. https://doi.org/10.1016/J.CLAY.2013.12.016.

[61]   A. Alujas, R. Fernández, R. Quintana, K.L. Scrivener, F. Martirena, Pozzolanic reactivity of low grade kaolinitic clays: Influence of calcination temperature and impact of calcination products on OPC hydration, Applied Clay Science. 108 (2015) 94–101. https://doi.org/10.1016/j.clay.2015.01.028.

[62]   R. Fernandez, Calcined Clayey Soils as a Potential Replacement For Cement in Developing Countries, Ecole Polytechnique Fédérale de Lausanne, 2009.

[63]   F. Avet, K. Scrivener, Investigation of the calcined kaolinite content on the hydration of Limestone Calcined Clay Cement (LC3), Cement and Concrete Research. 107 (2018) 124–135. https://doi.org/10.1016/j.cemconres.2018.02.016.

[64]   A. Negro, A. Bachiorrini, M. Murat, Interaction, in aqueous medium, between calcium carbonate and monocalcium aluminate at 5 °C, 20 °C and 40 °C, Bulletin de Minéralogie. 105 (1982) 284–290. https://doi.org/10.3406/BULMI.1982.7618.

[65]   C.H. Fentiman, Hydration of carbo-aluminous cement at different temperatures, Cement and Concrete Research. 15 (1985) 622–630. https://doi.org/10.1016/0008-8846(85)90061-4.

[66]   R.N. Edmonds, A.J. Majumdar, The hydration of mixtures of monocalcium aluminate and blastfurnace slag, Cement and Concrete Research. 19 (1989) 779–782. https://doi.org/10.1016/0008-8846(89)90048-3.

[67]   K. Scrivener, R. Snellings, B. Lothenbach, F. Group, A Practical Guide to Microstructural Analysis of Cementitious Materials, 2018. https://doi.org/10.1201/b19074.

[68] J.E. Rossen, K.L. Scrivener, Optimization of SEM-EDS to determine the C–A–S–H composition in matured cement paste samples, Materials Characterization. 123 (2017) 294–306. https://doi.org/10.1016/J.MATCHAR.2016.11.041.

[69] M. Dornak, J.R. Zungia, G. Anthony, T. Drimalas, K.J. Folliard, Development of Rapid, Cement-based Repair Materials for Transportation Structures, 2014. http://hdl.handle.net/2152/22348.

[70] Q.D. Nguyen, T. Kim, A. Castel, Mitigation of alkali-silica reaction by limestone calcined clay cement (LC3), Cement and Concrete Research. 137 (2020) 106176. https://doi.org/10.1016/J.CEMCONRES.2020.106176.

[71] F. Zunino, F. Martirena, K. Scrivener, Limestone calcined clay cements (LC3), ACI Materials Journal. 118 (2021) 49–60. https://doi.org/10.14359/51730422.

[72] B. Lothenbach, K. Scrivener, R.D. Hooton, Supplementary cementitious materials, Cement and Concrete Research. 41 (2011) 1244–1256. https://doi.org/10.1016/j.cemconres.2010.12.001.

[73] K.L. Scrivener, A. Capmas, Lea' s Chemistry of Cement and Concrete : Chapter 13, 2004. http://www.dbpia.co.kr/view/ar_view.asp?arid=1536305.

[74] V.S. Ramachandran, Cement hydration-Role of triethanolamine, CEMENT and CONCRETE RESEARCH. 6 (1976) 623–632.

[75] E. Berodier, Impact of the Supplementary Cementitious Materials on the kinetics and microstructural development of cement hydration, 2015. https://doi.org/10.5075/EPFL-THESIS-6417.

[76] P. Gu, J.J. Beaudoin, E.G. Quinn, R.E. Myers, Early strength development and hydration of ordinary portland cement/calcium aluminate cement pastes, Advanced Cement Based Materials. 6 (1997) 53–58. https://doi.org/10.1016/S1065-7355(97)00008-4.

[77] P. Gu, Y. Fu, J.J. Beaudoin, A study of the hydration and setting behaviour of OPC-HAC pastes, Cement and Concrete Research. 24 (1994) 682–694. https://doi.org/10.1016/0008-8846(94)90192-9.

[78] Tadros M. E., J. Skalny, R.S. Kalyoncu, Early Hydration of Tricalcium Silicate, Journal of the American Ceramic Society. 59 (1976) 344–347. https://doi.org/10.1111/J.1151-2916.1976.TB10980.X.

[79] J.F. Young, H.S. Tong, R.L. Berger, Compositions of solutions in contact with hydrating tricalcium silicate pastes, Journal of the American Ceramic Society. 60 (1977) 193–198. https://doi.org/10.1111/J.1151-2916.1977.TB14104.X.

[80] I. Odler, H. Dörr, Early hydration of tricalcium silicate II. The induction period, Cement and Concrete Research. 9 (1979) 277–284. https://doi.org/10.1016/0008-8846(79)90119-4.

[81] S. Garrault-Gauffinet, A. Nonat, Experimental investigation of calcium silicate hydrate (C-S-H) nucleation, Journal of Crystal Growth. 200 (1999) 565–574. https://doi.org/10.1016/S0022-0248(99)00051-2.

[82] P. Fierens, J.P. Verhaegen, Hydration of tricalcium silicate in paste-kinetics of calcium ions dissolution in the aqueous phase, Cement and Concrete Research. 6 (1976) 337–342.

[83] J.W. Bullard, R.J. Flatt, New Insights Into the Effect of Calcium Hydroxide Precipitation on the Kinetics of Tricalcium Silicate Hydration, Journal of the American Ceramic Society. 93 (2010) 1894–1903. https://doi.org/10.1111/J.1551-2916.2010.03656.X.

[84] L. Xu, P. Wang, G. De Schutter, G. Wu, Effect of calcium aluminate cement variety on the hydration of portland cement in blended system, Journal Wuhan University of Technology, Materials Science Edition. 29 (2014) 751–756. https://doi.org/10.1007/s11595-014-0991-7.

[85] P. Gu, J.J. Beaudoin, A conduction calorimetric study of early hydration of ordinary Portland cement/high alumina cement pastes, Journal of Materials Science. 32 (1997) 3875–3881. https://doi.org/10.1023/A:1018600412638.

[86] K. Scrivener, A. Ouzia, P. Juilland, A. Kunhi Mohamed, Advances in understanding cement hydration mechanisms, Cement and Concrete Research. 124 (2019) 105823. https://doi.org/10.1016/J.CEMCONRES.2019.105823.

[87] R.K. Iler, Effect of adsorbed alumina on the solubility of amorphous silica in water, Journal of Colloid and Interface Science. 43 (1973) 399–408. https://doi.org/10.1016/0021-9797(73)90386-X.

[88] T. Chappex, K.L. Scrivener, The effect of aluminum in solution on the dissolution of amorphous silica and its relation to cementitious systems, Journal of the American Ceramic Society. 96 (2013) 592–597. https://doi.org/10.1111/JACE.12098.

[89] L. Nicoleau, E. Schreiner, A. Nonat, Ion-specific effects influencing the dissolution of tricalcium silicate, Cement and Concrete Research. (2014). https://doi.org/10.1016/j.cemconres.2014.02.006.

[90] F. Begarin, S. Garrault, A. Nonat, L. Nicoleau, Hydration of alite containing aluminium, Advances in Applied Ceramics. 110 (2011) 127–130. https://doi.org/10.1179/1743676110Y.0000000007.

[91] G. Le Saoût, B. Lothenbach, A. Hori, T. Higuchi, F. Winnefeld, Hydration of Portland cement with additions of calcium sulfoaluminates, Cement and Concrete Research. 43 (2013) 81–94. https://doi.org/10.1016/J.CEMCONRES.2012.10.011.

[92] J. Nehring, D. Jansen, J. Neubauer, F. Goetz-Neunhoeffer, Hydration of C3S in presence of CA: Mineral-pore solution interaction, Journal of the American Ceramic Society. 102 (2019) 3152–3162. https://doi.org/10.1111/JACE.16197.

[93] L. Xu, P. Wang, G. Zhang, Calorimetric study on the influence of calcium sulfate on the hydration of Portland cement-calcium aluminate cement mixtures, Journal of Thermal Analysis and Calorimetry. 110 (2012) 725–731.

[94] J. Nehring, J. Neubauer, S. Berger, F. Goetz-Neunhoeffer, Acceleration of OPC by CAC in binary and ternary systems: The role of pore solution chemistry, Cement and Concrete Research. 107 (2018) 264–274. https://doi.org/10.1016/J.CEMCONRES.2018.02.012.

[95] S. Lamberet, Durability of ternary binders based on portland cement, calcium aluminate cement and calcium sulfate, Ecole Polytechnique Fédérale de Lausanne, 2005.

[96] B. Traynor, H. Uvegi, E. Olivetti, B. Lothenbach, R.J. Myers, Methodology for pH measurement in high alkali cementitious systems, Cement and Concrete Research. 135 (2020) 106122. https://doi.org/10.1016/J.CEMCONRES.2020.106122.

[97] L. Nicoleau, A. Nonat, D. Perrey, The di- and tricalcium silicate dissolutions, Cement and Concrete Research. 47 (2013) 14–30. https://doi.org/10.1016/J.CEMCONRES.2013.01.017.

[98] B. Lothenbach, M. Zajac, Application of thermodynamic modelling to hydrated cements, Cement and Concrete Research. 123 (2019) 105779. https://doi.org/10.1016/J.CEMCONRES.2019.105779.

[99] F. Georget, W. Wilson, K.L. Scrivener, edxia: Microstructure characterisation from quantified SEM-EDS hypermaps, Cement and Concrete Research. 141 (2021) 106327. https://doi.org/10.1016/J.CEMCONRES.2020.106327.

[100] A. Quennoz, K.L. Scrivener, Interactions between alite and C3A-gypsum hydrations in model cements, Cement and Concrete Research. 44 (2013) 46–54. https://doi.org/10.1016/j.cemconres.2012.10.018.

[101] E. Gallucci, P. Mathur, K. Scrivener, Microstructural development of early age hydration shells around cement grains, Cement and Concrete Research. 40 (2010) 4–13. https://doi.org/10.1016/j.cemconres.2009.09.015.

[102] R. Barbarulo, H. Peycelon, S. Leclercq, Chemical equilibria between C–S–H and ettringite, at 20 and 85 °C, Cement and Concrete Research. 37 (2007) 1176–1181. https://doi.org/10.1016/J.CEMCONRES.2007.04.013.

[103] D.G. Evans, R.C.T. Slade, Structural aspects of layered double hydroxides, Structure and Bonding. 119 (2005) 1–87. https://doi.org/10.1007/430_005.

[104] Y. Briki, F. Avet, M. Zajac, P. Bowen, M. ben Haha, K. Scrivener, Understanding of the factors slowing down metakaolin reaction in limestone calcined clay cement (LC3) at late ages, Cement and Concrete Research. 146 (2021) 106477. https://doi.org/10.1016/j.cemconres.2021.106477.

[105] A.C.A. Muller, K.L. Scrivener, J. Skibsted, A.M. Gajewicz, P.J. McDonald, Influence of silica fume on the microstructure of cement pastes: New insights from 1H NMR relaxometry, Cement and Concrete Research. 74 (2015) 116–125. https://doi.org/10.1016/j.cemconres.2015.04.005.

[106] P. Lura, O.M. Jensen, K. van Breugel, Autogenous shrinkage in high-performance cement paste: An evaluation of basic mechanisms, Cement and Concrete Research. 33 (2003) 223–232. https://doi.org/10.1016/S0008-8846(02)00890-6.

[107] F. Zunino, K. Scrivener, Microstructural developments of limestone calcined clay cement (LC3) pastes after long-term (3 years) hydration, Cement and Concrete Research. 153 (2022) 106693. https://doi.org/10.1016/J.CEMCONRES.2021.106693.

[108] F. Avet, E. Boehm-Courjault, K. Scrivener, Investigation of C-A-S-H composition, morphology and density in Limestone Calcined Clay Cement (LC3), Cement and Concrete Research. 115 (2019) 70–79. https://doi.org/10.1016/J.CEMCONRES.2018.10.011.

[109] M. Balonis, B. Lothenbach, G. le Saout, F.P. Glasser, Impact of chloride on the mineralogy of hydrated Portland cement systems, Cement and Concrete Research. 40 (2010) 1009–1022. https://doi.org/10.1016/J.CEMCONRES.2010.03.002.

[110] F. Georget, B. Lothenbach, W. Wilson, F. Zunino, K.L. Scrivener, Stability of hemicarbonate under cement paste-like conditions, Cement and Concrete Research. 153 (2022) 106692. https://doi.org/10.1016/J.CEMCONRES.2021.106692.

[111] H. Hirao, K. Yamada, H. Takahashi, H. Zibara, Chloride Binding of Cement Estimated by Binding Isotherms of Hydrates, Journal of Advanced Concrete Technology. 3 (2005) 77–84.

[112] H. Zibara, R.D. Hooton, M.D.A. Thomas, K. Stanish, Influence of the C/S and C/A ratios of hydration products on the chloride ion binding capacity of lime-SF and lime-MK mixtures, Cement and Concrete Research. 38 (2008) 422–426. https://doi.org/10.1016/J.CEMCONRES.2007.08.024.

[113] R. Loser, B. Lothenbach, A. Leemann, M. Tuchschmid, Chloride resistance of concrete and its binding capacity – Comparison between experimental results and thermodynamic modeling, Cement and Concrete Composites. 32 (2010) 34–42. https://doi.org/10.1016/J.CEMCONCOMP.2009.08.001.

[114] U.A. Birnin-Yauri, F.P. Glasser, Friedel's salt, Ca2Al(OH)6(Cl,OH)·2H2O: its solid solutions and their role in chloride binding, Cement and Concrete Research. 28 (1998) 1713–1723. https://doi.org/10.1016/S0008-8846(98)00162-8.

[115] Z. Shi, M.R. Geiker, B. Lothenbach, K. de Weerdt, S.F. Garzón, K. Enemark-Rasmussen, J. Skibsted, Friedel's salt profiles from thermogravimetric analysis and thermodynamic modelling of Portland cement-based mortars exposed to sodium chloride solution, Cement and Concrete Composites. 78 (2017) 73–83. https://doi.org/10.1016/J.CEMCONCOMP.2017.01.002.

[116] H. Maraghechi, F. Avet, H. Wong, H. Kamyab, K. Scrivener, Performance of Limestone Calcined Clay Cement (LC3) with various kaolinite contents with respect to chloride transport, Materials and Structures/Materiaux et Constructions. 51 (2018) 1–17. https://doi.org/10.1617/S11527-018-1255-3/FIGURES/18.

[117] W. Wilson, F. Georget, K. Scrivener, Unravelling chloride transport/microstructure relationships for blended-cement pastes with the mini-migration method, Cement and Concrete Research. 140 (2021). https://doi.org/10.1016/J.CEMCONRES.2020.106264.

[118] NT BUILD 443, Concrete, Hardened: Accelerated Chloride Penetration, (1995). www.nordtest.org (accessed March 8, 2022).

[119] T. Nishikawa, K. Suzuki, S. Ito, K. Sato, T. Takebe, Decomposition of synthesized ettringite by carbonation, Cement and Concrete Research. 22 (1992) 6–14. https://doi.org/10.1016/0008-8846(92)90130-N.

[120] K. Kobayashi, K. Suzuki, Y. Uno, Carbonation of concrete structures and decomposition of CSH, Cement and Concrete Research. 24 (1994) 55–61. https://doi.org/10.1016/0008-8846(94)90082-5.

[121] G.W. Groves, D.I. Rodway, I.G. Richardson, The carbonation of hardened cement pastes, Advances in Cement Research. 11 (1990) 117–125.

[122] F.P. Glasser, T. Matschei, Interactions Between Portland Cement and Carbon Dioxide, in: International Congress on the Chemistry of Cement, 2007.

[123] S. Zdenek, Carboniztion of porous concrete and its main binding componenta, Cement and Concrete Research. 1 (1971) 645–662.

[124] V.G. Papadakis, M.N. Fardis, C.G. Vayenas, Effect of composition, environmental factors and cement-lime mortar coating on concrete carbonation, Materials and Structures 1992 25:5. 25 (1992) 293–304. https://doi.org/10.1007/BF02472670.

[125] M.G. Richardson, Fundamentals of durable reinforced concrete, CRC Press, 2002.

[126] M. Antoni, J. Rossen, F. Martirena, K. Scrivener, Cement substitution by a combination of metakaolin and limestone, Cement and Concrete Research. 42 (2012) 1579–1589. https://doi.org/10.1016/j.cemconres.2012.09.006.

[127] B. Johannesson, P. Utgenannt, Microstructural changes caused by carbonation of cement mortar, Cement and Concrete Research. 31 (2001) 925–931. https://doi.org/10.1016/S0008-8846(01)00498-7.

[128] V. Shah, K. Scrivener, B. Bhattacharjee, S. Bishnoi, Changes in microstructure characteristics of cement paste on carbonation, Cement and Concrete Research. 109 (2018) 184–197. https://doi.org/10.1016/J.CEMCONRES.2018.04.016.

[129] V.T. Ngala, C.L. Page, Effects of carbonation on pore structure and diffusional properties of hydrated cement pastes, Cement and Concrete Research. 27 (1997) 995–1007. https://doi.org/10.1016/S0008-8846(97)00102-6.

[130] B. Šavija, M. Luković, Carbonation of cement paste: Understanding, challenges, and opportunities, Construction and Building Materials. 117 (2016) 285–301. https://doi.org/10.1016/J.CONBUILDMAT.2016.04.138.

[131] J. Xiao, J. Li, B. Zhu, Z. Fan, Experimental study on strength and ductility of carbonated concrete elements, Construction and Building Materials. 16 (2002) 187–192. https://doi.org/10.1016/S0950-0618(01)00034-4.

[132] N.R. Short, A.R. Brough, A.M.G. Seneviratne, P. Purnell, C.L. Page, Preliminary investigations of the phase composition and fine pore structure of super-critically carbonated cement pastes, Journal of Materials Science 2004 39:18. 39 (2004) 5683–5687. https://doi.org/10.1023/B:JMSC.0000040076.42260.CB.

[133] R. Folic, D. Zenunovic, Durability design of concrete structures, Part 2: Modelling and structural assessment, Facta Universitatis - Series: Architecture and Civil Engineering. 8 (2010) 45–66. https://doi.org/10.2298/fuace1001045f.

[134] H. Böhni, ed., Corrosion in reinforced concrete structures, Woodhead Publishing Limited, 2005. www.woodhead-publishing.com (accessed March 6, 2022).

[135] F. Avet, K. Scrivener, Influence of pH on the chloride binding capacity of Limestone Calcined Clay Cements (LC3), Cement and Concrete Research. 131 (2020) 106031. https://doi.org/10.1016/J.CEMCONRES.2020.106031.

[136] Z. Shi, M.R. Geiker, K. de Weerdt, T.A. Østnor, B. Lothenbach, F. Winnefeld, J. Skibsted, Role of calcium on chloride binding in hydrated Portland cement–metakaolin–limestone blends, Cement and Concrete Research. 95 (2017) 205–216. https://doi.org/10.1016/J.CEMCONRES.2017.02.003.

[137] M.S.H. Khan, Q.D. Nguyen, A. Castel, Carbonation of limestone calcined clay cement concrete, in: RILEM Bookseries, Springer Netherlands, 2018: pp. 238–243. https://doi.org/10.1007/978-94-024-1207-9_38.

[138] W. Soja, Carbonation of low carbon binders, Ecole Polytechnique Fédérale de Lausanne, 2019. https://doi.org/10.5075/epfl-thesis-9400 (accessed June 28, 2022).

[139] W. Wilson, J.N. Gonthier, F. Georget, K.L. Scrivener, Insights on chemical and physical chloride binding in blended cement pastes, Cement and Concrete Research. 156 (2022) 106747. https://doi.org/10.1016/J.CEMCONRES.2022.106747.

[140] S. Yoshida, Y. Elakneswaran, T. Nawa, Electrostatic properties of C–S–H and C-A-S-H for predicting calcium and chloride adsorption, Cement and Concrete Composites. 121 (2021) 104109. https://doi.org/10.1016/J.CEMCONCOMP.2021.104109.

[141] Z. Shi, B. Lothenbach, M.R. Geiker, J. Kaufmann, A. Leemann, S. Ferreiro, J. Skibsted, Experimental studies and thermodynamic modeling of the carbonation of Portland cement, metakaolin and limestone mortars, Cement and Concrete Research. 88 (2016) 60–72. https://doi.org/10.1016/J.CEMCONRES.2016.06.006.

[142] T. Chappex, K.L. Scrivener, The influence of aluminium on the dissolution of amorphous silica and its relation to alkali silica reaction, Cement and Concrete Research. 42 (2012) 1645–1649. https://doi.org/10.1016/J.CEMCONRES.2012.09.009.

[143] M. Bagheri, B. Lothenbach, K. Scrivener, The effect of paste composition aggregate mineralogy and temperature on the pore solution composition and the extent of ASR expansion, Materials and Structures (Submitted). (2022).

Curriculum vitae

Sarra EL HOUSSEINI

Date and place of birth	23.11.1993, Tunisia
Mail	sarra.elhousseini@epfl.ch / sarra.elhousseini@gmail.com

EDUCATION

2018-2022 PhD thesis at Ecole Polytechnique Federal de Lausanne (EPFL) in Laboratory of Construction Materials (LMC), Lausanne, Switzerland. Thesis: Hydration and durability of fast hardening binders incorporating supplementary cementitious materials.

2017-2018 Master research degree M2 in control and durability of materials, University of Burgundy, Dijon, France.

2014-2017 Engineering classes in Industrial chemistry, National Institute of Applied Science and Technology (INSAT), Tunis, Tunisia.

2012-2014 Preparatory classes in applied chemistry and biology, National Institute of Applied Science and Technology (INSAT), Tunis, Tunisia.

PROFESSIONAL QUALIFICATIONS

2018-2022 Research assistant at EPFL, Switzerland.

- Adapted the LC^3 mix design to improve its early age strength performance.
- Understood hydration mechanisms responsible of improving the strength performance.
- Supervised master projects on the incorporation of calcium aluminate cement and calcium sulfate in formulations based on Portland cement and SCM's.
- Gave a lecture about alternative cements during the yearly hold LC^3 doctoral school.

2018 Master thesis at Imerys aluminates, Vaulx milieu, France.

- Investigated the influence of incorporating calcined clay in a fixing mortar formulation.

2017   End of engineering study internship at Interdiscplinary Laboratory Carnot of Burgundy (ICB), Dijon, France.

- Studied the impact of setting retarders on the nucleation and growth of C-S-H.

2016   Internship at Zodiac Aerospace (Safran), Tunis, Tunisia

- Investigated the evaporation and drying processes of the adhesives used in the manufacturing of airplane defrosters.

LANGUAGES

Arabic *(native language)*, English *(fluent in speech and writing)* and French *(fluent in speech and writing)*.

PUBLICATIONS

Journal papers and patent under submission

Sub.2019   Hydraulic binder with low carbon footprint and high early strength

Sub.2022   Understanding interactions between calcined clay with Portland cement Calcium aluminate cement and Calcium sulfate in a fixing mortar formulation.

Sub.2022   Effect of the C/A ratio of the calcium aluminate cement on the hydration and performance of LC^3-CAC blends.

Sub.2022   Chloride ingress and carbonation resistance of LC^3-CAC blends.

INTERESTS

Hobbies

Badminton, hiking and sledging.